
Identifying the molecular function of MacroD2 and TARG1

Giuliana Katharina Möller



Munich 2019

Identifying the molecular function of MacroD2 and TARG1

Giuliana Katharina Möller

Aus dem Adolf-Butenandt-Institut
Lehrstuhl: Physiologische Chemie
im Biomedizinischen Zentrum
der Ludwig-Maximilians-Universität
München
Vorstand: Prof. Dr. Andreas Ladurner

Dissertation
zum Erwerb des Doktorgrades der Naturwissenschaften
an der Medizinischen Fakultät
der Ludwig-Maximilians-Universität München

vorgelegt von
Giuliana Katharina Möller
aus Karlsruhe

2019

Gedruckt mit der Genehmigung der Medizinischen Fakultät
der Ludwig–Maximilians–Universität München

Erstgutachter: Prof. Dr. Andreas G. Ladurner
Zweitgutachter: Prof. Dr. Alexander Dietrich
Dekan: Prof. Dr. med. dent. Reinhard Hickel
Tag der mündlichen Prüfung: 10.01.2020

Eidesstattliche Versicherung

Möller, Giuliana Katharina

Name, Vorname

Ich erkläre hiermit an Eides statt, dass ich die vorliegende Dissertation mit dem Thema

Identifying the molecular function of MacroD2 and TARG1

selbständig verfasst, mich außer der angegebenen keiner weiteren Hilfsmittel bedient und alle Erkenntnisse, die aus dem Schrifttum ganz oder annähernd übernommen sind, als solche kenntlich gemacht und nach ihrer Herkunft unter Bezeichnung der Fundstelle einzeln nachgewiesen habe.

Ich erkläre des Weiteren, dass die hier vorgelegte Dissertation nicht in gleicher oder in ähnlicher Form bei einer anderen Stelle zur Erlangung eines akademischen Grades eingereicht wurde.

München, 05.03.2019

Ort, Datum

Giuliana Katharina Möller

Unterschrift Doktorandin

Table of Contents

List of Figures	xii
List of Tables	xiii
Zusammenfassung	xvii
Abstract	xix
1 Introduction	1
1.1 Post-translational Modifications	1
1.2 Cellular ADP-ribosylation	3
1.2.1 ADP-ribosylation - Writers	3
1.2.2 Readers of ADP-ribose	7
1.2.3 Erasers of ADP-ribose	8
1.3 Cellular Function of PARP Enzymes	9
1.3.1 Function of PARylating PARPs	9
1.3.2 Functions of MARylating PARPs	10
1.4 Function of Macrodomain-containing Hydrolases - MacroD1, MacroD2, and TARG1	12
1.5 Actin Structure and Functions	13
1.6 EGFR signaling	16
2 Aims of this Thesis	21
2.1 Aim I: Deduce cellular function of MacroD2 by its interactors	21
2.2 Aim II: Identify the cellular function of MacroD2 and TARG1 by their loss-of-function phenotypes	22
3 Results	23
3.1 Identifying the Biological Function of MacroD2 by its Interaction Partners with BioID	23
3.1.1 BioID Validation	23
3.1.2 Identifying MacroD2 Interactors	30
3.2 Identifying the biological function of MacroD2 and TARG1 through loss-of-function phenotypes	37

3.2.1	Knockout Cell Line Generation and Validation	37
3.2.2	Identification of potential global proteome changes in cells lacking MacroD2	43
3.2.3	Function of MacroD2 and TARG1 in cellular proliferation	46
3.2.4	Function of MacroD2 and TARG1 in actin-regulated processes	49
3.2.5	Influence of MacroD2 and TARG1 on EGFR Signaling	58
4	Discussion	67
4.1	MacroD2 and TARG1 possess redundant functions in regulating the actin cytoskeleton - most likely through modulating EGFR signaling	67
4.1.1	Summary	67
4.1.2	Outlook	70
4.2	Interesting pathways which MacroD2 and TARG1 might influence	77
4.2.1	MacroD2 and TARG1 in neuronal function	77
4.2.2	MacroD2's and TARG1's role in DNA damage response in unstressed cells	82
5	Materials and Methods	85
5.1	Reagents	85
5.2	Antibodies	86
5.3	Buffers	87
5.4	Kits	89
5.5	Cloning	89
5.6	Plasmids	90
5.7	Cell Culture	90
5.8	Transfections	94
5.9	Knockdowns	94
5.10	Drug and Antibiotic treatments	94
5.11	Generation of CRISPR Knockout Cell Lines	95
5.11.1	Classic CRISPR	95
5.11.2	Nickase CRISPR	96
5.12	Genotyping of CRISPR Knockout Cell Lines	96
5.12.1	Classic CRISPR	96
5.12.2	Nickase CRISPR	96
5.13	Western blotting	97
5.14	Immunofluorescence	97
5.15	Microscopy	98
5.16	BioID Pulldowns	98
5.17	Mass Spectrometry	99
5.17.1	On-bead tryptic digest	99
5.17.2	Whole cell Proteome	99
5.17.3	Sample desalting	100
5.17.4	Mass Spectrometry Measurements	100

5.18	Mass Spec Data Analysis	101
5.19	Cell Cycle Profiling	101
5.20	xCelligence	102
5.21	Scratch Assay	102
5.22	Cell Migration Assay	102
5.22.1	Migration with and without EGF stimulation	102
5.22.2	Migration with and without FK866 treatment	103
5.23	EGFR Internalization Assay	103
5.24	EGFR Internalization Rescue	103
A	Appendix	105
A.1	BioID validation	105
A.2	Validation of knockout cell lines	110
A.3	Actin-regulated processes regulated by MacroD2 and/or TARG1	112
	References	117
	Acknowledgements	139

List of Figures

1.1	Phosphorylation is a representative PTM	2
1.2	Overview of human PARP family members with their domain structure . .	4
1.3	Changes in ADP-ribosylation status of proteins is represented in the ADP- ribosylation cycle	5
1.4	Overview of identified PAR reader domains	8
1.5	PARPs perform several cellular functions	11
1.6	Overview of actin networks involved in moving cells	15
1.7	EGFR signaling is a complex signaling pathway in human cells	18
3.1	BioID proximity ligation works by tagging proteins in close proximity to the bait with biotin	24
3.2	BioID constructs used in this study	25
3.3	N-terminally tagged MacroD2 fusion protein biotinylates itself and interac- tors well, while the C-terminally tagged MacroD2 fusion protein does not biotinylate itself or interactors well	26
3.4	All used BioID constructs exhibit the expected localization in human cells	29
3.5	The intensity of endogenously biotinylated proteins is comparable in all cell lines and replicates and MacroD2 is within the most intense peaks in all cell lines expressing MacroD2	31
3.6	In cells expressing BirA-MacroD2, many significantly enriched interactors could be identified over cells expressing BirA only	32
3.7	184 proteins are significantly enriched in cells expressing MacroD2-BirA over both controls (BirA only and HEK cells)	33
3.8	Significant MacroD2 interactors form a network of GO-terms with many connections in between GO-terms	35
3.9	Guide RNAs used for CRISPR/Cas9 knockout generation	38
3.10	Utilized Knockout Cell Lines show no detectable protein, which was targeted with CRISPR/Cas9, while GAPDH was expressed equally throughout all cell lines	39
3.11	Genotyping nickase-induced knockouts	42
3.12	The whole proteome of MacroD2 knockout (KO) cells compared to wildtype cells (U2OS) shows no major proteome changes	44

3.13	No significant changes in cell proliferation could be detected for any knock-out cell line compared to wild-type cells	47
3.14	Cell cycle profiles of WT and single KO cell lines show comparable cell cycle profiles	48
3.15	Example images of clonal U2OS (cWT2) staining against actin and focal adhesion proteins	50
3.16	Quantification of actin intensity and focal adhesion protein vinculin	51
3.17	Double knockout cell lines attach significantly slower than wildtype cells	52
3.18	MacroD2 knockout cell migrate slower than wild-type cells in a scratch assay	54
3.19	Double knockout cell migrate significantly slower than wildtype cells in a 96-well migration assay	56
3.20	NAD ⁺ depletion did not induce significantly faster migration in single or double knockout cells	57
3.21	MacroD2 knockout and double knockout cells do not induce cell migration sufficiently upon EGF-stimulation	59
3.22	Double knockout cells show clusters of EGFR upon EGF-treatment in the peri-nuclear area	60
3.23	Perinuclear EGFR foci after 30 minute EGF treatment are significantly enriched in double knockout cell lines	61
3.24	The increase in nuclear EGFR intensity upon 30 minute EGF-treatment is comparable in all wt and knockout cell lines	62
3.25	GFP-MacroD2 can reduce perinuclear EGFR accumulation upon EGF treatment in all double knockout cell lines	63
3.26	GFP-MacroD2 G188E, a non-ADP-ribose binding mutant, does not reduce perinuclear EGFR accumulation upon EGF treatment in all double knockout cell lines	64
3.27	GFP-TARG1 does reduce perinuclear EGFR accumulation upon EGF treatment in double knockout cell lines	65
4.1	Double knockout cell lines exhibit decreased cell attachment, migration and EGF-stimulated cell migration accompanied by an increase in perinuclear EGFR	71
A.1	Volcano plot of MacroD2 macrodomain and C-terminal domain interactors	111
A.2	mRNA levels of MacroD2 in MacroD2 KO cell lines	112
A.3	xCelligence measurements	113
A.4	Schematic representation of migration assay	114
A.5	Immunofluorescence images of all cell lines with actin and vinculin co-staining	115
A.6	Immunofluorescence images of all cell lines with Zyxin and Filamin A co-staining	116

List of Tables

3.1	Genotypes of MacroD2 and TARG1 knockout cell lines used in this thesis .	40
5.1	Used antibodies	86
5.2	Used plasmids with database location and glycerol stock availability	90
5.3	Used cell lines. Cell line name, content and selection	92
5.4	Drug Treatments	94
5.5	Antibiotic Treatments	95
5.6	CRISPR Target Sequences	95
A.1	MacroD2 significant interactors	105
A.2	Percent of cells in different cell cycle phases	112

ADP	Adenosine-diphosphate
bp	Base pair
BSA	Bovine serum albumine
DMEM	Dulbecco's Modified Eagle Medium
DNA	Desoxyribonucleic acid
DTT	Dithiothreitol
EDTA	Ethylen-diamin-tetra-acetic acid
EVC	Empty vector control
FA	Formic acid
FBS	Fetal bovine serum
FL	Full-length
FSC	Forward scatter
HEK	Human Embryonic Kidney cell line
HRP	Horse Raddish Peroxidase
iPS	Induced pluripotent stem cells
kb	Kilo base pairs
KO	Knockout
MD	Macrodomain
PAGE	Polyacrylamide Gel Electrophoresis
PARG	Poly-ADP-ribose glycosylase
PARP	Poly-ADP-ribose-polymerase
PBS	Phosphate Buffered Saline
PBS-T	Phosphate Buffered Saline supplemented with 0.5% Tween 20
Pen/Strep	Penicillin and streptomycin
PFA	Paraformaldehyde
PI	Propidium iodide
SDS	Sodium dodecyl sulfate
SSC	Side scatter
TBS	Tris Buffered Saline
TBS-T	Tris Buffered Saline supplemented with 0.5% Tween 20
TFA	Trifluoroacetic acid
Tris	Tris(hydroxymethyl)aminomethane
UV	Ultraviolet
U2OS	Human osteosarcoma cell line
WT	Wild-type

Zusammenfassung

Humane Zellen müssen in einer angemessenen Zeit auf Umwelteinflüsse reagieren. Ein Weg diese schnelle Reaktionszeit zu ermöglichen ist es kleine chemische oder biologische Verbindungen an Proteine anzuhängen, die sogenannten post-translationalen Modifikationen. Post-translationalen Modifikationen werden von verschiedenen Enzymklassen abhängig von der Art der post-translationalen Modifikation angehängt, gelesen und entfernt.

Eine der post-translationalen Modifikationen ist die ADP-Ribosylierung, eine Modifikation, bei der entweder eine oder mehrere ADP-Riboseeinheiten von der PARP-Enzymfamilie an Proteine angehängt werden. ADP-Ribosylierung spielt bei einer Vielzahl von zellulären Signaltransduktionswegen und in einer großen Zahl von essentiellen zellulären Funktionen eine wichtige Rolle, wie zum Beispiel DNA-Reparatur, Transkription und dem Zellzyklus. Proteine, welche nur mit einer einzigen ADP-Riboseeinheit versehen sind, werden als mono-ADP-ribosyliert (MARyliert) bezeichnet. In MARylierten Proteinen, bei denen die ADP-Riboseeinheit über eine saure Aminosäure an das Protein gebunden ist, kann die Modifikation von drei Enzymen entfernt werden - MacroD1, MacroD2 und TARG1. Während MacroD1 ausschließlich mitochondrial lokalisiert ist, sind sowohl MacroD2 als auch TARG1 im Zellkern und im Zytoplasma lokalisiert. Die Funktion von MacroD2 und TARG1 ist bisher weitestgehend unbekannt. Beide Enzyme werden in der Literatur mit DNA-Schäden und neurologischen Symptomen in Verbindung gebracht. Aus diesem Grund war das Ziel dieser Dissertation die Entschlüsselung der Funktion beider Enzyme in humanen Zellen.

Hierfür habe ich einen zweigleisigen Ansatz gewählt. Im ersten Ansatz habe ich Proteininteraktionspartner von MacroD2 mit der BioID-Methode identifiziert. Hierbei habe ich die BioID-Methode gewählt, da diese Methode zur Detektion von schwachen und transienten Interaktionen entwickelt wurde und ADP-Ribosylierung schnell an Proteine angehängt und entfernt wird. Unter den mit BioID identifizierten Interaktoren von MacroD2 habe ich viele Proteine der Gen-Ontologie-Begriffe gefunden, welche mit Aktin und fokalen Adhäsionen verbunden sind. Dieses Ergebnis führte zu der Hypothese, dass MacroD2 in der Regulation des Aktinzytoskeletts beteiligt sein könnte.

Im zweiten Ansatz habe ich Zellen mit CRISPR/Cas hergestellt, in welchen MacroD2, TARG1 oder beide Enzyme fehlen, und diese validiert. Mit diesen Zellen habe ich systematisch nach Phänotypen gesucht, welche mit den Interaktoren von MacroD2 zusammenhängen. Ich habe alle Zelllinien in Hinsicht auf die Signalintensität und Lokalisation des Aktinzytoskeletts und der fokalen Adhäsionen mit Immunfluoreszenzexperimenten untersucht, habe hierbei aber keine Defizite erkannt. Danach habe ich untersucht, ob diese

Zellen Probleme mit Aktin-regulierten Prozessen, wie Zellmigration und -anhaftung, aufweisen. Ich habe festgestellt, dass nur Zellen, in denen beide Enzyme fehlen, erhebliche Probleme mit Zellmigration und -anhaftung aufweisen.

Um herauszufinden, wie Zellmigration und -anhaftung in Zellen ohne MacroD2 und TARG1 dereguliert sind, habe ich den epidermal growth factor receptor (EGFR)-Signaltransduktionsweg untersucht. Ich habe herausgefunden, dass Zellen ohne MacroD2 und TARG1 nicht in einem ausreichenden Maß auf die Stimulation mit EGF reagieren und dass EGFR nach der Behandlung mit EGF in perinuklearen Punkten angehäuft wird.

Zusammengefasst konnte ich zeigen, dass Zellen ohne MacroD2 und TARG1 Probleme mit der Zellmigration und -anhaftung ebenso wie eine Deregulierung des EGFR-Signaltransduktionsweges aufweisen. Die Tatsache, dass MacroD2 und TARG1 in ungestressten Zellen in Zellmigration, -anhaftung und im EGFR-Signaltransduktionsweg füreinander kompensieren können, deutet darauf hin, dass beide Enzyme zumindest teilweise redundant sind.

Abstract

Human cells need to react to environmental stimuli in a timely manner. One way to achieve this fast reaction time is the attachment of small chemical or biological units to proteins, so-called post-translational modifications. Post-translational modifications are added, read, and removed by different sets of enzymes dependent on the type of post-translational modification.

One type of post-translational modification is ADP-ribosylation, a modification where either single or multiple units of ADP-ribose are added to proteins by a family of enzymes called PARPs. ADP-ribosylation is involved in a plethora of cellular pathways and in a multitude of essential cellular functions such as DNA damage repair, transcription, and the cell cycle. Proteins modified with a single ADP-ribose moiety are called mono-ADP-ribosylated (MARylated). In MARylated proteins, where the ADP-ribose moiety is linked to the protein via acidic amino acids, the modification can be reversed by three enzymes - MacroD1, MacroD2, and TARG1. While MacroD1 is exclusively mitochondrial, both MacroD2 and TARG1 are present in the nucleus and cytoplasm. Not much is known about the function of MacroD2 and TARG1 so far. Both enzymes are connected to the response to DNA damage and to neurological defects in literature. Therefore, the aim of this thesis was to identify which functions both enzymes possess in human cells.

To this end, I utilized a two-pronged approach. Firstly, I identified protein interaction partners of MacroD2 with the BioID approach. I used BioID since this system was generated to identify weak and transient interactions which is necessary since ADP-ribosylation is rapidly added and removed. With the interactors of MacroD2 identified with the BioID approach, I found that many proteins with gene ontology terms related to actin and focal adhesions were enriched. This led to the hypothesis that MacroD2 might be involved in the regulation of the actin cytoskeleton.

As a second prong, I generated and validated CRISPR/Cas knockout cell lines lacking either MacroD2, TARG1 or both enzymes. With those cell lines I systematically screened for phenotypes related to the identified MacroD2 interactors. I screened all cell lines for defects in intensity or localization of the actin cytoskeleton and focal adhesions with immunofluorescence experiments. I could not identify any defects. Subsequently, I addressed if the knockout cell lines had defects in actin regulated processes such as cell migration and attachment. I realized that only cells lacking both MacroD2 and TARG1 had tremendous defects in cell migration and attachment.

In order to identify how cell migration and attachment were deregulated in cells lacking

MacroD2 and TARG1, I tested epidermal growth factor receptor (EGFR) signaling as a possible deregulated pathway. I found that cells lacking both enzymes did not increase cell migration in response to EGF treatment and that EGFR was accumulated in perinuclear foci after EGF treatment.

In summary, I could show that cells lacking MacroD2 and TARG1 had defects in cell migration and attachment, as well as deregulated EGFR signaling. The fact that MacroD2 and TARG1 can compensate for each other in cell migration, attachment, and EGFR signaling suggests that they perform at least partially redundant functions in unstressed cells.

Chapter 1

Introduction

1.1 Post-translational Modifications

Cells need to rapidly react to internal and external changes such as DNA damage or environmental growth factors. This can be achieved by changing the function and activity of proteins as well as their protein-protein interactions through post-translational modifications (PTMs). PTMs can be small chemical groups or proteins which can be bound to one or multiple amino acid residues of proteins. The importance of PTMs on cell signaling was long known but the sheer variety of cellular PTMs, with over 200 types of PTMs known, became clear only due to improved detection methods, especially in mass spectrometry. Some of the best studied PTMs are phosphorylation, ubiquitination, acetylation, and methylation. Each single type of PTM is added, read, and removed by different sets of proteins in human cells leading to massive signaling networks. Defects in enzymes adding or removing PTMs are known to be the reason for numerous diseases including cancer (Deribe et al., 2010; Seet et al., 2006).

A good example for the influence of PTMs on proteins is protein phosphorylation, which was the first identified PTM. Phosphorylation was first observed in 1906 on a protein called vitellin (Levene and Alsberg, 1906). The phosphorylation of vitellin was later defined to be a phosphorylated serine (Lipmann and Levene, 1932). In general, proteins are phosphorylated with a single phosphate at serine, tyrosine or threonine amino acids by enzymes called kinases. Kinases can phosphorylate proteins on different amino acids based on different environmental stimuli. As a direct example to explain readers, writers, and erasers for phosphorylation, I have chosen Epidermal Growth Factor Receptor (EGFR). The reader, writer, and eraser terminology for PTMs was first used by Baker, Allis, and Wang (Baker et al., 2008). EGFR is a tyrosine kinase receptor involved in a network responding to extracellular growth stimuli, which phosphorylates (writer) itself at multiple distinct tyrosine amino acids depending on the external stimuli. Phosphorylation can be read by many proteins with phospho-recognition domains (reader). Examples of those domains are Src homology 2 (SH2) domains binding to phosphorylated tyrosine, as depicted in figure 1.1. SH2 domains are found commonly in adaptor proteins responsible for signal transduc-

tion from receptor proteins to downstream kinases, starting a signal cascades inside cells, e.g. CT10 regulator of kinase (CRK) binding EGFR. In case of phospho-binding motifs, it is well documented that distinct binding domains require specific consensus sequences in their target proteins for efficient binding (Deribe et al., 2010; Seet et al., 2006). Enzymes removing phospho-groups from proteins are called phosphatases (eraser) and they oppose kinases (figure 1.1). Phosphatases are important to modulate and switch off signaling processes in cells. They dephosphorylate EGFR and are highly specific in their protein and phospho-amino acid target selection (Tiganis, 2002). Phosphorylation controls major cellular processes such as cell growth, cell cycle and proliferation, differentiation, and the DNA damage response (Deribe et al., 2010).

Phosphorylation is regulated by many different enzymes resulting in a complex regulatory network. This is true for all known and studied PTMs. Each PTM is tightly regulated by a vast array of writers, readers, and erasers. Networks regulating specific PTMs are not disconnected from each other but intertwine with each other resulting in a massive, interconnected signaling network. Different types of PTMs can target the same or neighboring amino acids in the same protein and positively or negatively influence the binding of their respective writers, readers or erasers at their target sites. PTMs can be mutually exclusive, e.g. methylation and acetylation of lysine 9 of histone H3 or antagonistic, e.g. phosphorylation of serine 10 of histone 3 which displaces the reader of methylation (HP1) from lysine 9. On the other hand PTMs can set the stage to allow another PTM to modify the same protein in a cooperative or sequential manner, e.g. phosphorylation and ubiquitination of EGFR (Seet et al., 2006).

Understanding these highly interconnected networks is a challenge we need to address in depth in the future and holds the key to understand diseases better.

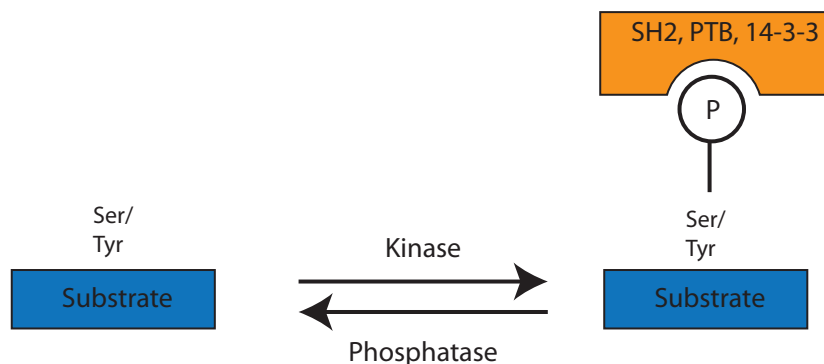


Figure 1.1: Phosphorylation is a representative PTM. Enzymes adding and reversing the PTM and some representative recognition domains are depicted. Adapted from (Deribe et al., 2010)

1.2 Cellular ADP-ribosylation

1.2.1 ADP-ribosylation - Writers

As described in the previous chapter, PTMs are very important for cellular functions and are highly intertwined with each other. Apart from needing to understand the huge network formed by the entirety of all possible PTMs, it is important to understand the function of each individual PTM on its own - with all its readers, writers, and erasers. One very interesting and important cellular PTM is ADP-ribosylation.

ADP-ribosylation is a very dynamic and complex post-translational protein modification which is mainly added by the poly-ADP-ribose polymerase (PARP) family of ADP-ribosyl transferases (ARTs). PARP enzymes utilize NAD^+ to form negatively charged ADP-ribose units on proteins and release nicotinamide. Poly-ADP-ribose chains can be linear or branched and of different size. PAR was first discovered in 1963 by Chambon et al. (Chambon et al., 1963) and has started the discovery of a plethora of chemical and biological findings. The use of NAD^+ connects ADP-ribosylation with metabolic processes in the cell (for review see ref. (Barkauskaite et al., 2013)).

PARPs can add ADP-ribose to acidic amino acids (aspartate and glutamate) and lysine residues (Chapman et al., 2013; Martello et al., 2016). It was discovered recently that proteins can be ADP-ribosylated on serine residues. This form of ADP-ribose is added to target proteins by PARP1 or PARP2 together with histone PARylation factor 1 (HPF1). Serine modified ADP-ribosylated proteins are histones and proteins belonging to the DNA damage response (Bonfiglio et al., 2017; Fontana et al., 2017; Gibbs-Seymour et al., 2016; Leidecker et al., 2016).

Ten out of the 17 PARP family members add only single ADP-ribose moieties to proteins, so-called mono(ADP-ribosylation) (MARylation), while five PARPs (PARP1, PARP2, PARP4, PARP5a, PARP5b) generate poly-ADP-ribose on proteins (PARylation) by adding further ADP-ribose units onto the first unit. Two PARP family members (PARP9 and PARP13) are enzymatically inactive (Feijs et al., 2013c).

PARP enzymes possess a catalytic PARP domain, with a catalytic triad responsible for NAD^+ binding. PARylating PARPs' catalytic triad consists of the amino acids H-Y-E (histidine-tyrosine-glutamate), where glutamate (E) is responsible to add additional ADP-ribose moieties to the first moiety. MARylating PARPs on the other hand have a catalytic triad where glutamate is mutated to isoleucine, leucine, threonine, valine or tyrosine. The H-Y-E catalytic triad can also be found in Diphtheria-like bacterial ARTs, which gave rise to the alternative name ARTDs for PARPs (Hottiger et al., 2010). PARP enzymes have various domains apart from their catalytic domain and can be clustered into four distinct groups based on their domain content: DNA-dependent, Tankyrases, Macrocontaining, CCCH-containing. The PARPs without any of the before mentioned domains are termed unclassified. DNA-dependent PARPs contain a WGR domain, a domain named after its conserved central motive (W-G-R; tryptophan-glycine-arginine). The WGR domain enables binding of the WGR domain of PARP2 in collaboration with its catalytic domain to damaged DNA (Riccio et al., 2016).

Tankyrases are characterized by their protein-binding Ankyrin repeats. Macro- and CCCH-containing PARPs are characterized by their macrodomain and their CCCH zinc finger, respectively. Macrodomains bind ADP-ribose while CCCH zinc fingers bind viral RNA. Groups and domain structures of all PARPs are depicted in figure 1.2 (Daugherty et al., 2014; Hottiger et al., 2010; Li and Chen, 2014).

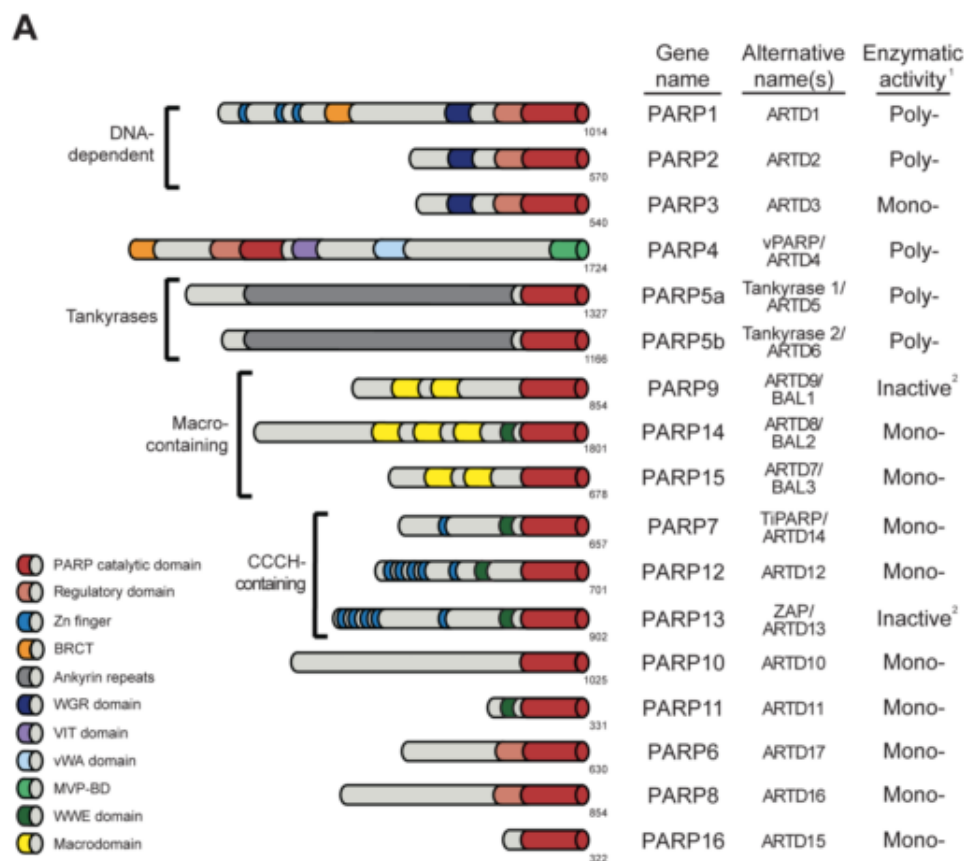


Figure 1.2: Human PARP family members are depicted with schematic domain structure, alternative names, PARP subgroups, and ADP-ribose transferase activity. Figure from <http://journals.plos.org/plosgenetics/article?id=10.1371/journal.pgen.1004403> (18.10.2017) (Daugherty et al., 2014).

Apart from PARPs, there are five extracellular or secreted polymerases - so-called ADP-ribosyl transferases cholera toxin-like (ARTCs) - which MARylate proteins on arginine residues. ARTCs have a R-S-E (arginine-serine-glutamate) catalytic triad, which is also found in the cholera toxin. ART1-4 are anchored to the plasma membrane whereas ART5 is secreted. ART1 was shown to regulate innate immunity and cell-cell contacts (Bütepage et al., 2015; Hottiger et al., 2010; Mashimo et al., 2014).

Members of the Sirtuin family (Sirt2, Sirt4, and Sirt6) were identified to possess MARylation activity, too. Sirtuin family members catalyze the deacetylation of target proteins

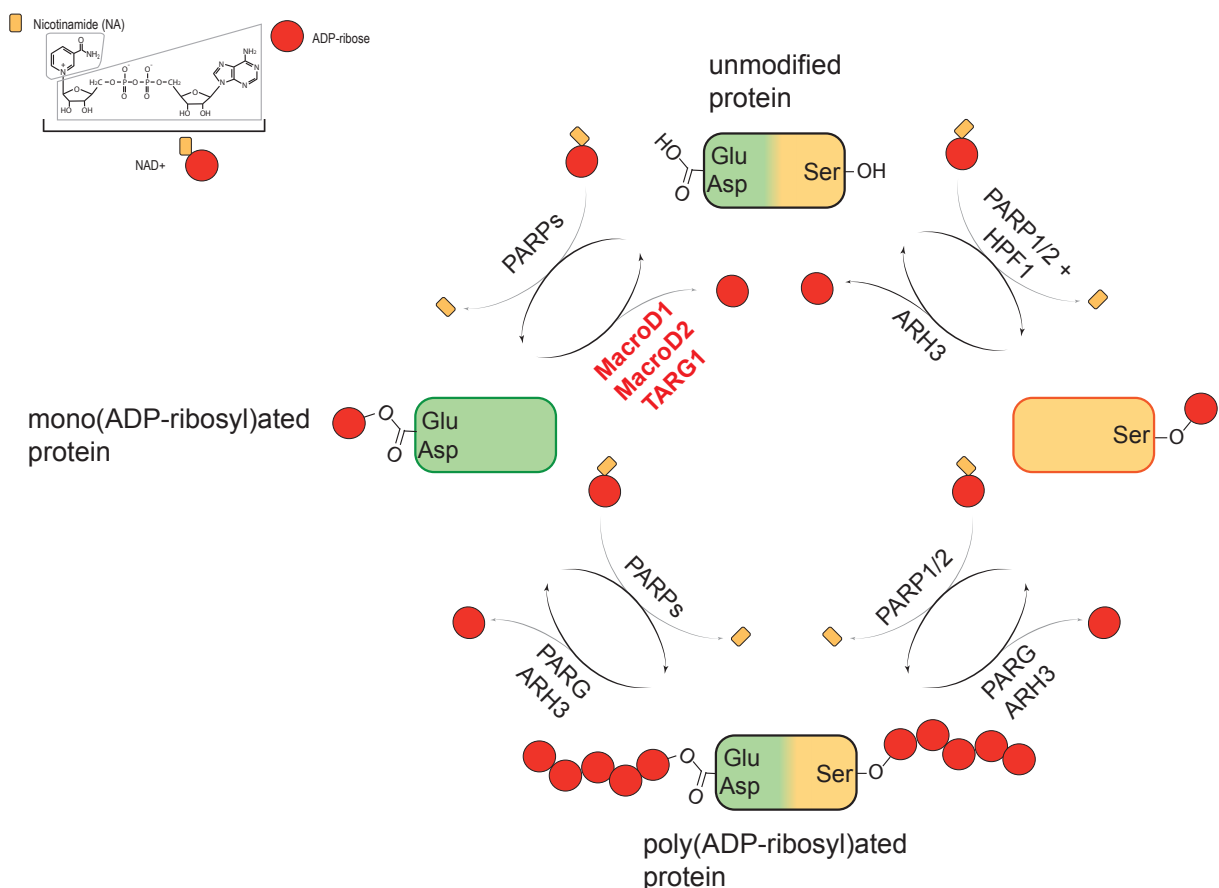


Figure 1.3: ADP-ribosylation cycle is depicted schematically. When a protein (top) undergoes mono(ADP-ribosyl)ation the ADP-ribose (red circle) can be transferred from NAD⁺ to a acidic amino acid (glutamate (Glu) or aspartate (Asp; left)) or a serine (Ser; right). It is also possible for multiple units of ADP-ribose to be added to a protein at a given target site in a process known as poly(ADP-ribosyl)ation (bottom). The enzymes PARP1 and PARP2 are involved in ADP-ribosylation of both Glu/Asp and Ser, with histone PARylation factor 1 (HPF1) acting as a cofactor in the mono(ADP-ribosyl)ation of serine. PARP3, PARP5a and PARP5b can add further units of ADP-ribose to MARylated proteins. The enzymes involved in the reversal of both mono- and poly(ADP-ribosyl)ation are shown. Fontana et al. have shown that ADP-ribosylhydrolase 3 (ARH3) is exclusively responsible for reversing the mono(ADP-ribosyl)ation of Ser, and that it is also involved (with PARG) in reversing the poly(ADP-ribosyl)ation of Ser (Fontana et al., 2017). Adapted from (Moeller and Timinszky, 2017)

in a NAD⁺ dependent fashion and produce O-acetyl-ADP-ribose on these target proteins (Bütepage et al., 2015). It was shown that Sirtuin proteins MARylate target proteins on arginine residues (Mashimo et al., 2014). Sirt4 was shown to MARylate Glutamate

dehydrogenase (GDH) on a cysteine residue, providing an additional link between ADP-ribosylation and cellular metabolism (Choi et al., 2005).

1.2.2 Readers of ADP-ribose

To relay the message of any PTM, the presence of so-called readers is important. Readers need to be able to bind to specific PTMs and to interact with other proteins to result in local or global cellular changes. To bind ADP-ribosylated proteins, four classical binding domains are known: macrodomains, PAR-binding motifs (PBMs), WWE-domains, and PAR-binding zinc-fingers (PBZs). A PBM is a loosely defined 20 amino-acid cluster of hydrophobic amino acids spaced by basic residues found in DNA damage checkpoint proteins (Pleschke et al., 2000). *In silico* analysis predicts PBM motifs in more than 800 proteins (Gagné et al., 2008). WWE-domains are named after their conserved tryptophan and glutamate amino acids and were found in PARPs as well as ubiquitin ligases (Wang et al., 2012). PBZ domains were discovered originally in two DNA damage response proteins (aprataxin and PNK-like factor & checkpoint with forkhead and ring finger domains) which contain a zinc finger motif able to bind to PAR (Ahel et al., 2008). In recent years, new PAR reader modules emerged, such as FHAs/BRCT (forkhead associated), oligonucleotide/oligosaccharide-binding (OB)-fold, RNA recognition motif (RRM), serine-arginine (SR) repeats, glycine arginine (KR)-rich motifs, PilT N-terminus (PIN) domain, and RG/RGG repeats, as depicted in figure 1.4. FHAs/BRCT motifs are well known for their ability to recognize phosphorylated proteins but were shown in recent years to also bind PAR during DNA damage response *in vivo* and *in vitro*. In this class of PAR-binders, it is remarkable that the FHA domain of e.g. APTX interacts with iso-ADP-ribose while the BRCT domain of e.g. Ligase 4 recognizes ADP-ribose (Li et al., 2013) itself. The OB-fold is a single stranded DNA or RNA binding motif but was shown to bind to PAR *in vivo* and *in vitro* under DNA damage conditions. The first identified protein with a PAR-binding OB-fold was human ssDNA-binding protein 1 (hssB1) (Zhang et al., 2014). RRM domains, as their name already suggests, are known for their RNA recognition capability. In 2003, heterogeneous nuclear ribonucleoprotein (hnRNP), such as hnRNP A1, containing two RRM motifs, was found to bind PAR (Gagné et al., 2003). SR repeats are known as splice regulators and for binding RNA in general. Alternate splicing factor/splice factor 2 (ASF/SF2), a SF-protein family of splice factors, binds to PAR (Malanga et al., 2008). Furthermore, KR motifs in the ras-GAP SH3-binding proteins (G3BP) bind PAR under genotoxic stress conditions, thereby influencing stress granule assembly (Isabelle et al., 2012). PIN domains are known DNA and RNA binding domains with nucleolytic activity and are responsible for the binding of EXO1, a RAD2 family nuclease member, to PAR under DNA damage conditions. In the same publication, other PIN containing proteins were shown to bind PAR in pulldown experiments, introducing PIN as PAR binding domains (Zhang et al., 2015). RG/RGG repeats - regions rich in arginine and glycine - are known RNA binding motifs and were shown to bind to PAR. This was first shown for the RG repeat domain of the nuclease MRE11 in 2008 (Haince et al., 2008).

In summary, ADP-ribose can be bound by a number of domains, some of which were known to bind to other substrates, such as phosphate, ssDNA, and RNA. This indicates that ADP-ribosylation might cross-talk with other PTMs and cellular pathways e.g., stress granule formation and DNA repair.

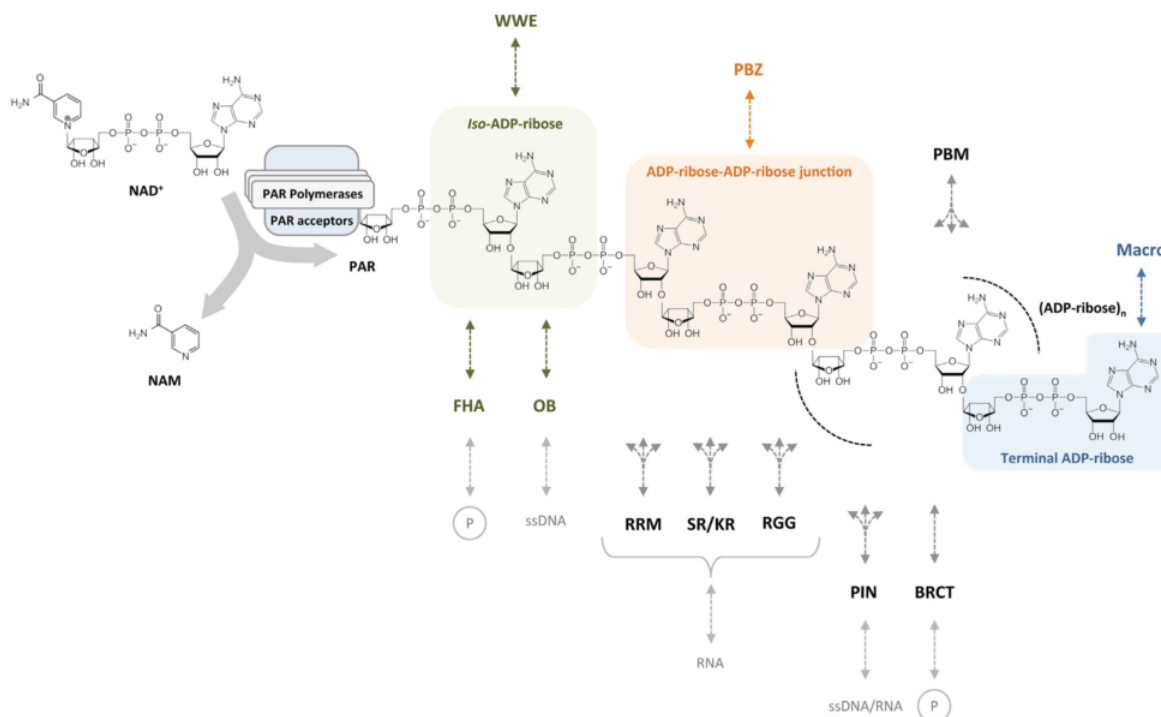


Figure 1.4: Overview of identified PAR reader domains. Different PAR reader domains with their PAR site (if known) and alternative substrate binding possibilities (Teloni and Altmeyer, 2016). Reprint with permission from Oxford University Press.

Different reader domains can detect different features of the PAR chains. Macrodomains are globular reader domains recognizing mono-ADP-ribose, poly-ADP-ribose as well as O-acetyl-ADP-ribose. Structural data suggests that macrodomains recognize the last ADP-ribose moiety only, indicating a “2’ OH PAR capping activity” for macrodomains (Timinszky et al., 2009). All other known readers recognize features in PAR. The WWE-domain, OB-fold, and FHA-domain bind to iso-ADP-ribose, a structure formed by two consecutive ADP-ribose moieties in a PAR chain. While PBZ does not bind to iso-ADP-ribose, it binds to another distinct structure formed by two consecutive ADP-ribose moieties in a PAR chain (figure 1.4). The binding mechanism for PBM, RRM, SR repeats, KR-rich motifs, and PIN domains is not known yet, but their binding might result from electrostatic interactions (for review see (Ryu et al., 2015; Teloni and Altmeyer, 2016)).

1.2.3 Erasers of ADP-ribose

In order to terminate signals coming from PTMs, those signals need to stop once the cellular output is achieved. Erasers remove PTMs and revert proteins back to their unmodified state. Poly-ADP-ribose glycohydrolase (PARG), a macrodomain-containing hydrolase of PAR, removes PAR from proteins but leaves the most protein proximal ADP-ribose moiety

behind. Apart from PARG, ARH3 can remove PAR from target proteins - although less efficiently than PARG (Niere et al., 2012; Oka et al., 2006). ARH3 can degrade PAR from target proteins as well as degrade free PAR chains and therefore protect proteins from PAR-induced apoptosis (Mashimo et al., 2013). It was shown that ARH3 hydrolysis depends on magnesium ions and is as such different from the mechanism of PARG-mediated PAR hydrolysis, which depends on its macrodomain fold (Mueller-Dieckmann et al., 2006; Oka et al., 2006; Slade et al., 2011). ARH3 can not remove the most protein proximal acidic amino acid or arginine linked ADP-ribose unit but can remove serine linked ADP-ribose as depicted in figure 1.3 (Bonfiglio et al., 2017; Fontana et al., 2017; Gibbs-Seymour et al., 2016; Leidecker et al., 2016). ARH1 was shown to remove arginine linked mono-ADP-ribose (Mashimo et al., 2014; Mueller-Dieckmann et al., 2006; Niere et al., 2012). Like ARH3, ARH1 does not possess a macrodomain to bind to ADP-ribose but binds in a magnesium-dependent manner (Mueller-Dieckmann et al., 2006; Oka et al., 2006). Three macrodomain-containing glycohydrolases, TARG1, MacroD1, and MacroD2, are able to remove the most protein proximal ADP-ribose moieties from proteins if they are linked via acidic amino acids as depicted in figure 1.3 (Jankevicius et al., 2013; Sharifi et al., 2013). I will discuss macrodomain-containing glycohydrolases in further detail later in the introduction.

1.3 Cellular Function of PARP Enzymes

PARP enzymes are very important for human cells, since they regulate a plethora of cellular functions. Some functions are performed by groups of PARPs, consisting of a mixture of MARylating/PARylating PARPs, while others are performed by single PARP enzymes. As an example of a single PARP performing one cellular function, PARP16 is connected with the unfolded protein response in the endoplasmatic reticulum (ER) (Jwa and Chang, 2012) 1.5. In a study where all PARP genes were knocked out in human cells and the lack of function phenotype was reported, the loss of PARP5a, a PARylating Tankyrase, and PARP7, a CCCH-containing MARylating PARP, resulted in mitotic defects. PARP5a and PARP15, an unclassified PARP, showed membrane defects, whereas PARP9 and PARP14, both containing macrodomains, showed actin cytoskeletal defects (Vyas et al., 2013). It was also shown that one PARylating PARP (PARP5a), a number of MARylating PARPs (PARP12, PARP14, PARP15), a catalytically inactive PARP (PARP13), as well as two PARG isoforms are components of cytoplasmic stress granules. The PARPs identified in stress granules were from three PARP groups - Tankyrase, CCCH zinc finger, and Macrodomain-containing (Leung et al., 2011).

1.3.1 Function of PARylating PARPs

According to literature, PARylating PARPs (PARP1, PARP2, PARP4, PARP5a, PARP5b) are connected with functions such as DNA damage regulation, telomere length regulation, cell cycle progression, and cell death, as depicted in figure 1.5 (Daniels et al., 2015; Hottiger,

2015a; Wei and Yu, 2016). Some functions of PARP1 and PARP5a are discussed in more detail in the following paragraphs.

The most studied PARP enzyme is PARP1. PARP1 is predominantly involved in the DNA damage response by its recruitment to DNA damage sites and subsequent activation. Active PARP1 PARylates itself and serves as a docking site for DNA damage response enzymes and chromatin remodelers including but not limited to ALC1, macroH2A1.1, CHFR, and APLF (Feijs et al., 2013a). ADP-ribose is added to target proteins at serine residues by PARP1 or PARP2, and HPF1 (figure 1.3). Target proteins are histones and proteins belonging to the DNA damage response (Bonfiglio et al., 2017; Fontana et al., 2017; Gibbs-Seymour et al., 2016; Leidecker et al., 2016). Another PARylating PARP is PARP5a/Tankyrase1. PARP5a is involved in the Wnt signaling pathway which in itself regulates many important cellular functions such as proliferation and migration (Huelsenken and Behrens, 2002). PARP5a PARylates axin, an integral part of the Wnt complex. PAR on axin is bound by RNF146, a WWE-domain containing E3 ubiquitin ligase which stimulates the ubiquitination and subsequently the degradation of axin which in turn activates Wnt signaling (Callow et al., 2011; Zhang et al., 2011).

1.3.2 Functions of MARylating PARPs

In recent years the importance of MARylation for human cells became more apparent even though there are still many questions to be resolved. One of the major problems in driving the discovery of new functions of MARylation is that there is no MAR-specific antibody available and that the direct detection of MARylated proteins, without detecting PARylated proteins, remains impossible with mass spectrometry. However, more and more research emerges which indicates that MAR performs important functions in human cells. MARylating PARPs were shown to be involved in functions such as cell structure and motility (PARP11 and PARP14) as well as translation and mRNA stability (PARP12, PARP14, PARP15) as depicted in figure 1.5 (Daniels et al., 2015; Vyas and Chang, 2014). Examples of functions of MARylating PARPs are discussed in more detail in the following paragraphs.

It was shown that PARP14 regulates transcription. PARP14 functions as a molecular switch by binding to the promoters of STAT6 target genes and recruiting HDAC2 and HDAC3 (histone deacetylases) to these under non-stimulated condition. Upon IL-4 stimulation, PARP14 MARylates itself, as well as HDAC2 and HDAC3 and displaces them from the promoter of STAT6 target genes. PARP14 allows efficient binding of STAT6 to its target site and subsequent transcriptional activity (Mehrotra et al., 2011).

PARP10 inhibits the activation of NF- κ B in response to IL1 β and TNF α . PARP10 binds to poly-ubiquitinated NEMO, an important regulator of NF- κ B signaling, and thereby inhibits NF- κ B mediated transcription of pro-inflammatory target genes (Verheugd et al., 2013). PARP14 promotes the Warburg effect, the usage of aerobic glycolysis in cancer cells, by inhibiting the metabolic activity of PKM2, a key regulator of the Warburg effect, through inhibition of JNK signaling in hepatocellular carcinoma (Iansante et al., 2015).

New developments in mass spectrometry and chemical genetic engineering showed that every MARYlating PARP analyzed so far MARYlates specific target proteins and therefore performs distinct functions in human cells. PARP10, apart from its already mentioned function in NF- κ B signaling, was shown to MARYlate proteins involved in mRNA metabolism, protein transport, and cellular metabolism while PARP11 was shown to MARYlate proteins from gene ontology-terms (GO-terms) of RNA transport and nuclear membrane organization. The same paper showed that different PARPs have mainly non-overlapping target proteins. They showed that previously published datasets for PARP1 and PARP2 (PARylating PARPs) also showed non-overlapping targets as well as some common targets. PARP10 and PARP2 show the most overlap with 29% common targets. Whereas PARP11 only had two overlapping targets in common with PARP2, it had no target in common with PARP1 and six common targets with PARP10 (Carter-O'Connell et al., 2014, 2016).

This supports the hypothesis that MARYlation and PARylation perform important, mostly non-overlapping functions in human cells.

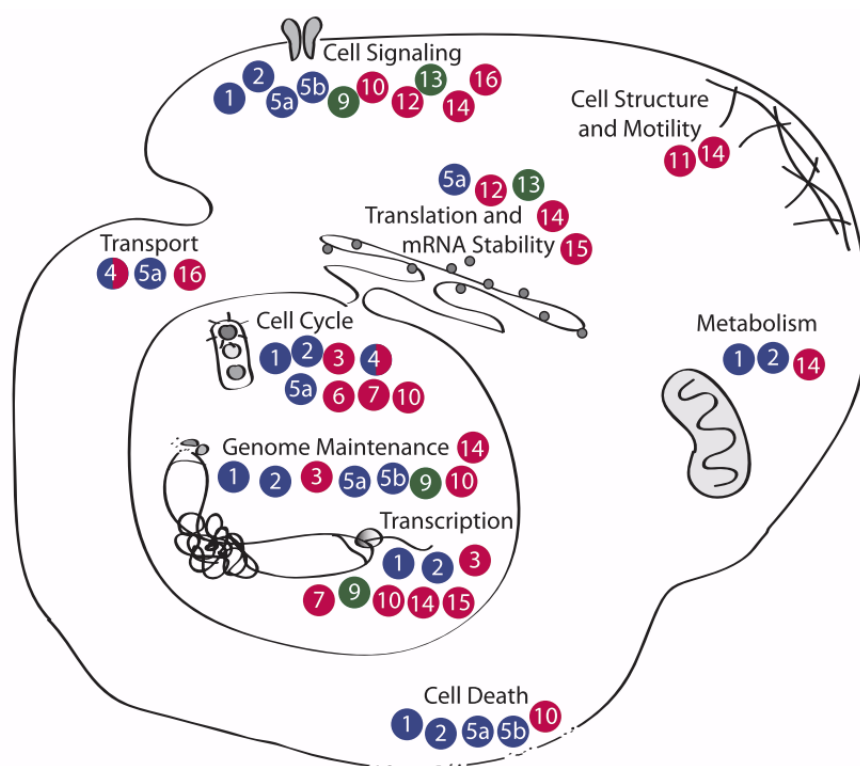


Figure 1.5: PARPs perform several cellular functions. MARYlating and PARylating PARPs perform important cellular functions. PARylating PARPs are shown in blue, MARYlating PARPs in red, PARPs without enzymatic function in green. Numbers depict number of PARP enzyme e.g. 1 is PARP1 (Daniels et al., 2015). Reprint with permission from Elsevier.

1.4 Function of Macrodomain-containing Hydrolases - MacroD1, MacroD2, and TARG1

MacroD1, MacroD2, and TARG1 contain a macrodomain, responsible for binding and removing acidic amino acid-linked mono-ADP-ribose from target proteins. MacroD1 is localized to mitochondria, whereas MacroD2 and TARG1 are both in the nucleus and the cytoplasm. Mutant, non-mitochondrial MacroD1, MacroD2, and TARG1 can recruit to DNA damage sites in response to laser micro-irradiation (Jankevicius et al., 2013; Sharifi et al., 2013). It is not clear if these glycohydrolases perform non-redundant functions in cells (Feijs et al., 2013c). An *in vitro* MARYlated peptide binding assay revealed that of catalytically inactive MacroD2 and TARG1, only TARG1 shows specificity for the amino acid sequence surrounding the ADP-ribosylated site. This indicates that TARG1 might bind distinct sets of proteins, whereas MacroD2 might tolerate a more diverse amino acid sequence context and might therefore tolerate a broader range of target proteins (Kistemaker et al., 2016).

Not much is known regarding the cellular function of MacroD2. MacroD2 was shown to activate GSK-3 β , an important component of Wnt signaling, by removing inhibitory mono-ADP-ribose (Rosenthal et al., 2013).

The possible involvement of MacroD2 and TARG1 in the response to DNA damage is discussed in further detail below. Upon DNA damage - induction of DNA double strand breaks - the unstructured C-terminal domain of MacroD2 is phosphorylated by ATM at two SQ motives and MacroD2 is subsequently exported from the nucleus into the cytoplasm in a PARYlating PARP independent manner. Export of MacroD2 correlates with decreased presence at DNA damage sites. This might indicate that the export of MacroD2 regulates the ADP-ribosylation status of proteins recruited to DNA damage sites (Golia et al., 2017). This indicates that MacroD2 is involved in the response to DNA damage, we do however not know yet, if MacroD2 is involved in other cellular responses and signaling pathways, especially in unstressed cells. TARG1 was shown to recruit to DNA damage sites as well and was shown to be important for DNA repair since cells depleted of TARG1 show increased sensitivity to DNA damage induced by hydrogen peroxide and methyl methanosulfonate (Sharifi et al., 2013). Furthermore, both MacroD2 and TARG1 were shown to de-ADP-ribosylate PARP10, which is involved in DNA damage (Jankevicius et al., 2013; Sharifi et al., 2013). These findings strongly suggest that both MacroD2 and TARG1 are involved in the response to DNA damage.

Apart from its potential function in the DNA damage response, MacroD2 might be connected to human cancers based on findings in several studies. MacroD2 overexpression was detected in two of five patients with tamoxifen resistant breast cancer and mediates tamoxifen resistance in two breast cancer cell lines. Depletion of MacroD2 in breast cancer cell lines resulted in reduced tumor load in xenographs. It was additionally shown that patients with at least two-fold MacroD2 overexpression in the cancer genome atlas breast cancer database showed worse survival rates (Mohseni et al., 2014). Additionally, several independent studies correlated MacroD2 with colorectal cancer. In one study fifteen colo-

rectal cancer cell lines were analyzed for frequent gains and losses. MacroD2 was frequently lost in half of the colorectal cancer cell lines (Briffa et al., 2015). In another study, chromosomal breakpoints in 352 primary advanced colorectal cancer samples were determined. MacroD2 had the highest prevalence of chromosomal breaks (41%) (van den Broek et al., 2015). In DNA copy number analyses of more than one thousand cancer cell lines from ten tumor types, MacroD2 showed focal deletions. They found that the MacroD2 gene represents a common fragile site in colorectal cancer (Rajaram et al., 2013). Another study identified MacroD2 as a focal deletion site and postulates that focal deletions in cancer cells result from replicate stress (Dereli-Öz et al., 2011).

Apart from functions in DNA damage response and a potential role of MacroD2 in cancer, MacroD2 and TARG1 are connected in literature to neurological disorders. TARG1 was found to be homozygously mutated in patients with severe neurodegeneration (Sharifi et al., 2013). The deletion of MacroD2 was shown in a patient with Kabuki syndrome, which entails mental retardation (Maas et al., 2007). It has been shown and debated whether defects in MacroD2 lead to neurological disorders such as familial schizophrenia (Xu et al., 2009), autism-like traits (Anney et al., 2010; Frye et al., 2016; Jones et al., 2014), and genetic generalized epilepsy (Mefford, 2016), stroke (Debette et al., 2010), and multiple sclerosis (Baranzini et al., 2009). Small nucleotide polymorphisms (SNPs) in the locus of MacroD2 were found to influence temporal lobe volume (Kohannim et al., 2012).

In summary, MacroD2 and TARG1 are involved in the response to DNA damage and neuronal disorders. MacroD2 was additionally shown to be involved in breast and colorectal cancer in several studies. This indicates that both MacroD2 and TARG1 are important for the health of human cells.

1.5 Actin Structure and Functions

ADP-ribosylation has many indispensable functions in human cells and was shown to be involved in the regulation of the actin cytoskeleton. Firstly, actin can be ADP-ribosylated at arginine residues by botulinum toxin and was found to be ADP-ribosylated in chicken (Heine et al., 2008; Terashima et al., 1995). Secondly, it was shown that PARP1 inhibition results in a block of actin rearrangement (Rom et al., 2015). Thirdly, the knockdown of PARP9 and PARP14 resulted in actin cytoskeletal defects (Vyas et al., 2013). Lastly, downregulation of PARP1 and PARP9 led to decreased cell migration (Aguiar et al., 2000; Cavone et al., 2011; Rodríguez et al., 2013; Ullrich et al., 2001). To understand how ADP-ribosylation influences the actin cytoskeleton, it is important to address the functions and the structures of actin.

Actin is a versatile player in human cells and is involved in a plethora of pathways. Actin transitions between two forms: the globular G-form and the filamentous F-form. Both forms exist in the nucleus and the cytoplasm. The transition from one form to the other is regulated by a multitude of cellular proteins, most prominently actin-binding proteins (ABPs), and results in regulated actin dynamics (for review see ref. (Dominguez and Holmes, 2011)). Actin filaments can form sophisticated structures such as cross-linked networks,

bundles, and contractile structures, which are very important for cell and nuclear shape as well as cell motility (Blanchoin et al., 2014; Dominguez and Holmes, 2011; Revenu et al., 2004) although it became clear in recent years that actin has important functions apart from the aforementioned. It is an important part of some chromatin remodeler complexes such as INO80, TIP60 and BAF. Furthermore, nuclear actin is involved in gene expression, i.e., its binding to all classes of RNA polymerases is required for their activity (Kapoor and Shen, 2014). Additionally, it was shown that actin is involved in efficient DNA repair (Belin et al., 2015). Chromatin structure, gene expression and DNA repair are also connected to ADP-ribosylation.

In the following paragraphs I want to discuss some actin-regulated processes - cell attachment and migration - since they are connected to ADP-ribosylation in the literature (Aguiar et al., 2000; Cavone et al., 2011; Rodríguez et al., 2013; Ullrich et al., 2001; Vyas et al., 2013) and will be connected to the cellular function of MacroD2 and TARG1 in this thesis. Cell migration is important for a multitude of cellular processes and its deregulation can result in various diseases. It is important in, e.g., neural development, immune response, and wound healing. Misregulation of cell migration and attachment is involved in cancer metastasis and various vascular and inflammatory diseases (Gardel et al., 2010). In order for cells to attach to any kind of surface the cells need to be able to produce focal adhesions. For cell attachment, small nascent adhesions mature through focal complexes to focal adhesions. These steps coincide with increased tension from the cell to the surface. Focal adhesions consist of many different focal adhesion proteins such as vinculin and zyxin (Blanchoin et al., 2014; Dominguez and Holmes, 2011; Gardel et al., 2010; Revenu et al., 2004), both of which were identified in this thesis as MacroD2 interactors.

Cell migration depends on the ability of actin and focal adhesions to generate directional forces. The structure of the F-actin networks and their dynamics, required for cell migration, is tightly regulated by signaling molecules and effectors (Blanchoin et al., 2014; Gardel et al., 2010; Magi et al., 2012), such as EGFR signaling in human, mouse, and *Drosophila* border cells (Jékely et al., 2005; Lauand et al., 2013; Yamaoka et al., 2011).

Apart from actin's function in migration in general, it is necessary for directed migration as well. Chemotaxis is the ability of cells to sense environmental cues, so-called chemoattractants, and to induce migration in the direction of the highest concentration of this cue. It is essential for a multitude of processes such as neuron migration during nervous system development and immune cell migration to chase their bait (inflammation or infection signals) (Wang, 2009).

Since MacroD2 and TARG1 are connected to neuronal defects (Anney et al., 2010; Baranzini et al., 2009; Debette et al., 2010; Frye et al., 2016; Jones et al., 2014; Kohannim et al., 2012; Maas et al., 2007; Mefford, 2016; Sharifi et al., 2013) and proper neuronal development depends on directed cell migration (Cooper, 2013), I will introduce directed cell migration, also known as chemotaxis, in the following paragraphs. Chemotaxis requires that the cell recognizes the chemotactic cue, e.g. chemokines or growth factors, such as epidermal growth factor (EGF), and starts a signal cascade leading to actin cytoskeletal remodeling (Roussos et al., 2011; Van Haastert and Devreotes, 2004; Wang, 2009). It usually refers to cells sensing a chemoattractant gradient but cells can also increase mi-

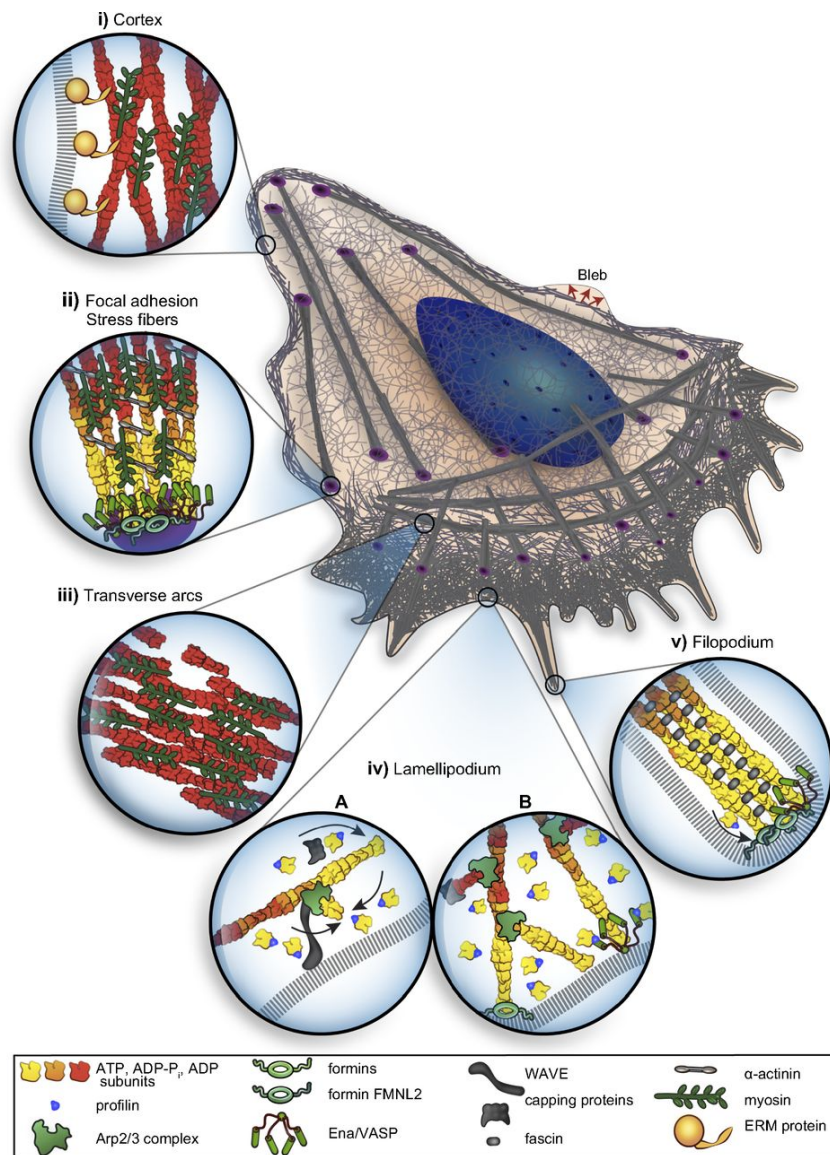


Figure 1.6: Overview of actin networks in moving cells. Moving cells have distinct actin organizations throughout the cell. From (Blanchoin et al., 2014). Permission for reprint was granted.

gration speed in response to a uniform chemoattractant distribution. One theory why cells react to uniform chemoattractant distribution is that cells generate their own gradients by degrading chemoattractants locally (Tweedy et al., 2016). Many different cancer cell types use chemotactic pathways for increased cell motility and invasiveness and use chemotactic cues, particularly secretion of chemokines, to shape the tumor micro-environment to be more metastatic (Roussos et al., 2011). Alterations of growth factors during embryogenesis were shown to lead to neuronal defects such as attention-deficit/hyperactivity disorder (ADHS) and autism spectrum disorders (ASD).

As the heterozygous deletion of MacroD2 was also associated with ASD (Frye et al., 2016), it is tempting to speculate that the regulation of cell migration through ADP-ribosylation underlies the many observed connections from MacroD2 and TARG1 deficiencies and neuronal defects.

1.6 EGFR signaling

In order to better understand directed cell migration, it is important to understand the cues which start this process. Cues resulting in directed cell migration are often growth factors binding to growth factor receptors, which in turn regulate the actin skeleton to allow migration. Therefore, it is important to understand how one of the major growth factor receptor signaling pathways works in human cells.

The epidermal growth factor receptor (EGFR) is the founding member of the ErbB family of single pass transmembrane-receptor tyrosine kinases. Apart from EGFR, which is also known as ErbB1/Her1, the family consists of three additional members. ErbB receptors can homo- and heterodimerize with each other, resulting in many different combinations. ErbB receptors are well known as proto-oncogenes since they promote pro-oncogenic cellular processes such as proliferation, motility, attachment, and many more. EGFR is commonly upregulated in a vast number of cancers (for review see ref. (Brand et al., 2013; Lo and Hung, 2006)), including colorectal cancer which is connected to MacroD2 in literature (Briffa et al., 2015; van den Broek et al., 2015). It was shown that many types of cancer contain EGFR in their nucleus and that this is connected to tumor proliferation and progression. Moreover, nuclear EGFR was linked to resistance to cancer therapeutics (for review see ref. (Brand et al., 2013; Lo and Hung, 2006)).

Connections between ADP-ribosylation and EGFR signaling were published and seem to be clinically relevant to cancer therapy. Inhibition of both EGFR and PARP1/PARP2 in triple negative breast cancer cells (breast cancer cells lacking estrogen receptor, progesterone receptor, and EGFR) resulted in delayed growth *in vivo* due to decreased DNA double strand break repair (Nowsheen et al., 2012). EGFR activating mutations in lung cancer patients were sensitive to PARP inhibition with an inhibitor targeting PARylating PARPs (Olaparib) (Pfäffle et al., 2013). PARP inhibition was shown to suppress the growth of EGFR mutant lung cancer and glioblastoma cells by suppressing pyruvate kinase isoform M2 (PKM2) nuclear retention. PKM2 translocates to the nucleus in a PAR-dependent manner where it promotes tumor growth and proliferation (Li et al., 2016). EGFR activation through EGF binding prior to radiation treatment induces PARP1 activity and results in decreased cell survival upon radiation in two prostate carcinoma cell lines (Hagan et al., 2007).

The relevance of EGFR to cancer therapy might stem from an emerging theme in EGFR research where EGFR is connected to DNA damage signaling. One study reports that nuclear EGFR phosphorylates PCNA resulting in increased chromatin binding of PCNA and increased DNA repair (Birge et al., 1992). It was also shown that radiation-induced DNA damage results in the activation of EGFR and subsequent nuclear transport

in caveolin-containing vesicles. Nuclear EGFR directly phosphorylates DNA-PK resulting in increased DNA repair. In this study the activation and nuclear transport of EGFR depends on Src activity (Dittmann et al., 2008). Both studies show the interesting connection of nuclear EGFR signaling with DNA repair, which is the first identified function of PARP enzymes and provides another link between EGFR signaling and ADP-ribosylation.

In summary, EGFR is a known proto-oncogene involved in a multitude of human cancers and seems to be intertwined with ADP-ribosylation.

In the following paragraph, I will give a general introduction into EGFR signaling and signal outputs which will be relevant for my results. Upon stimulation with activators/growth factors or upon stress induction, EGFR dimerizes and transphosphorylates itself in the C-terminal tail. Phosphorylated EGFR starts a wide range of signal cascades and results in the expression of target genes, many of which are connected to cellular proliferation. This leads to global and complex changes in human cells (Tan et al., 2016; Wee and Wang, 2017). EGFR activates the MAPK, PI3K-Akt, SRC, PLC, and JAK-STAT pathways (figure 1.7). All of these pathways are interlinked and have various feedback loops, giving rise to a whole EGFR signaling network (Oda et al., 2005).

EGF activation was shown to result in receptor poly-ubiquitination in the kinase domain of EGFR (Huang et al., 2006; Tong et al., 2014). Ubiquitinated EGFR is internalized in endosomes (clathrin-dependent and -independent) and stays active upon endocytosis while interacting with some adapter proteins such as Shc and Eps8 (Burke et al., 2001). Active EGFR internalization in clathrin-coated pits depends on the interaction of EGFR with EPS15, which in turn interacts with the clathrin adaptor protein 2 (AP2) (Benmerah et al., 1998; Carbone et al., 1997; van Delft et al., 1997). From endosomes, EGFR is recycled back to the plasma membrane or transported to lysosomes and subsequently degraded.

EGFR can be transported in vesicles from the endosomes to the Golgi apparatus where retrograde transport to the ER is mediated by coat-protein complex I (COPI). The transport into the ER is mediated by EGFR-Sec61 association (Liao and Carpenter, 2007). The nuclear localization signal in EGFR mediates the nuclear transport through the nuclear pore complex by binding to importin- $\alpha 1\beta 1$ and nucleoporin (Lo et al., 2006). EGFR functions as a co-transcription factor for several genes in the nucleus (figure 1.7) (Brand et al., 2011; Wee and Wang, 2017). Nuclear EGFR promotes cell cycle progression by co-regulating the expression of cyclooxygenase-2 (Coffey et al., 1997), cyclin D1 (Lin et al., 2001), iNOS (Lo et al., 2005), c-myc (Jaganathan et al., 2011), and Aurora-A (Hung et al., 2008). Furthermore, it was shown that the co-transcriptional activity of nuclear EGFR is SUMO1 dependent (Packham et al., 2015).

EGFR signaling triggers cell migration and actin reorganization. However, studies show that actin influences EGFR internalization creating an interesting feedback loop between actin and EGFR. Dynamic actin filaments are necessary for endosomal sorting of EGFR (Ohashi et al., 2011). EGF treatment induces co-localization of F-actin with EGFR and induces actin polymerization (Rijken et al., 1991). The interaction between actin and EGFR diminishes EGFR activation by autophosphorylation *in vitro* (Tang and Gross, 2003).

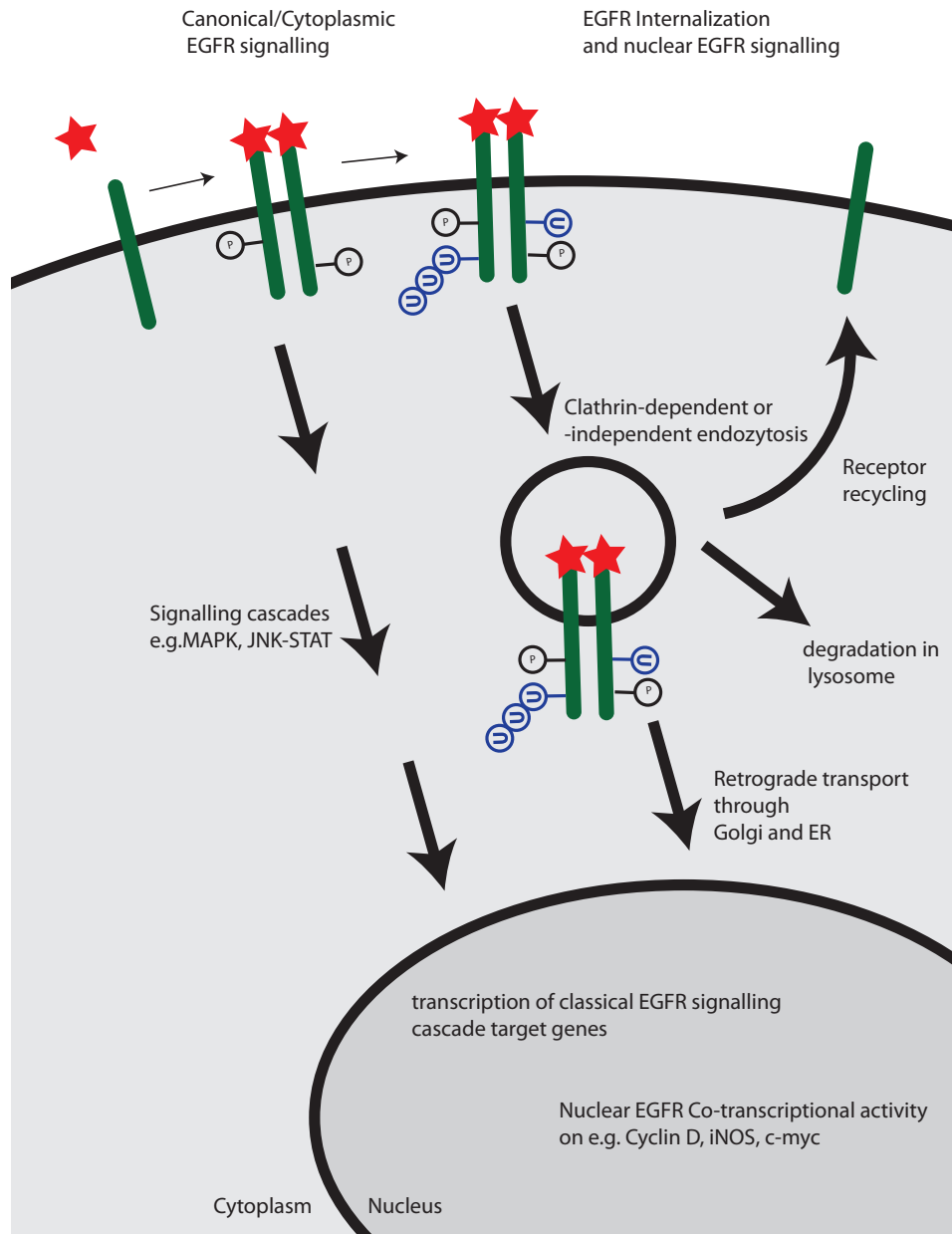


Figure 1.7: Scheme of EGFR signaling. EGF (red star) activates EGFR (green). EGFR heterodimerizes and autophosphorylates (p) itself. Phosphorylated EGFR can start many canonical downstream signaling cascades. Upon ubiquitination (u) EGFR gets internalized in vesicles. EGFR containing vesicles can be recycled back to the plasma membrane, degraded in lysosomes or transported via Golgi and ER to the nucleus. Nuclear EGFR functions as a co-transcription factor in the expression of target genes such as c-myc. Adapted from (Brand et al., 2011; Haglund and Dikic, 2012; Lo and Hung, 2006; Madhus and Stang, 2009)

In summary, EGFR signaling is a network that is tightly regulated by at least three PTMs: phosphorylation, ubiquitination, and SUMOylation (Packham et al., 2015; Tong et al., 2014) and is most likely linked to ADP-ribosylation as well. EGFR activation results in major cellular changes, such as actin-dependent cell migration, DNA repair and proliferation.

Chapter 2

Aims of this Thesis

ADP-ribosylation is a very dynamic post-translational modification of target proteins. Although the most studied Poly-ADP-ribose polymerases (PARPs) add multiple units of ADP-ribose onto target proteins, the majority of PARP family members were shown to only add a single ADP-ribose moiety to target proteins, leading to mono-ADP-ribosylated or MA-Rylated proteins. ADP-ribosylation poses an exciting mechanism for cells to regulate functional outputs of a plethora of proteins. Cellular pathways regulated by ADP-ribosylation are, among others, the response to DNA damage, cellular motility and metabolism.

So far it is not known what cellular function the removal of mono-ADP-ribose from proteins has. Three enzymes responsible for the removal of mono-ADP-ribose from acidic amino acids of target proteins, MacroD1, MacroD2, and TARG1 were identified. While MacroD1 is mitochondrial, both MacroD2 and TARG1 are nuclear and cytoplasmic.

MacroD2 and TARG1 possess the same enzymatic function in human cells and are localized to the same cellular compartments. However, it is not known if they have the same cellular functions and regulate the same pathways.

This thesis is broken down into two main aims to deduce the cellular function of MacroD2 and TARG1 in unstressed human cells.

2.1 Aim I: Deduce cellular function of MacroD2 by its interactors

In order to address the cellular function of MacroD2 in unstressed cells I wanted to identify its interaction partners. In order to do that I chose the BioID system - a method established to detect transient and weak interactions through biotinylation of proteins in close proximity to MacroD2 with BirA, a biotin ligase. The addition and removal of mono-ADP-ribose to and from proteins is transient and BioID was designed especially for detecting this type of interaction. Furthermore, since the labeling of interactors is done *in vivo* and based on the very strong interaction between biotin (the labeling agent) and streptavidin, very harsh washing conditions can be used, which in collaboration with a small labeling radius should result in low background labeling.

For the BioID experimental setup, I decided to establish stable cell lines with inducible expression of the MacroD2-BirA fusion protein. To validate the expression and localization of the fusion protein as well as the biotinylation of target proteins I planned to utilize immunofluorescence experiments and western blotting. These methods should show if the fusion protein was localized correctly, and if it was expressed and biotinylates other proteins in my chosen cell system. After validating BioID in my chosen cell system, I planned to perform pulldowns of biotinylated target proteins with streptavidin beads and perform on-bead digestion with mass spectrometry. To validate the mass spectroscopy results, I aimed to generate intensity plots of MacroD2 and endogenously biotinylated proteins. Since MacroD2 is the most proximal protein to BirA and should therefore be highly biotinylated, MacroD2 should be one of the proteins detected most frequently in mass spectrometry in samples expressing MacroD2-BirA. Furthermore, intensity plots of endogenously biotinylated proteins should show that these are present in equal amount throughout all utilized cell lines and replicates. Overall, using the BioID system should enable me to deduce cellular pathways regulated by MacroD2 in an unbiased approach.

2.2 Aim II: Identify the cellular function of MacroD2 and TARG1 by their loss-of-function phenotypes

The second aim was to identify the function of MacroD2 and TARG1 by their loss of function phenotypes. Loss-of-function phenotypes result from the disturbance of cellular functions in the absence of one or more proteins of interest, in my thesis MacroD2 and TARG1. In order to achieve this, I aimed to generate MacroD2, TARG1, and MacroD2/TARG1 double knockout cell lines with the CRISPR/Cas system in human U2OS cells. I chose to validate all cell lines at protein and DNA level with western blotting and genotyping. I wanted to use these cell lines to investigate possible phenotypes suggested by the BioID interactors. Due to the results of the BioID experiments I chose to investigate all cell lines lacking MacroD2 and/or TARG1 for defects in their actin and focal adhesion structure and localization, defects in actin-regulated processes (such as cell attachment and cell migration), and EGFR signaling defects.

Chapter 3

Results

MacroD2 and TARG1 are enzymes removing acidic amino acid-linked protein proximal ADP-ribose units from target proteins. Both enzymes are localized to the nucleus and cytoplasm. Not much is known about the cellular functions of both enzymes and whether they possess redundant functions in human cells (for review see ref. (Barkauskaite et al., 2013; Feijs et al., 2013c)). The aim of my thesis was to identify what cellular functions MacroD2 and TARG1 possess in unstressed human cells. I planned to address the cellular functions of both enzymes by their loss-of-function phenotypes and investigated possible functions and deregulated pathways based on interaction partners of MacroD2 identified with the BioID approach.

3.1 Identifying the Biological Function of MacroD2 by its Interaction Partners with BioID

3.1.1 BioID Validation

The cellular functions of MacroD2 are still mainly unknown, the only exception being MacroD2's recruitment to sites of DNA damage and subsequent export from the nucleus in a matter of minutes (Golia et al., 2017). To investigate possible roles of MacroD2 in untreated cells, I chose to identify protein interaction partners. Identified interactors falling into specific GO-terms indicate possible functions for MacroD2. To that end, I used the BioID system because ADP-ribosylation is a very dynamic post-translational modification (PTM) and BioID was designed to identify weak and transient protein-protein interaction partners. BioID relies on the promiscuous biotin ligase BirA from *E. coli* to biotinylate proteins in close proximity (approximately 10 nm) to fusion proteins *in vivo* (Kim et al., 2014; Roux et al., 2012). *In vivo* biotinylated proteins are isolated from cells, denatured and subsequently precipitated on streptavidin beads under harsh washing conditions to ensure minimal unspecific protein detection. Bound proteins are trypsin-digested and identified by mass spectrometry (figure 3.1). Since this method does not rely on the continuous interaction between interacting target proteins and MacroD2 throughout the whole pulldown

but rather on the tight interaction between biotin and streptavidin, interaction partners are retained even in harsh washing steps. Another advantage of this approach is that it only enriches proteins which are very close (10 nm) to the fusion protein *in vivo* instead of entire protein complexes. This, in combination with harsh washing conditions, increases the chance of identifying direct over indirect interactors compared to conventional pulldowns (Kim et al., 2014; Roux et al., 2012).

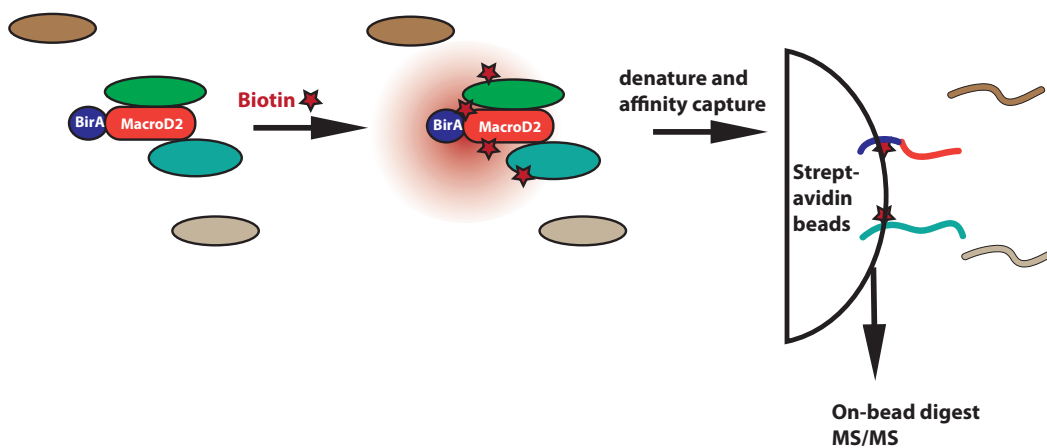


Figure 3.1: Schematic representation of BioID proximity ligation. MacroD2 is fused to BirA, a promiscuous biotin ligase. Upon biotin addition to the cell media, proteins in close proximity to the fusion protein (bait) (10 nm) get biotinylated *in vivo*. Cells are then lysed and denatured. Denatured proteins are captured by streptavidin beads which allows for very harsh washing conditions. Captured proteins are subjected to on-bead tryptic digest and analyzed with mass spectrometry. Adapted from (Kim et al., 2014; Roux et al., 2012)

For the BioID experiments, I generated stable cell lines with inducible expression of the MacroD2 fusion proteins for the BioID experiments. I chose HEK Trex cells since the integration of plasmids into their genome can be accomplished with flippase which results in integration of the plasmids at the same site in the cells' genome. This leads to more comparable expression of different integrated constructs between different cell lines. Additionally, HEK Trex cells allow for inducible expression of the MacroD2 fusion proteins at the same time as biotinylation of target proteins via addition of biotin to the medium.

In order to identify MacroD2 interactors and to investigate if both domains of MacroD2 possess distinct functions and therefore interact with distinct sets of proteins in unstressed conditions, as they do under DNA damage condition (Golia et al., 2017), I generated constructs containing full and partial MacroD2. All constructs were either C- or N-terminally tagged with BirA. Constructs with MacroD2 contain either full-length MacroD2 or partial MacroD2 (macrodomain-only or C-terminal domain-only) and were tagged with BirA

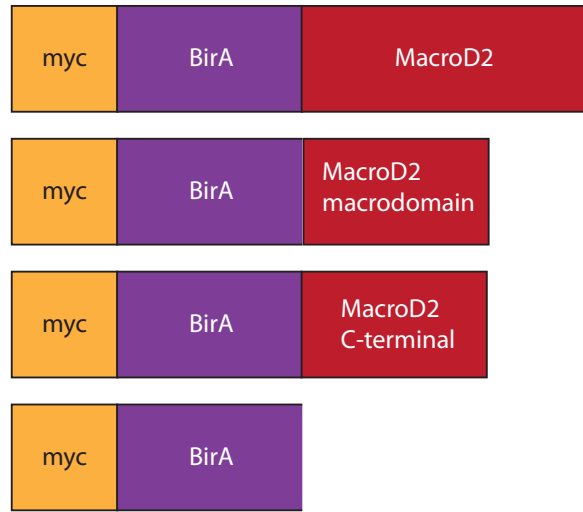


Figure 3.2: Schematic representation of used BioID constructs tagging MacroD2 N-terminally. All constructs are myc tagged and contain the biotin ligase BirA. All but the empty vector control contain MacroD2 fully or partially.

and a widely used tag - myc in N-terminally tagged constructs or hemagglutinin (HA) in C-terminally tagged constructs - for easy detection with antibodies. The empty vector control (EVC) contains only the biotin ligase BirA and the tag. N-terminally tagged constructs are depicted in figure 3.2. C-terminal constructs are mirror images of N-terminal constructs, with myc being replaced by HA, e.g. MacroD2 full-length constructs contain MacroD2 C-terminally tagged with BirA, C-terminally tagged with HA.

I generated HEK Trex cells with all genome-integrated constructs as described above. Cell lines were incubated for 24 hours with both doxycyclin to induce expression of the fusion proteins as well as biotin to induce biotinylation of target proteins by BirA, as suggested in the original literature (Roux et al., 2012). After incubation for 24 hours, I examined the fusion protein expression and biotinylation of target proteins in cell lines expressing C- and N-terminally tagged full-length MacroD2 and compared them to their respective empty vector controls to address if the fusion proteins are expressed and can tag interaction partners. To this end, I lysed the cells and performed pulldowns with magnetic streptavidin beads and detected biotinylated proteins using streptavidin-HRP of the input, unbound, and pulldown fractions on western blot (figure 3.3, see section 5.16 in the Methods chapter).

In order to show that the biotin-streptavidin pulldowns work in the chosen harsh conditions, endogenously biotinylated proteins can be used as a proxy for all biotinylated proteins. Their presence and signal strength was analyzed in all fractions (input, unbound, and pulldown) in all used cell lines. Endogenously biotinylated proteins - pyruvate carboxylase at 130 kDa, acetyl-CoA carboxylase at 265 kDa, propionyl-CoA carboxylase at 80 kDa, and methylcrotonyl-CoA carboxylase at 81 kDa - are mitochondrially expressed

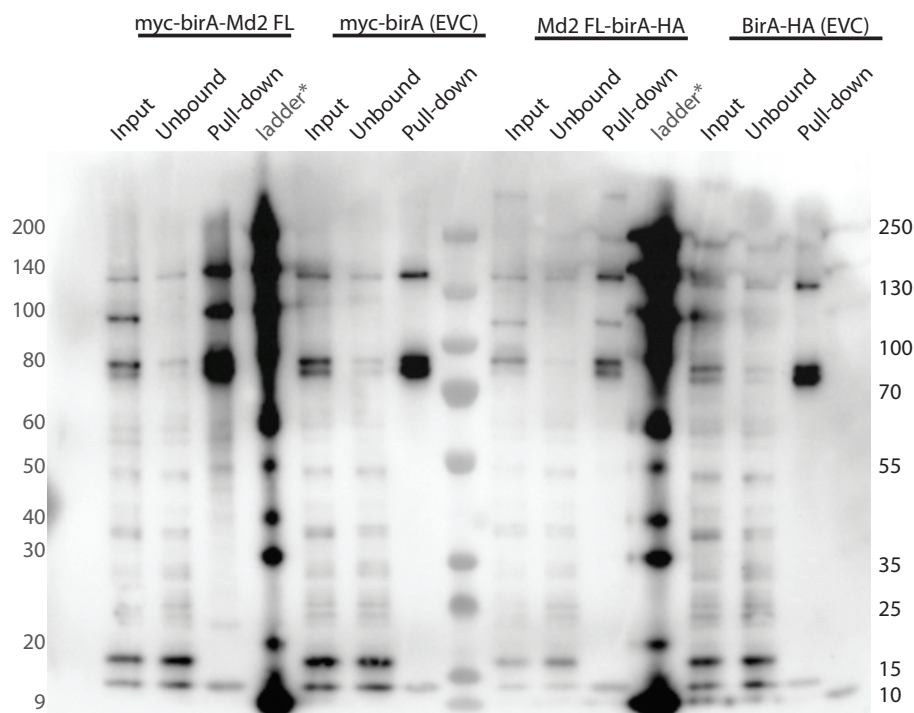


Figure 3.3: N-terminally tagged MacroD2 fusion protein biotinylates itself and interactors well, while the C-terminally tagged MacroD2 fusion protein does not biotinylate itself or interactors well. Pulldown of C- and N-terminally BirA-tagged MacroD2 full-length and corresponding empty vector control is depicted. Fractions of cells expressing N-terminally tagged MacroD2 are labeled with myc-BirA-Md2 FL, fractions expressing the corresponding empty vector control with myc-BirA. Fractions with C-terminally tagged MacroD2 are labeled Md2 FL-BirA-HA and the corresponding empty vector control birA-HA. Expression of constructs was induced with doxycyclin and biotinylation of interaction partners was induced with biotin. 20 μ L of each fraction, input (of 4.8 mL total sample), unbound (of 4.8 mL total sample) and pulldown (of 1.5 mL total sample), were loaded. Biotinylated proteins were detected with streptavidin-HRP. Left band size is for biotinylated protein ladder in kDa, right for prestained protein ladder (middle) in kDa.

proteins present in all input samples (line1, 5, 9, 13) of the streptavidin western blot (figure 3.3). They are visible as strong bands at 130 kDa and as a double band at 80 kDa. When comparing input with pulldown fractions, their signal strength is increased in pulldown samples. This indicates that pulldowns of biotinylated proteins are successful in the chosen conditions *per se*.

To address if BirA works in C- and N-terminally tagged MacroD2 constructs, i.e. if it biotinylates the fusion protein and proteins in close proximity, the extent of self-biotinylation of the MacroD2 fusion proteins can be assessed. MacroD2 should be the most biotinylated protein in the cell lysate, since it is the most proximal protein to itself. In fi-

figure 3.3 the C- and N-terminally tagged MacroD2-BirA fusion proteins both run at about 100 kDa. MacroD2 fusion proteins can only be detected in fractions of cells expressing MacroD2 (lane 1-3 and 9-11) but not in any fractions of the empty vector controls (lane 5-7 and 13-15). This indicates that the expression and self-biotinylation of C- and N-terminal fusion proteins is successful in cell lines expressing them.

Next I wanted to address if there are differences in biotinylation strength between C- and N-terminally tagged constructs. To this end, I compared N-terminally tagged MacroD2 (lane 1-3) and C-terminally tagged MacroD2 (lane 9-11) in all fractions. It becomes clear that the abundance of the MacroD2 fusion protein running at 100 kDa is increased in the pulldown fraction over the input fraction for N-terminal tagged MacroD2 (compare lane 1 to lane 3). This indicates that the pulldown of N-terminally tagged MacroD2 was successful under the chosen conditions.

In C-terminally tagged MacroD2, however, the abundance in the pulldown fraction is comparable to the input fraction (compare lane 9 to 11). This indicates that C-terminally tagged MacroD2 could not be isolated from the lysate to the same extent as the N-terminal fusion protein, resulting either from insufficient self-biotinylation of C-terminally tagged MacroD2 or problems in pulldown efficiency. Since endogenously biotinylated proteins could be enriched to some extent, insufficient self-biotinylation is more likely to cause this problem.

Next it is important to address if interacting proteins are biotinylated and can be isolated in the pulldown in order to identify which proteins interact with MacroD2. To address this issue, it is necessary to compare protein signals that are increased in the pulldown fraction over the input or unbound fraction in cells expressing the fusion proteins. On the other hand, to ensure that these proteins are specific interactors and not randomly biotinylated proteins or proteins binding to beads unspecifically, these proteins need to be present in the pulldown fraction of cells expressing the fusion protein and absent in the pulldown fraction of the empty vector controls.

In the N-terminally tagged MacroD2 pulldown fraction (lane 3) an overall smear of biotinylated proteins is detectable compared to the input and unbound fraction (lanes 1-2). Additionally, there were several distinct bands not present in the unbound or input fraction running at 50 kDa, faint bands around 45, 40, and 25 kDa (figure 3.3; as described in methods section 5.16). This indicates that proteins in close proximity to the N-terminally tagged MacroD2 fusion protein are biotinylated and could be isolated with the streptavidin pulldown. To address if these proteins are specific, one has to compare the pulldown fraction of the cell line expressing N-terminally tagged MacroD2 (lane 3) over the respective pulldown fraction of the empty vector control (lane 7). The only bands visible in the pulldown fraction of the empty vector control are the endogenously biotinylated proteins (130 and 80 kDa) and one band running at 10-15 kDa which is present in all fractions. This indicates that the bands in the pulldown fraction of cells expressing N-terminally tagged MacroD2 are specific.

The pulldown of the C-terminally tagged MacroD2 fusion protein expressing cell line (lane 11) does not show any distinct bands apart from the endogenously biotinylated proteins (130 and 80 kDa), the fusion protein (100 kDa) and the band at 10-15 kDa

present in all fractions. Additionally, very little biotinylated proteins are present in the pulldown fraction in general. This indicates that no or very little interactors of MacroD2 could be biotinylated or isolated with the streptavidin pulldown.

In summary, the N-terminally tagged MacroD2 fusion protein biotinylates itself and interactors well and biotinylated proteins could be isolated in the pulldown fraction. This is not the case for the C-terminally tagged MacroD2 fusion. Furthermore, all previous studies from our laboratory were using N-terminally GFP-tagged MacroD2 constructs to show the recruitment and export of MacroD2 (Golia et al., 2017; Jankevicius et al., 2013). Since N-terminally tagged MacroD2 constructs performed better in the pulldown assay and to ensure comparability to previous studies from our laboratory, only N-terminally tagged constructs were used for further experiments.

Apart from validating the expression of the fusion protein (detected with the myc-tag) and the biotinylation of itself and its interaction partners (detected via biotin), it is important to ensure that the fusion protein and its interactors are localized to the appropriate cellular compartments. Improper location of the fusion protein would result in the identification of false interaction partners.

To this end, I performed immunofluorescence experiments (figure 3.4) staining the fusion protein with an anti-myc antibody, biotinylated proteins representing interactors with streptavidin Alexa-568, and nuclei with Hoechst. The localization was compared to known localization patterns of GFP-tagged MacroD2 and its partial fragments. The GFP-tagged MacroD2 constructs with MacroD2 full-length, macrodomain-only, and C-terminal domain-only were analyzed in our laboratory in previous studies (Golia et al., 2017). The GFP-tagged MacroD2 full-length showed nuclear and cytoplasmic staining with more intense cytoplasmic staining. The macrodomain-only and the intrinsically unstructured C-terminal domain-only constructs showed equal nuclear and cytoplasmic staining.

All MacroD2 fusion constructs showed the expected localization. MacroD2 full-length localized in the nucleus and the cytoplasm with enhanced cytoplasmic staining. The macrodomain (MD) of MacroD2 as well as the C-terminal domain (CTD) localized to the nucleus and cytoplasm to the same extent. This shows that all fusion proteins follow the expected localization observed with GFP-fusion constructs. The biotin staining representing self-biotinylated MacroD2 and MacroD2 interactors is present in the same locations and nuclear/cytoplasmic ratios as the fusion protein, except for strong staining in punctate clusters close to the nucleus. That signal is in fact the only visible signal in the empty vector control (figure 3.4). The pattern of these punctate clusters resembles the shape and size of mitochondria and might therefore stem from endogenously biotinylated proteins since they are expressed in mitochondria. Since the punctate staining is strong it must stem from highly biotinylated proteins in the cells. In order to assess which biotinylated proteins are abundantly present in cells, the input fraction of the pulldowns can be used. In the empty vector control, the strongest signals stem from endogenously biotinylated proteins. In the input fraction of cells expressing the MacroD2-BirA fusion, endogenously biotinylated proteins are highly biotinylated as well (figure 3.3 lanes 1 and 5). Therefore, the punctate staining cluster most likely represents endogenously biotinylated proteins.

After validating the expression and localization of the fusion proteins as well as the

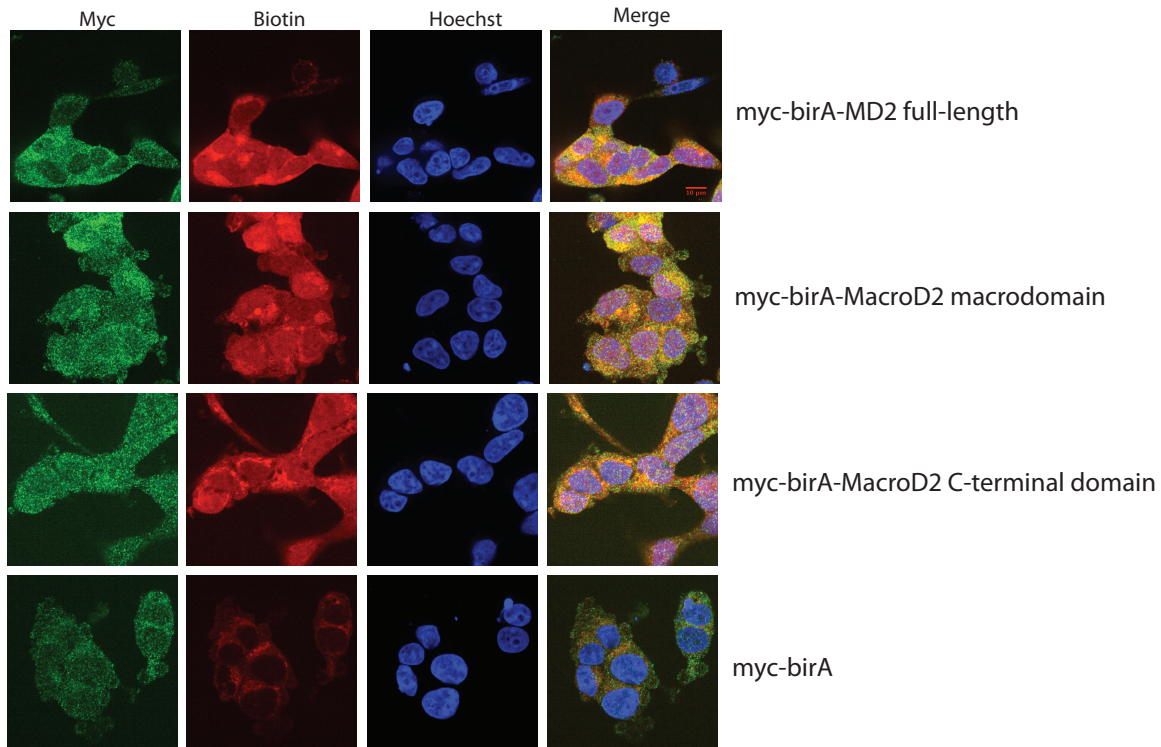


Figure 3.4: All used BioID constructs exhibit the expected localization in human cells. Immunofluorescence experiments of all used cell lines are depicted. The fusion construct was detected with anti-myc antibody and biotinylated proteins were detected with streptavidin-Alexa568. Nuclei were stained with Hoechst. BirA-tagged MacroD2 constructs localize to the nucleus and the cytoplasm in the same manner as GFP-tagged constructs, tested and published from Gyula Timinszkys laboratory (Golia et al., 2017). Scale bar 10 μm

biotinylation of specific interactors and their localization, it remains to assess if the mass spectrometric detection, of those proteins works properly. Mass Spectrometry experiments were performed by Dr. Andreas Schmidt of the Proteomics Core Unit at the LMU. The MacroD2 fusion proteins and endogenously biotinylated proteins can be used as a proxy for all biotinylated proteins in the mass spectrometric detection, since we know from the pulldown that they are the most biotinylated proteins in the lysates (figure 3.3 lane 1). They should therefore be the most abundantly detected proteins.

To validate the mass spectrometric identification of proteins in the biotin pulldowns, I generated intensity plots of endogenously biotinylated proteins (Pyruvat carboxylase, Proprionyl-CoA carboxylase, Methylcrotonyl-CoA carboxylase) in Perseus (figure 3.5A). Intensity plots show the intensity of all proteins as \log_2 -transformed normalized iBAQ values in all used samples. iBAQ values are a measure for protein intensity from label-free quantifications and are calculated as the sum of all identified peptide intensities over all theoretical peptides. Protein intensities of chosen proteins are depicted as red lines.

The intensity plot of endogenously biotinylated proteins shows that they are among the most abundant proteins in all samples, including control samples (HEK Trex cells and empty vector control cells) as depicted in figure 3.5A. This was expected based on the pulldown experiments. Therefore, the pulldown and detection of biotinylated proteins was successful in all used samples of all cell lines.

Since the biotinylation of proteins in the BioID system relies on the distance to the biotin ligase BirA (Kim et al., 2014; Roux et al., 2012) the most biotinylated and enriched protein should be MacroD2 in all samples containing the MacroD2-BirA fusion proteins. In the intensity plot for MacroD2 this is true for all samples with MacroD2 full-length. For the samples expressing partial MacroD2 (macrodomain-only or C-terminal domain-only) this is only partly true since the intensity of MacroD2 in these samples is lower than in full-length MacroD2 samples. The intensity of MacroD2 in samples expressing partial MacroD2 is lower due to the way iBAQ values are calculated. The intensity of MacroD2 in iBAQ values is calculated as the sum of all peptide intensities of MacroD2 over all theoretical peptides identifiable in full-length MacroD2. Since the number of possible peptides is lower in partial MacroD2 than in full-length MacroD2, this artificially dampens the intensity in these samples. In samples expressing partial MacroD2, MacroD2 is within the five most abundantly identified proteins, whereas the control samples only contain low levels of MacroD2 (figure 3.5B). MacroD2 was expected to be present in low abundance in control samples since they do not express a MacroD2-BirA fusion protein.

With endogenously biotinylated proteins and MacroD2 as a proxy for all proteins, I could show that isolated interactors can be detected using mass spectrometry.

In summary, with the pulldown experiments I could show that MacroD2 fusion proteins can biotinylate themselves and interactors. With the immunofluorescence experiments I was able to demonstrate that all constructs are localized as expected and the intensity plots I determined that proteins isolated with the streptavidin pulldown can be detected with mass spectrometry.

3.1.2 Identifying MacroD2 Interactors

To assess which proteins are specifically interacting with MacroD2 it is necessary to determine which proteins were enriched in samples expressing the MacroD2-BirA fusion proteins over the control samples (empty vector control and HEK Trex). To this end, I generated a volcano plot in Perseus of samples expressing MacroD2 full-length over the empty vector control samples. Volcano plots depict each identified protein as a grey square which is localized on the volcano plot according to its difference in iBAQ values between two sample types (x-axis) and the logarithm of their corresponding p-value (y-axis). In this plot, it depicts the difference in iBAQ values of all proteins between samples expressing MacroD2-BirA and samples expressing only BirA, the empty vector control. All proteins significantly enriched in either of the samples are above the cut-off line (black). The cut-off line in Perseus is drawn based on false discovery rate (FDR) calculation for multiple samples (Tyanova et al., 2016) and a minimal fold change (s0 value) between both samples. In other words, proteins significantly enriched in samples containing MacroD2-BirA are

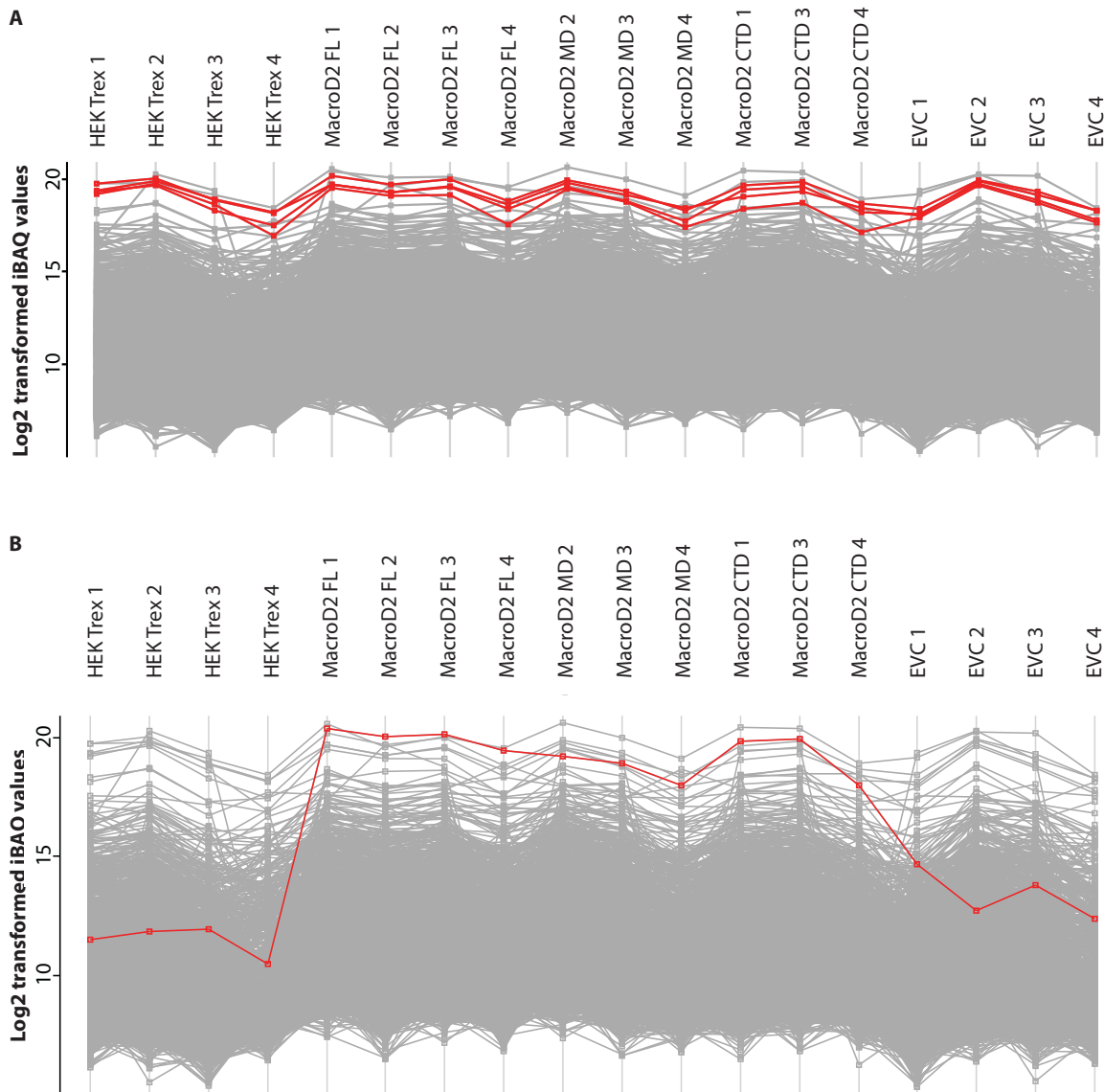


Figure 3.5: The intensity of endogenously biotinylated proteins is comparable in all cell lines and replicates and MacroD2 is within the most intense peaks in all cell lines expressing MacroD2. Intensity plots of all MS/MS samples as log₂-transformed normalized iBAQ values are depicted. (A) Intensity of endogenously biotinylated proteins (red lines) over the intensity of all detected proteins (grey) across all samples. (B) Intensity of MacroD2 (single red line) over the intensity of all detected proteins (grey) across all samples.

located at the upper right section above the cut-off line.

This volcano plot shows that a greater number of identified proteins were enriched in the sample containing the MacroD2 fusion protein (figure 3.6) which can also be seen by

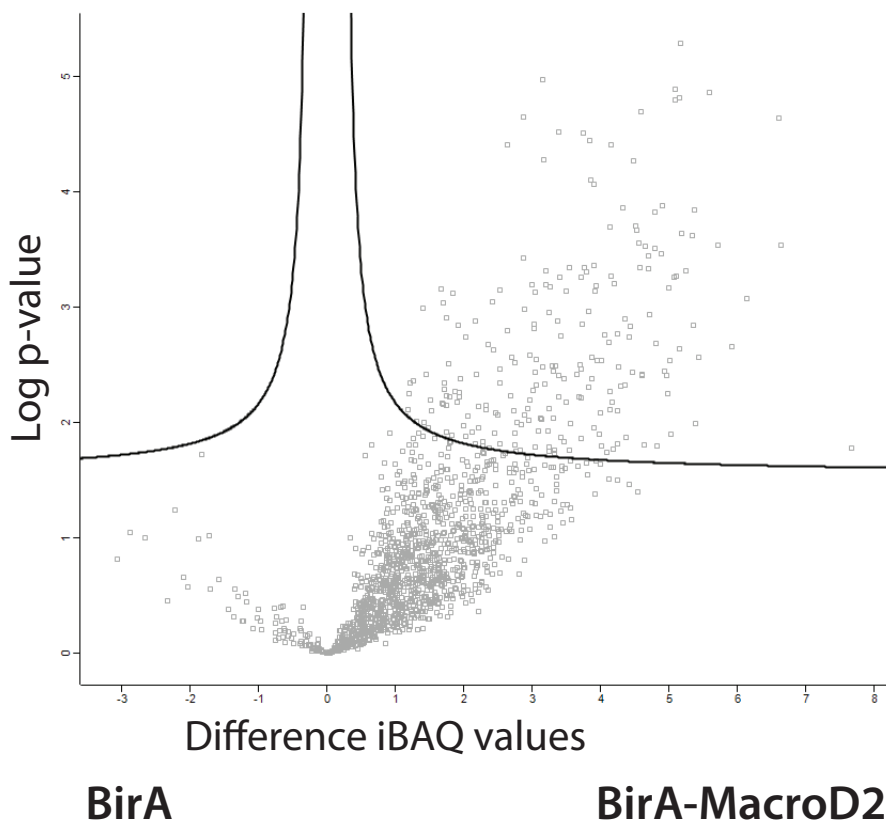


Figure 3.6: In cells expressing BirA-MacroD2, many significantly enriched interactors could be identified over cells expressing BirA only. Volcano plot of samples expressing the MacroD2 full-length fusion protein against the empty vector control is depicted. iBAQ value intensity differences of individual proteins detected are plotted against the logarithm of their p-value. Measurements are indicated as grey boxes. Significantly changed proteins are above the black cut-off line ($s_0=0.1$, $FDR=0.05$). Generated in Perseus (Tyanova et al., 2016).

the maximum difference in iBAQ values of proteins in samples containing the MacroD2 fusion being almost double as high as the difference for proteins in samples of the empty vector control. This serves as an additional quality control for the pulldown efficiency and protein detection by mass spectrometry since we would expect more biotinylated proteins in the samples with the fusion proteins in successful experiments. This correlates with the streptavidin staining in the immunofluorescence experiments (figure 3.4). There, the biotin staining in the empty vector control samples showed very faint staining intensity outside the unspecific staining of endogenously biotinylated proteins observed in mitochondria.

I calculated a second volcano plot of samples containing the MacroD2 fusion proteins, this time over samples of the second control cell line, i.e. HEK Trex cells, in Perseus ($s_0=0.1$,

FDR 0.05). The comparison of interactors over two control cell lines allows for more reliable detection of specific interactors when only those proteins are considered that are enriched over both controls. I calculated a venn diagram of all significantly enriched proteins in MacroD2 full-length samples over samples of HEK Trex as well as all significantly enriched proteins in MacroD2 full-length samples over samples of BirA-only (depicted in figure 3.6) to identify proteins enriched in samples containing the MacroD2-BirA fusion over both control samples.

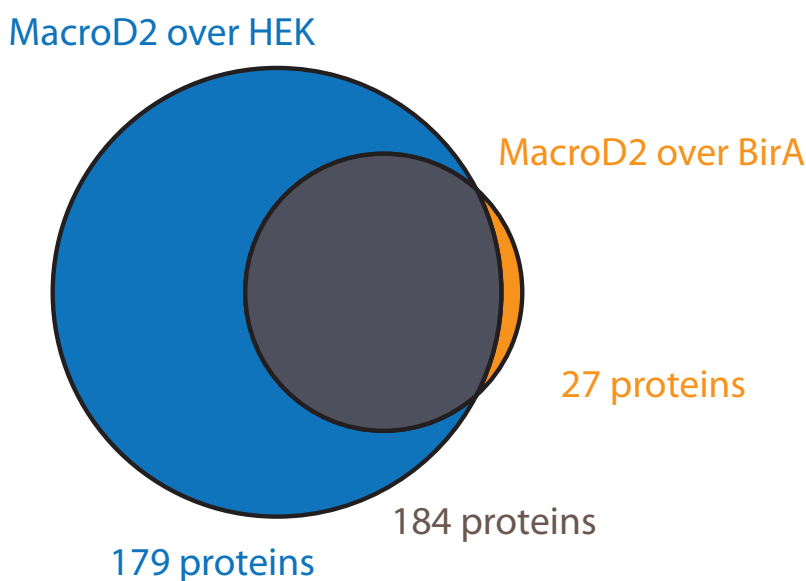


Figure 3.7: 184 proteins are significantly enriched in cells expressing MacroD2-BirA over both controls (BirA only and HEK cells). Venn diagram of significantly enriched proteins in the samples of MacroD2 full-length over samples expressing BirA-only (MacroD2 over BirA) and significantly enriched proteins in the samples of MacroD2 full-length over samples of HEK Trex cells (MacroD2 over HEK). Aubergine colored overlap represents proteins (184) significantly enriched in samples containing MacroD2-BirA fusion over samples from both controls. Proteins only enriched over HEK (179) are depicted in blue, proteins enriched only over BirA (27) are depicted in orange. Significantly enriched proteins over both controls were defined in volcano plots in Perseus. Overlap of significantly enriched proteins over both controls was calculated with Venny2.0 (Oliveros, Juan Carlos, 2007–2015) and redrawn to scale with adobe illustrator

As depicted in figure 3.7, there is a big overlap in proteins enriched over both samples (47 %). Very few proteins enriched over the empty vector control (27; 7 %) were not enriched over HEK Trex samples. There where, however, many proteins enriched in MacroD2-BirA samples over HEK Trex samples which were not enriched in the MacroD2-BirA containing

samples over empty vector control samples. This might stem from the fact that the biotin ligase BirA in the empty vector control randomly biotinylates proteins in close proximity to itself. This background biotinylation would not be present in the HEK Trex cells since they are not expressing BirA at all. Therefore, samples containing MacroD2-BirA fusion proteins would show an enrichment of background biotinylated proteins over samples of HEK Trex cell, but not over samples containing BirA. Proteins randomly biotinylated by BirA would be significantly enriched over HEK Trex cells but do not represent genuine interactors of MacroD2. This is visible in the venn diagram (figure 3.7) since the number of significant enriched proteins in samples containing MacroD2-BirA fusion proteins over samples from HEK Trex is about double the number of significantly enriched proteins over samples containing BirA-only.

To address the question if both domains of MacroD2 - macrodomain and C-terminal domain - interact with distinct sets of proteins in unstressed cells, I compared protein intensities between both samples using a volcano plot. The hypothesis that they might interact with distinct sets of proteins stems from the fact that both domains have distinct functions under DNA damage conditions. The macrodomain of MacroD2 was shown to bind to sites of DNA damage in the nucleus whereas the C-terminal domain of MacroD2 was shown to be phosphorylated by ATM upon DNA damage which leads to nuclear to cytoplasmic transport of MacroD2 (Golia et al., 2017; Jankevicius et al., 2013). However, in untreated cells, the majority of proteins identified in cells expressing only the macrodomain of MacroD2 were also identified in samples of cells expressing only its C-terminal domain, as depicted in the volcano plot A.1. In this plot most proteins had comparable intensities in both samples. Additionally, no proteins were significantly enriched over either one of the samples. The absence of distinct sets of interactors indicates that the individual domains of MacroD2 might not have distinct functions in the absence of DNA damage. Therefore, I decided to focus on the interactors of full-length MacroD2.

In order to explore the function MacroD2 possesses in non-stressed cells, I examined all proteins significantly enriched over both controls (figure 3.7 intersection - aubergine colored, table A.1) and calculated significant GO-term interaction networks using ClueGo, a Cytoscape plugin (Bindea et al., 2009). In the resulting network, proteins belonging to connected GO-terms are clustered together and depicted as colored circles. Related GO-terms are connected according to chance-corrected kappa statistics (determines association strength between GO-terms) and labeled by the parental GO-term. The size of the circle is based on the enrichment significance of the GO-term (Bindea et al., 2009). For MacroD2 full-length, the largest network of GO-terms is related to the actin cytoskeleton - “focal adhesion”, “actin cytoskeleton”, “actin binding”, “actin filament binding”, and “actin filament” (figure 3.8). In addition to actin cytoskeleton related GO-terms, proteins belonging to large GO-term clusters belong to GO-terms related to “microtubule”, “regulation of viral processes”, and “regulation of cell morphology involved in differentiation” (figure 3.8; green, purple and ochre clusters).

In summary, I could show that the BioID system utilized showed robust results for MacroD2 in expression, localization, biotinylation of interactors, pulldowns, and protein identification with mass spectrometry. The most abundant GO-term network for proteins

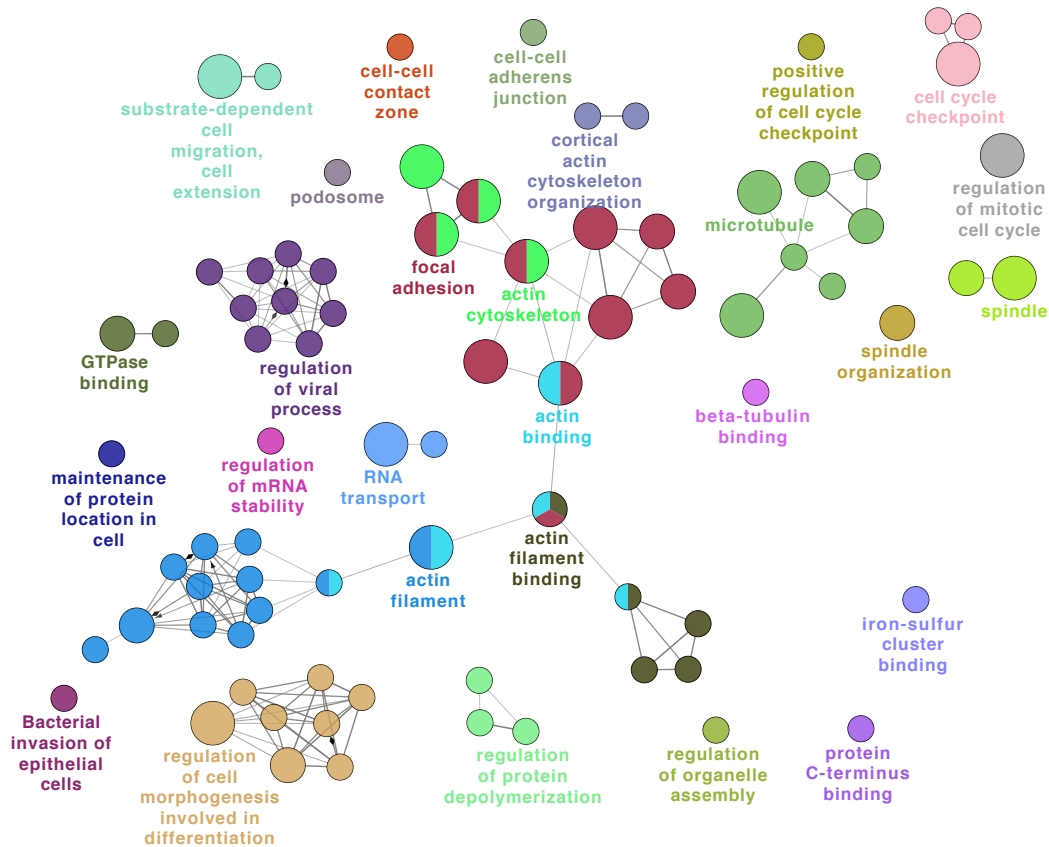


Figure 3.8: Significant MacroD2 interactors form a network of GO-terms with many connections in between GO-terms. Network of significant GO-terms for proteins significantly enriched in MacroD2 full-length over both control cell lines (empty vector control and HEK Trex) is depicted. Figure was generated using the ClueGo plugin for Cytoscape. Significantly enriched GO-terms are depicted as colored circles. Circle size reflects significance of GO-terms (smaller p-Value equals bigger circle). Different circle colors represents different GO-term groups, defined by the most significant GO-term of a color group. Circles are connected based on kappa scores (Bindea et al., 2009).

significantly interacting with MacroD2 full-length identified in this study belongs to the actin cytoskeleton. The next step in order to identify the cellular function of MacroD2 is to use the MacroD2 interactors identified with the BioID system to hypothesize probable loss-of-function phenotypes which can then be investigated in MacroD2, as well as in TARG1 and MacroD2/TARG1 knockout cell lines. Since more than 180 interactors were identified with this approach, we decided to screen for phenotypes connected with the actin cytoskeleton using knockout cell lines instead of validating good candidates individually by e.g. pull-downs.

3.2 Identifying the biological function of MacroD2 and TARG1 through loss-of-function phenotypes

3.2.1 Knockout Cell Line Generation and Validation

To address which biological functions MacroD2 and TARG1 possess in human cells I wanted to explore their loss-of-function phenotypes. I generated knockout cell lines with CRISPR/Cas9 in human osteosarcoma cells (U2OS). U2OS cells are easy to handle due to their cancerous origin, but are still a good model system for human cells in general since they are mainly triploid without major changes in many cancer relevant signaling pathways such as EGFR/ErbB, mTor, cell cycle, and insulin signaling (Akan et al., 2012). Additionally, U2OS cells express both MacroD2 and TARG1 in amounts detectable on western blot (figure 3.10) enabling fast and easy screening of possible knockout clones at the protein level.

For the generation of single knockout cell lines U2OS cells were transfected with plasmids containing the appropriate guide RNA and Cas9. U2OS cells were transfected with a single, GFP-containing plasmid. Successfully transfected cells were then isolated with FACS and expanded. After screening all cell lines for the loss of MacroD2 or TARG1 on western blot, cell lines lacking the proteins were genotyped by subcloning and Sanger sequencing.

For double knockout cell lines, two MacroD2 knockout cell lines were transfected with four plasmids, each containing one guide RNA and nickase Cas9. Transfected cells were isolated with antibiotic resistance and screened for the loss of MacroD2 and TARG1 on western blot. Cell lines lacking both proteins were genotyped using PCR.

The generation and characterization of all cell lines is described in more detail in the next sections.

For the generation of the MacroD2 knockout cell lines I used two distinct guide RNAs with classical Cas9 to minimize the possibility of potential off-target effects being present in both cell lines lacking MacroD2. Off-target effects result from binding of guide RNAs to DNA sequences similar to the target site resulting in unwanted insertions and deletions in those sites. One guide RNA targets Exon 6 and the other exon 7 of MacroD2 as depicted in figure 3.9. I chose these guides targeting the middle of the macrodomain of MacroD2 - spanning exon 3 to 9 - in order to induce protein folding problems in case any mRNA is expressed despite all alleles containing premature stop-codons which should activate non-sense mediated mRNA decay. Both guide RNAs targeting MacroD2 resulted in the generation of cell lines lacking MacroD2 on western blot.

For TARG1 knockout cell lines, only one of the two utilized classical Cas9 guide RNAs generated knockout cell lines. I used guide RNAs targeting the middle of the macrodomain of TARG1 (on exon 3 as depicted in figure 3.9) in order to ensure that no folded protein can be generated, as discussed for MacroD2 knockout cell lines in detail.

Apart from screening all cell lines for the loss of MacroD2 or TARG1 protein on western blot, knockout cell lines generated with the classical Cas9 enzyme were genotyped by PCR

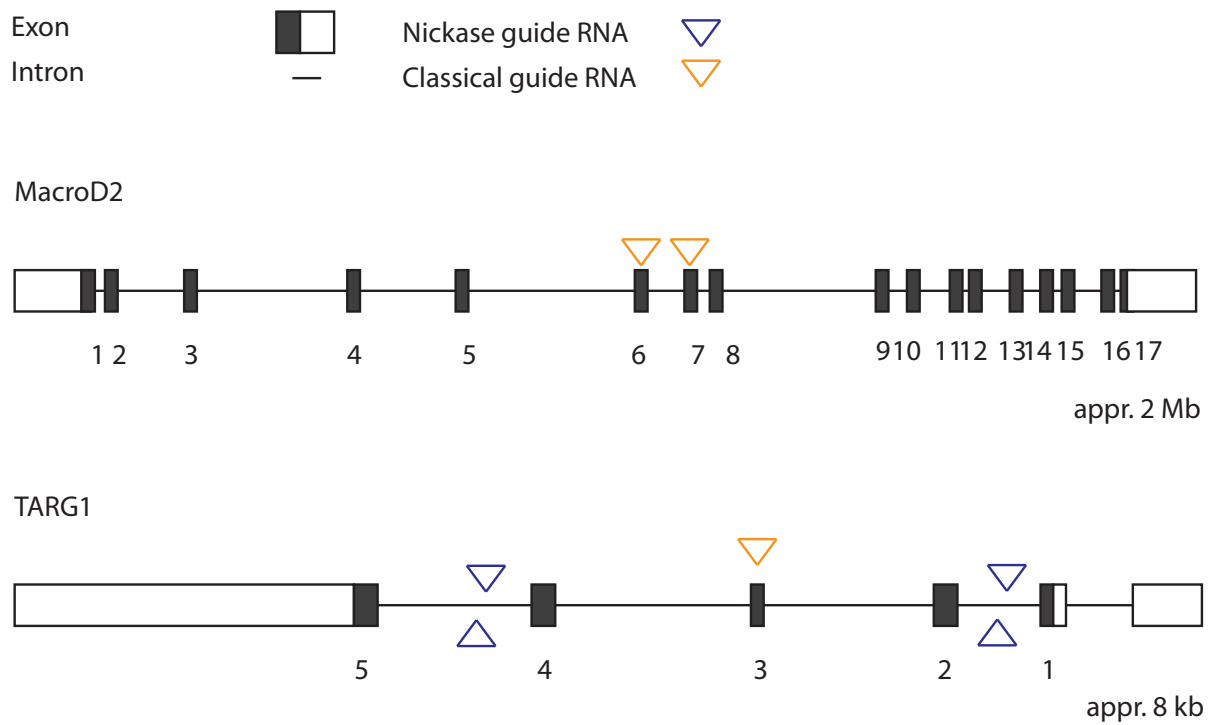


Figure 3.9: Guide RNAs used for CRISPR/Cas9 knockout generation. Chosen guide RNAs are depicted on schematic genes of MacroD2 and TARG1

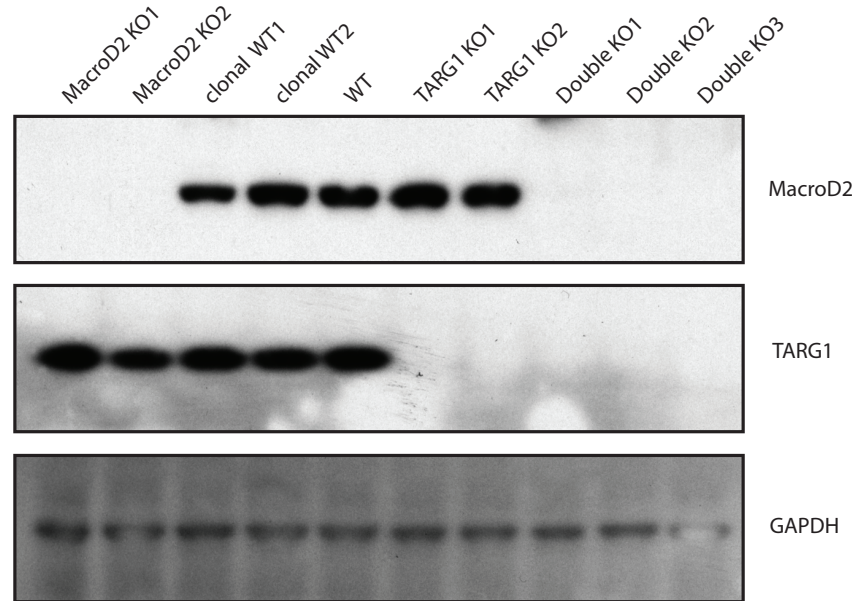


Figure 3.10: Utilized Knockout Cell Lines show no detectable protein, which was targeted with CRISPR/Cas9, while GAPDH was expressed equally throughout all cell lines. MacroD2, TARG1 and double knockout cell lines were generated with CRISPR/Cas9. Protein lysates were analyzed in a western blot with anti-MacroD2 and anti-TARG1 antibodies. Loading was controlled with GAPDH.

amplification of an approximately one kilobase pair region surrounding the used cut site of Cas9 (3 bp upstream of the PAM (Ran et al., 2013)) and subcloned into a small vector (pBluescript II KS+). Multiple subcloned plasmids were sequence verified to ensure that all three alleles of the cells contained insertions or deletions resulting in premature stop codons. Since U2OS is mainly triploid (Akan et al., 2012) I wanted to find three distinct alleles in the knockout cell lines, which is the case if all three alleles had distinct mutations. With this method I can be certain that no wild-type alleles are present but I might have dismissed knockout cells from further analysis, which had the same mutation on more than one allele. All used cell lines had three distinct insertions or deletions in all three alleles resulting in premature stop codons, as depicted in table 3.1.

Additionally to validating MacroD2 knockout cell lines at the DNA (table 3.1) and protein level (figure 3.10), the cell lines were validated at the RNA level with RT-qPCR (performed by Irene Chen, figure A.2). MacroD2 knockout cell lines show strongly diminished MacroD2 mRNA levels compared to mRNA levels found in wild-type cells. This indicates that nonsense mediated decay is activated in these cell lines.

Double knockout cell lines were generated by knocking TARG1 out with the double nickase system (Ran et al., 2013) in both previously identified MacroD2 knockout cell lines (see purple triangles in figure 3.9). For the double nickase system our group received

Table 3.1: Genotypes of MacroD2 and TARG1 knockout (KO) cell lines. PCR amplification and subcloning of a 1 kb region around the cut site (generated by Cas9 three base pairs upstream of the PAM sequence of the used targets (Ran et al., 2013)). Insertions or deletions differing from wild-type U2OS sequence are noted.

Cell line	Allele 1	Allele 2	Allele 3
MacroD2 KO1	2 base insertion (AT)	13 base deletion	2 base deletion (AT)
MacroD2 KO2	2 base deletion (AG)	22 base deletion	1 base deletion (G)
TARG1 KO1	1 base insertion (C)	7 base deletion (GCGCCCA)	7 base deletion (CCAGCGC)
TARG1 KO2	2 base deletion (CC)	2 base deletion (GC)	7 base deletion (GCATGGG)

the constructs from the Lüscher laboratory. Nickase Cas9 is a mutant Cas9 which only cuts one strand of DNA. With the double nickase approach, double strand breaks are generated using two guide RNAs targeting nickase Cas9 to opposite strands of the target DNA. The double nickase approach leads to two single strand breaks in opposite strands in close proximity to each other (Ran et al., 2013). To generate a large deletion in TARG1, two double strand breaks were generated with four guide RNAs. The advantage of using nickase over classical Cas9 is that with the necessity of two guide RNAs binding to both strands of DNA the possibility of off-target effects is drastically decreased. Furthermore, with inducing a large deletion from two double strand breaks, screening for knockout cells was possible with PCR without further subcloning and sequencing steps. For the double knockout cell lines a large region of TARG1 genomic DNA between intron 2 and 5 (2.8 kb) was removed with the use of two double nickase-induced double strand breaks as depicted in figure 3.9.

To genotype double knockout cell lines, I can use PCR. If the deletion in the TARG1 genomic DNA was successful, we can assume that the two ends where the double strand breaks were introduced get ligated frequently, leading to a new sequence not present in the wild-type genomic DNA. I chose to PCR amplify a 1000 bp fragment of TARG1 genomic DNA which is only detected with PCR if the genomic DNA of TARG1 upstream of the first introduced double strand break is ligated to the genomic DNA downstream of the second double strand break. This PCR amplicon existing due to a successful deletion of the 2.8 kb fragment from TARG1 genomic DNA is called mutant amplicon in the following text. The presence of this amplicon shows that all or some of the alleles of the examined cell lines contain the desired deletion. To ensure that there are no alleles of wild-type TARG1 present in the genomic DNA of double knockout cell lines, I chose to PCR amplify a 500 bp fragment which lies within the genomic DNA of TARG1 which was designed to be removed from the genomic DNA (between both double strand breaks). This fragment is called wild-type amplicon in the following.

In figure 3.11, an agarose gel with wild-type and mutant amplicons from 9 cell lines is depicted. The mutant 1 kb amplicons of cell lines are shown on the left, on the right side the wild-type amplicons are depicted. An example of a successful deletion of the large fragment of TARG1 can be seen on lane 6 (TARG1 KO clone 1), since there is no PCR product detectable for the wild-type amplicon but a strong band of the resulting mutant amplicon. An example for an unsuccessful deletion can be seen in lane 2 (Double KO clone 4), since there is no mutant amplicon but a strong band for the wild-type amplicon which was supposed to be deleted.

One of the three double knockout cell lines used in this study (Double KO3; lane 5) showed no amplification of the deleted wild-type allele and had two distinct amplicon sizes for the mutant alleles. Detecting two distinct mutant amplicons indicates that one of the alleles gained some bases between both double strand breaks due to DNA repair. Therefore, it is homozygous for the mutation and does not possess a functioning TARG1 gene anymore. In one other used double knockout cell line (Double KO1, lane 1), the wild-type allele was strongly reduced and a much stronger mutant allele is visible. For the third cell line (Double KO2, lane 4) the wild-type amplicon was weaker but there was no mutant amplicon visible (figure 3.11). This might indicate that these cell lines only lost some alleles of TARG1, it is however possible that TARG1 is mutated in all alleles. This would be reasonable if the deleted fragment was re-inserted either invertedly or with small insertions or deletions resulting in premature stop codon-inducing frame shifts. Another possibility is that the cell lines only had small insertions or deletions at one of the two double strand breaks resulting in frame shift mutations without exclusion of the 2.8 kb fragment, which therefore could be detected in the PCR. Additionally, it is not known if all alleles in U2OS cells are active, i.e. are used for transcription of TARG1. All three double knockout cell lines were used in this study, since neither TARG1 nor MacroD2 could be detected at the protein level (figure 3.10).

All generated cell lines were analyzed in multiple biological replicates for the absence of MacroD2 and TARG1 on western blot. As shown in figure 3.10, all cell lines have lost the appropriate proteins, e.g. all single knockout cell lines lacked either MacroD2 or TARG1 while maintaining normal levels of the other protein and housekeeping genes (in this case GAPDH), while double KO cells lack both proteins while maintaining constant GAPDH levels.

In summary, all used cell lines were characterized at the protein level with western blotting and at the DNA level by genotyping to assess their genetic changes. One representative image of all cell lines used in this study is depicted in figure 3.10, showing expected protein patterns in all cell lines. The fact that none of the double knockout cell lines shows a signal for TARG1 indicates that all three double knockout cell lines lack TARG1. Therefore, I have generated and validated knockout cell lines of MacroD2, TARG1 and MacroD2/TARG1. When all clonal cell lines were generated it became clear that there are two morphologically distinct subpopulations of U2OS cells present in the parental, non-clonal U2OS cell lines. One subpopulation consists of longer cells, whereas the other subpopulation consists of rounder cells. I made sure that one clone of each morphology was selected within each genotype (morphology of subpopulations represented in knockout cell lines can be seen in

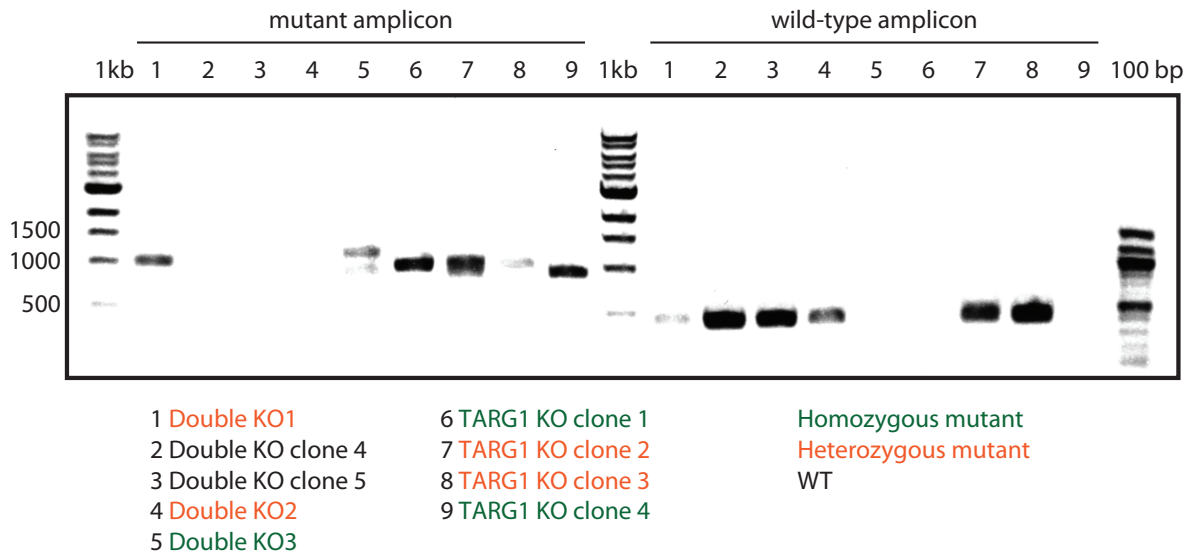


Figure 3.11: Genotyping of nickase-induced double knockout cell lines. Detection of PCR fragments of wild-type amplicons with primers amplifying a 500 bp region of exon 4 and detection of mutant/KO amplicons with primers amplifying a 1 kb fragment (about 600 bp in intron 5 and 300 bp in exon 2) run on a 1 % agarose gel.

figure A.5).

3.2.2 Identification of potential global proteome changes in cells lacking MacroD2

MacroD2 is connected with protein stability and gene expression in literature, therefore I wanted to address if cells lacking MacroD2 experience global proteome changes. It was shown that MacroD2 is a positive modulator of the heat shock response (Raychaudhuri et al., 2014) and activates GSK-3 β (Rosenthal et al., 2013). Active GSK-3 β leads to the degradation of β -catenin and to the inactivation of the Wnt pathway (Wu and Pan, 2010).

Additionally, PARPs and PAR were shown to influence gene expression (Gupte et al., 2017; MacPherson et al., 2013; Mehrotra et al., 2011; Rouleau et al., 2011; Szántó et al., 2012) on multiple levels as discussed in further detail below. For example, PARP1-mediated PARylation of C/EBP β attenuates the transcription of genes involved in adipogenesis (Luo et al., 2017), and macrodomain containing PARPs (PARP9, PARP14, PARP15) were shown to repress transcription in a luciferase assay (Aguar et al., 2005). PAR itself was shown to relieve repression of gene expression by mRNA degradation and miRNA-mediated translational repression (Leung et al., 2011) and to activate the nuclear proteasome in response to oxidative damage (Mayer-Kuckuk et al., 1999; Ullrich et al., 1999).

Additionally to their function in gene expression, PARPs influence protein degradation. For example, PARP16 was shown to be involved in protein degradation in the unfolded protein response (Jwa and Chang, 2012) and PARP5a was shown to PARylate axin leading to its degradation through the PAR-binding E3 ubiquitin ligase RNF146 (Callow et al., 2011).

To identify any global changes in protein levels in cells lacking MacroD2, I performed whole cell proteome analysis in unstressed MacroD2 knockout cells and wild-type U2OS cells. For whole cell proteome analysis all proteins and their abundance in whole cell lysates are identified with label-free mass spectrometry. With this method more than 5000 proteins and their abundance could be identified in U2OS and one of the MacroD2 knockout cell lines. To address if any of the identified proteins were more abundant in the wild-type or knockout cell line, I compared the protein intensity (x-axis) and the significance of this intensity difference (y-axis) between both cell lines with a volcano plot (figure 3.12).

In the resulting volcano plot (depicted in figure 3.12) there are almost no significant changes in protein intensities visible between the MacroD2 knockout cell line and U2OS wild-type cells for untreated cells. This can be determined from the volcano plot since no grey squares, representing protein intensity and significance, are depicted above the black cut-off line, except for Calponin-1, which is enriched in U2OS cells. Calponin-1 has not been connected with ADP-ribosylation in literature so far. It is an actin filament-associated regulatory protein expressed mainly in smooth muscle cells (Liu and Jin, 2016).

For comparison, major changes in the whole proteome of human cells could be detected between wild-type and TANKyase 1 (PARP5a) and TANKyrase 2 (PARP5b) double knockout cells. In this study, over 7000 proteins were detected from which 608 proteins (about 8 % of detected proteins) showed significant abundance changes between both cell lines (false discovery rate (FDR) = 0.05) with almost equal distribution between increased and decreased proteins (287 to 321, respectively) (Bhardwaj et al., 2017). This indicates

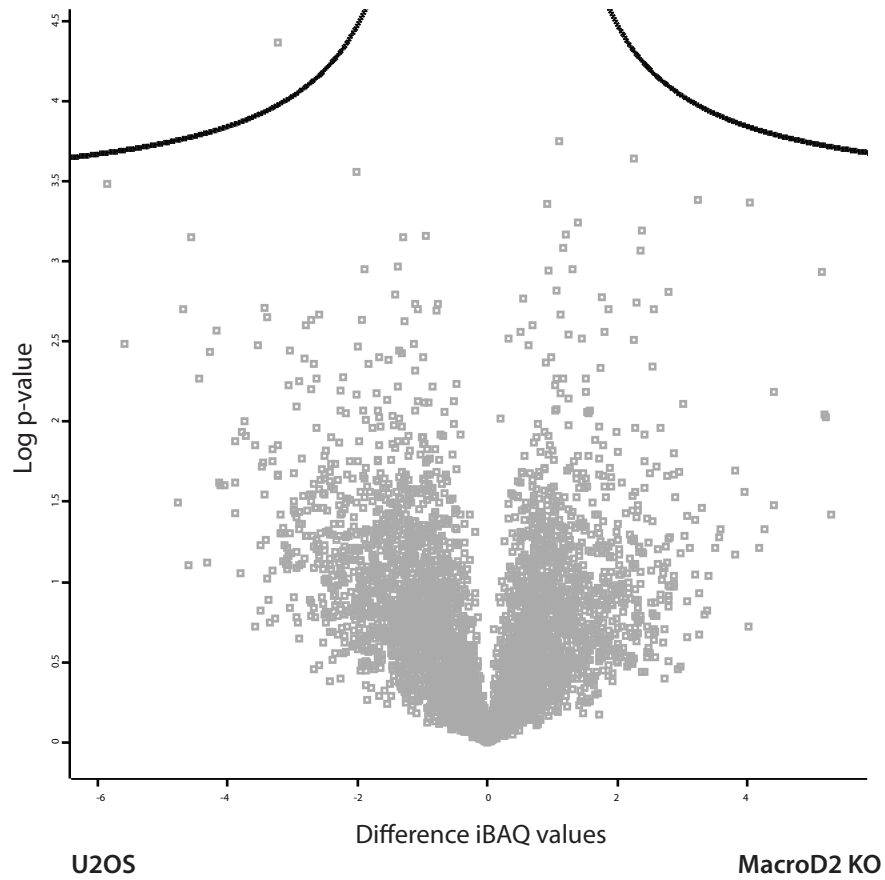


Figure 3.12: The whole proteome of MacroD2 knockout (KO) cells compared to wildtype cells (U2OS) shows no major proteome changes. Volcano plot of whole proteome of MacroD2KO against U2OS (WT). iBAQ value intensity differences of individual detected are plotted against their p-value. Significantly changed proteins are on top of the cut-off line ($s_0=0.1$, FDR 0.05). Generated in Perseus

that with major protein abundance changes in MacroD2 knockout cells over wild-type cells, the volcano plot should also show a similar ratio of significant changes in protein abundance when applying the same statistics - in both cases a FDR of 0.05. However, major abundance changes could not be observed for MacroD2 knockout cells, where only one protein was significantly more abundant in wild-type cells .

However, mass spectrometric approaches to detect a cell's whole proteome can so far only detect a fraction of all proteins of a cell. Abundant proteins, i.e., proteins expressed in multiple copies (up to 20000000) per cell, are more likely detected than proteins which are less abundant. This results from the fact that the 1000 most highly expressed proteins in a cell account for 80 % of the proteome mass, and a fraction of the proteome cannot be detected since the measured values for the proteins were below the detection limit. Apart from proteins expressed in so few copies that they fall below the detection limit, proteins cannot be detected for other technical reasons as well. For example, proteins can be lost during cell lysis, tryptic digest or any other step in sample preparation (Milo, 2013). In a study from 2011, more than 10000 distinct proteins could be detected in U2OS cells and the observed protein copy numbers of U2OS cells span at least seven orders of magnitude. Furthermore, they showed that highly expressed proteins perform core functions such as energy metabolism and translation, while low abundant proteins perform regulatory functions. This study does, however, still not show all proteins present in U2OS cells due to detection limits, e.g., an underrepresentation of membrane-bound proteins (Beck et al., 2011). If one uses the hypothesis that one gene results in one protein, human cells should express about 20000 distinct proteins. Since different proteins can result from the same gene through alternative splicing, single amino acid polymorphisms, and post-translational modifications, more proteins can originate from one gene and more proteins could be present in a human cell at a given time (Ponomarenko et al., 2016).

With these limitations in mind, I can conclude that with more than 5000 proteins detected I was able to detect about half the number of proteins experimentally detectable in U2OS cells (10000 proteins) and about a quarter of the theoretically detectable proteins (20000 proteins resulting from 20000 genes) (Beck et al., 2011; Ponomarenko et al., 2016). With 5000 proteins detected, I most likely mainly detected most abundant proteins, which are statistically most likely involved in core functions such as energy metabolism, but only a minor fraction of low abundance, regulatory proteins (Beck et al., 2011). Additionally, MacroD2 and TARG1 could not be detected in the wild-type or MacroD2 knockout cell lines. This might be due to the low abundance of MacroD2 and TARG1 in U2OS cells. MacroD1 was detected in both cell lines in equal quantities.

This result implies that within the limitations of the whole cell proteome detection, any phenotypic changes (which will be discussed in the following chapters) between MacroD2 knockout cells and U2OS wild-type cells should not result from major global proteome changes. However, this result most likely includes mainly abundant proteins with a minor fraction of low abundance proteins.

3.2.3 Function of MacroD2 and TARG1 in cellular proliferation

Since MacroD2 was interacting in the BioID with a big cluster of proteins belonging to the GO-term of “microtubule” and with minor clusters as well as single GO-terms connected to “positive regulation of cell cycle checkpoint”, “cell cycle checkpoint”, “regulation of mitotic cell cycle”, “spindle”, and “spindle organization” (figure 3.8), I tested if MacroD2 and/or TARG1 regulate cellular proliferation. To address if any of the generated cell lines possessed defects in cell proliferation, I measured cellular proliferation with xCelligence. xCelligence is a method where cells are seeded in a specific chamber of an E-plate and the electrical flow in the chamber is measured over time. Cell attachment and proliferation impede electrical flow in the chamber directly but to a different extent, as depicted in figure A.3A. Cell attachment results in a rapid increase in impedance, whereas proliferation results in a slow increase in impedance until the maximum impedance is reached at cell confluence (figure A.3B). The doubling time of all cell lines can be calculated in xCelligence from the impedance curve, and a box plot showing the doubling time of all knockout and wild-type cell lines in triplicate was generated.

None of the cell lines showed significantly different proliferation from wild-type cells. However, all single knockout cell lines had shorter doubling time than wild-type cell lines, whereas all double knockout cell lines had increased doubling time over wild-type. Double knockout cell lines proliferate significantly slower than single knockout cell lines (p-value ≤ 0.05 over TARG1 KO, p-value ≤ 0.01 over MacroD2 KO) (figure 3.13). It can be concluded from these results that most likely neither MacroD2 nor TARG1 influence cell proliferation significantly. It is very likely that TARG1 is completely absent in all three double knockout cell lines, since all three used double knockout cell lines proliferate slower than wild-type cells and significantly slower than both MacroD2 knockout cell lines.

Even though only minor changes in doubling time between knockout cells and wild-type cells were observed in the xCelligence measurement, I investigated if MacroD2 or TARG1 influence the cell cycle. Thereto I performed a cell cycle analysis experiment with FACS analysis of changing DNA content over the cell cycle. DNA content is measured through the DNA dye propidium iodide. In human cells, cell populations are distributed in a way that most cells are either in G1- or G2-phase. Cells in G1-phase have the minimal amount of DNA present over the course of the cell cycle and most cells in a population are in G1-phase. During S-phase the DNA is replicated and cells possess a DNA content between the content observed in G1-phase and G2-phase. In a population relatively few cells are in S-phase. Cells in G2-phase possess double the amount of DNA observed for cells in G1-phase since their whole genome was duplicated.

The results from the cell cycle analysis of propidium iodide stained cells show that for wild-type cell lines about 50 % of cells are in G1-phase, about 10 % of cells are in S-phase and below 30 % of cells are in G2-phase. Both MacroD2 and TARG1 knockout cell lines show very similar proportions of cells in all cell cycle phases (results of two replicates are shown in table A.2). Cell cycle profiles, depicting DNA content on the x-axis and cell number on the y-axis, were drawn from the FACS measurements of more than 10000 propidium iodide stained cells for all single knockout cell lines and wild-type cell lines. No

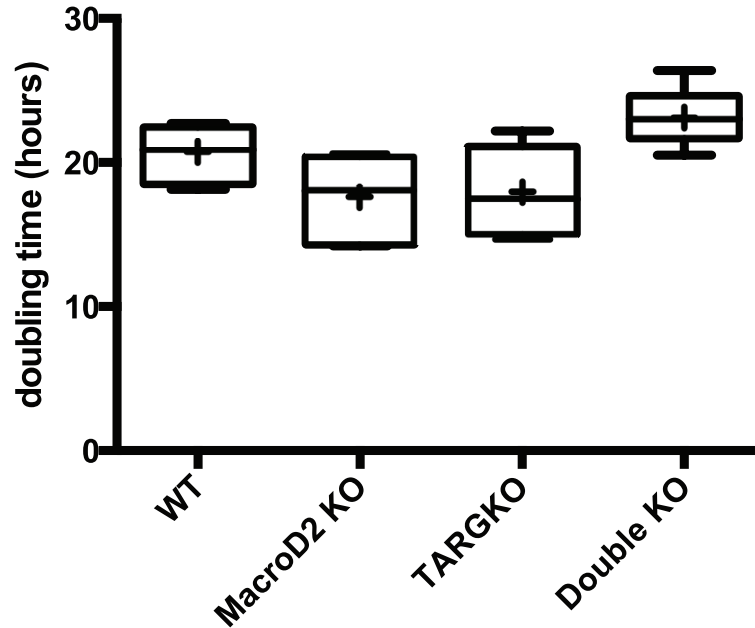


Figure 3.13: No significant changes in cell proliferation could be detected for any knockout cell line compared to wild-type cells. xCelligence measurements of cellular proliferation. Electric flow in cells is measured. Upon attachment or proliferation of cells, electric flow is hindered/impeded. Impedance correlates directly with cell proliferation. Box plots of xCelligence measurements of proliferation with xCelligence in two MacroD2, two TARG1, three double knockout and three wildtype cell lines. Median with 95 % CI from three replicates. Statistics done in Perseus with Kruskal-Wallis test.

major cell cycle changes were detectable for any single knockout cell lines compared to wild-type cells (representative examples in figure 3.14). From the cell cycle profiles conclusions can be drawn apart from changes in the proportion of cells in different cell cycle stages, e.g. cells with mitotic defects resulting in polyploidy would exhibit a population of cells with DNA content higher than regular G2-phase content, and apoptotic, necrotic or majorly aneuploid cells would exhibit a population of cells with DNA content below regular G1-phase cells. Since there are no cell lines showing higher DNA content than G2-phase DNA content, these cells have not changed their ploidy. Additionally, all cell lines seem to be healthy since there are only minor fractions of sub G1-phase DNA content.

This indicates that the minor increase in cell proliferation detected with xCelligence for any single knockout cell lines does not result from major changes in the cell cycle, from changes in ploidy, or from poor health of cells, all of which would be detectable in bulk analysis of unsynchronized cells. Additional to xCelligence and cell cycle profiles indicating no proliferation defects, all cell lines were passaged at the same rate, indicating

similar doubling time as well.

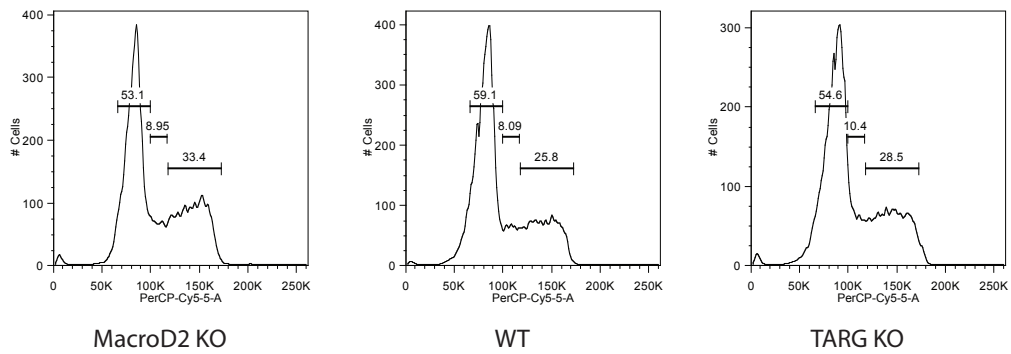


Figure 3.14: Cell cycle profiles of WT and single KO cell lines show comparable cell cycle profiles. Cell cycle profiles of wild-type (WT) and single knockout (KO) cell lines with propidium iodide staining. DNA content (measured by propidium iodide staining intensity) is depicted on the x-axis, cell number is depicted on the y-axis. Example images for one cell line per genotype.

3.2.4 Function of MacroD2 and TARG1 in actin-regulated processes

The results from the BioID showed that MacroD2 is interacting with many proteins from actin-related GO-terms such as “actin filament binding” and “focal adhesion” (figure 3.8). Therefore, I wanted to investigate if any of the knockout cell lines had defects in their actin cytoskeleton, focal adhesions or in actin-regulated cellular functions. Typical functions of the actin cytoskeleton are cell attachment and migration (Blanchoin et al., 2014; Dominguez and Holmes, 2011; Revenu et al., 2004).

Deregulations in the Actin cytoskeleton or Focal Adhesions

Zyxin, vinculin, and filamin A as well as many actin binding proteins were significant interactors of MacroD2 in the BioID screen (see table A.1). Zyxin is a focal adhesion protein implicated in actin stress fiber maintenance and repair (Smith et al., 2010). Vinculin is a focal adhesion protein involved in cell attachment and migration (Gardel et al., 2010). Filamin A, a 2647 amino acid long actin binding protein, provides a dynamic structural framework in human cells. It interacts with a plethora of human proteins (Yue et al., 2013). Mutations in filamin A were identified in various human cancers (Feng and Walsh, 2004). Filamin A is also involved in cell adhesion (Kim and McCulloch, 2011), provides a scaffold for many nuclear and cytoplasmic signaling proteins in cancer progression (Yue et al., 2013), such as the internalization of active EGFR (Fiori et al., 2009), and was shown to be required for efficient DNA double strand break repair (Yue et al., 2009).

In order to assess if the loss of MacroD2 and/or TARG1 results in changes in the actin cytoskeleton or in focal adhesions, I performed a number of immunofluorescence experiments. To assess changes to actin fiber localization and intensity as well as localization, size, and intensity of focal adhesions, I stained cells with anti-actin antibody and anti-vinculin antibody. Additionally, I performed a second set of immunofluorescence experiments staining for zyxin and filamin A. A representative staining of actin, vinculin, zyxin, and filamin A observed in all replicates of wild-type cells and all wild-type cell lines (clonal U2OS cell line 2 (cWT2) chosen) is depicted in figure 3.15. Actin staining is predominantly visible at cell attachment sites on the outside of the cells. Additionally, small finger-like structures, probably filopodia, contain strong actin staining. Vinculin staining is strong at foci at cell attachment sites at all cell borders. Zyxin staining is visible in strong fibers running from the cell border towards the nucleus. Filamin A staining was observed all over the cell and excluded from the nucleus - it looks like a meshwork generated from many thin filaments. All staining closely resembles expected staining patterns of the used proteins (for example staining patterns observed in literature see refs. (Austen et al., 2015; Feng et al., 2006; Gardel et al., 2010; Smith et al., 2010)).

When comparing the actin, vinculin, zyxin, and filamin A stainings in all used cell lines to each other (two cell lines each from MacroD2 KO, TARG1 KO, MacroD2/TARG1 double KO and clonal wild-type; figures A.5 and A.6) only minor differences were visible. In figure A.5 all cell lines showed very similar actin staining. Actin staining was visible at

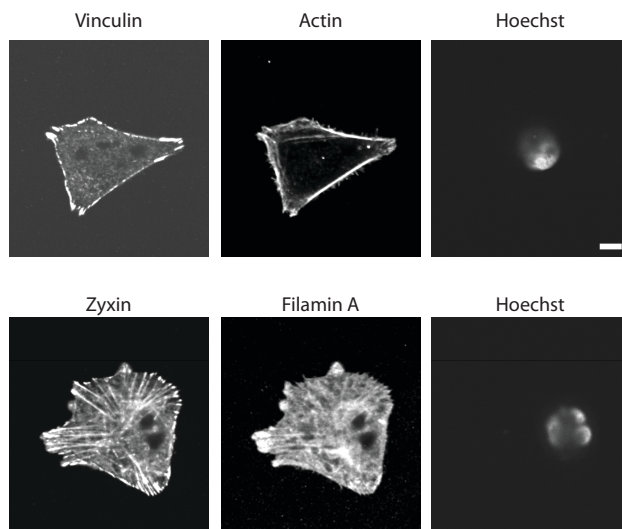


Figure 3.15: Example images of clonal U2OS (cWT2) staining against actin, focal adhesion proteins zyxin and vinculin as well as filamin A. Nuclei were stained with Hoechst. Images of the cells on the attachment site were captured close to the glass surface. Scale bar is 10 μm

cell attachment sites on all cell borders with comparable staining intensity and in small extrusions from the cell body. The vinculin staining was visible on all cell borders in all cell lines, however one clone from each genotype showed additional staining in the cell body (cWT1, MacroD2 KO2, TARG1 KO2, double KO2). This difference might stem from the fact that the U2OS cell line used to generate all clonal and knockout cell lines had two subpopulations. One population had more round morphology (cWT2, MacroD2 KO1, TARG1 KO1 and double KO1), whereas the other showed a more elongated morphology. All used cell lines were chosen in a way that both subpopulations were present. Since apart from the changes correlating with different morphologies there were no detectable defects in location or intensity visible in the immunofluorescence images, I quantified the global intensity of actin (figure 3.16A), the number of vinculin foci per cells (figure 3.16B), the area of focal adhesions (figure 3.16C), and the major axis length of vinculin foci (figure 3.16D). There was no trend visible between the different cell line types, only between the different morphological clones within one cell line type. For example, one of the clonal U2OS cell lines (cU2OS1) showed a higher actin staining intensity, but that cell line also has a high variability in actin intensity between cells, while the second cell line (cU2OS2) has comparable intensity to all other cell lines with similar variance between cells. Therefore, cells lacking MacroD2, TARG1 or both have no detectable differences in staining of actin or vinculin, in both intensity and pattern/location. Differences between two cell lines of one genotype were as strong as differences between the genotypes.

Location, morphology and intensity of zyxin and filamin A were addressed in a second

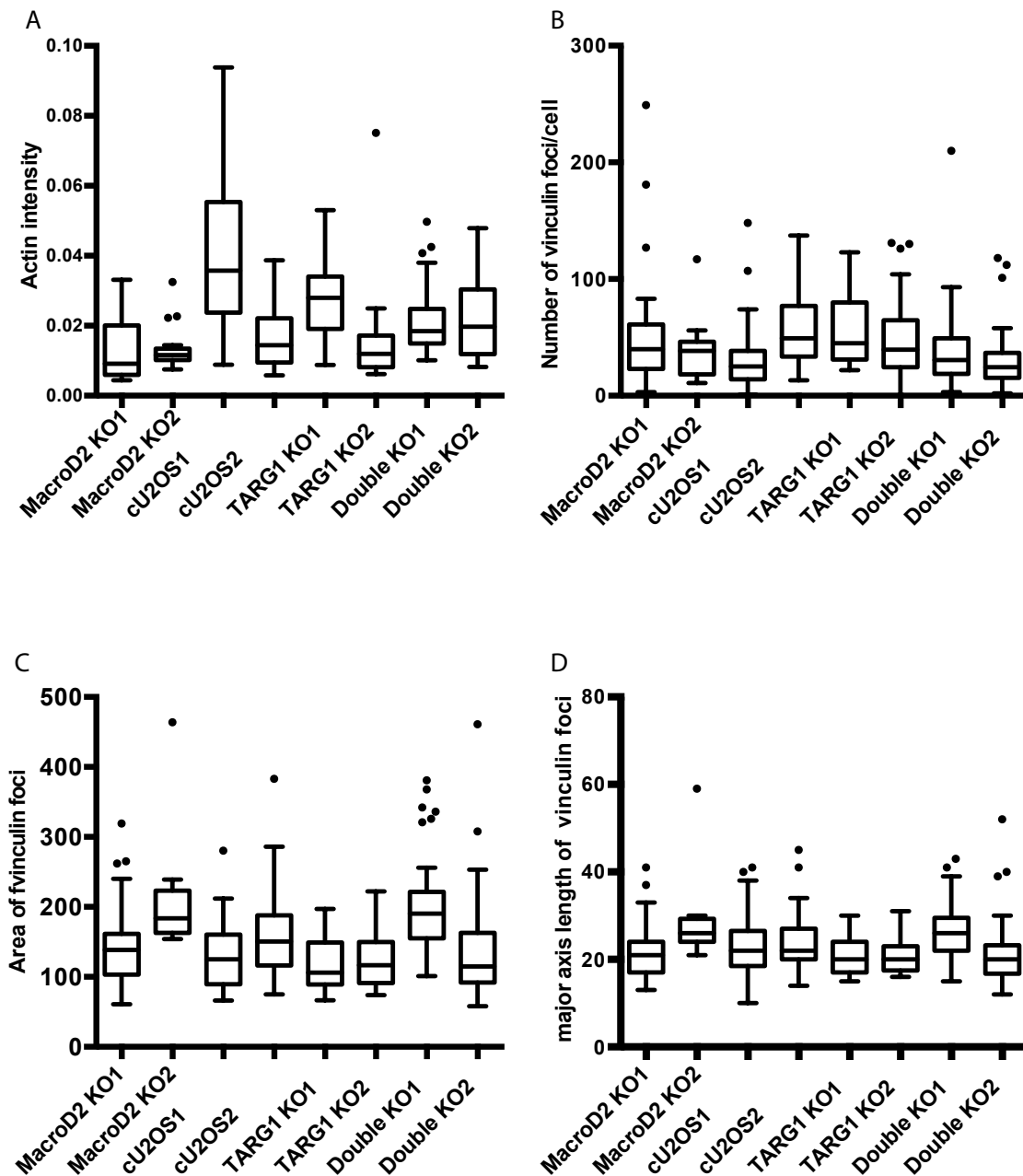


Figure 3.16: Quantification of actin intensity and vinculin foci number, area, and major axis length. Identification and measurements with cell profiler. Graphic representation with GraphPad Prism 7.0 7.0. Box plot with 95 % confidence interval.

set of immunofluorescence experiments (figure A.6). Zyxin staining was visible at cell borders and as filaments going from cell border to the nucleus in various degrees throughout all used cell lines. Overall staining intensity of zyxin was similar in all cell lines. There

was no trend visible between different cell types or morphologies. Filamin A staining was similar throughout all used cell lines. The staining pattern was the same in all cell lines, with staining throughout the cell with low nuclear staining.

Taken together these experiments show that there were no major changes in the intensity or localization of actin, vinculin, zyxin or filamin A at cell attachment sites.

Function in Cell Attachment

Cell attachment is regulated mainly by dynamic changes of the actin cytoskeleton and focal adhesion maturation. MacroD2 was shown to interact with many focal adhesion proteins and proteins binding to the actin cytoskeleton (figure 3.8). In order to address if MacroD2 and/or TARG1 have an effect on cell attachment, cell attachment was measured in all knockout and wild-type cell lines using xCelligence (figure 3.17). xCelligence works by measuring impedance changes (figure A.3A and B, we well as chapter 3.2.3). Attachment can be calculated as the slope of the resulting curve during the fast increase of impedance.

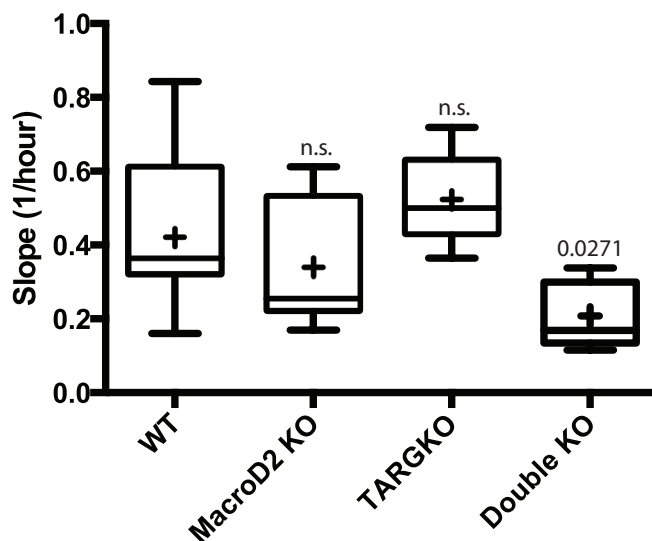


Figure 3.17: Double knockout cell lines migrate significantly slower than wildtype cells. Cell Attachment measured with xCelligence. 5000 cells per well were seeded in E-plates and cell attachment measured. Attachment can be calculated as the slope of the resulting curve during the fast increase phase (figure A.3B, leftmost section of the graph (1)). Box plots calculated from attachment measurements with xCelligence experiments in two MacroD2, two TARG1, three double knockout, and three wild-type cell lines. Median with 95% confidence interval from three replicates. Statistics with Kruskal-Wallis test.

The attachment speed of all cell lines from three biological replicates each was used to calculate box plot graphs (figure 3.17). In this graph it is visible that MacroD2 knock-

out and TARG1 knockout cell lines do not attach significantly different from wild-type cells. Double knockout cell lines, however, showed a significantly decreased attachment speed when compared to wild-type cell lines. This indicates that MacroD2 and TARG1 are functionally redundant in cell attachment since only the double knockout cell lines had defects in cell attachment. Furthermore, the fact that cells lacking MacroD2 and TARG1 have cell attachment defects supports the finding from the BioID screen which indicated that MacroD2 interacts with proteins associated with the GO-terms related to the actin cytoskeleton and/or with focal adhesion (figure 3.8).

Function in Cell Migration

Using the BioID approach, MacroD2 was shown to interact with a plethora of actin-related proteins. Therefore, I wanted to address if MacroD2 and/or TARG1 influence additional actin regulated processes to cell attachment. Cell migration is another actin-regulated process which is influenced by a large number of cell signaling pathways (Magi et al., 2012). An additional indicator that MacroD2 and/or TARG1 might influence cell migration stems from the fact that it was shown that PARP1 and PARP9 influence cell migration in various cell types (Aguiar et al., 2000; Cavone et al., 2011; Rodríguez et al., 2013; Ullrich et al., 2001). Therefore, I investigated if the lack of MacroD2 and/or TARG1 results in cell migration defects with scratch assays.

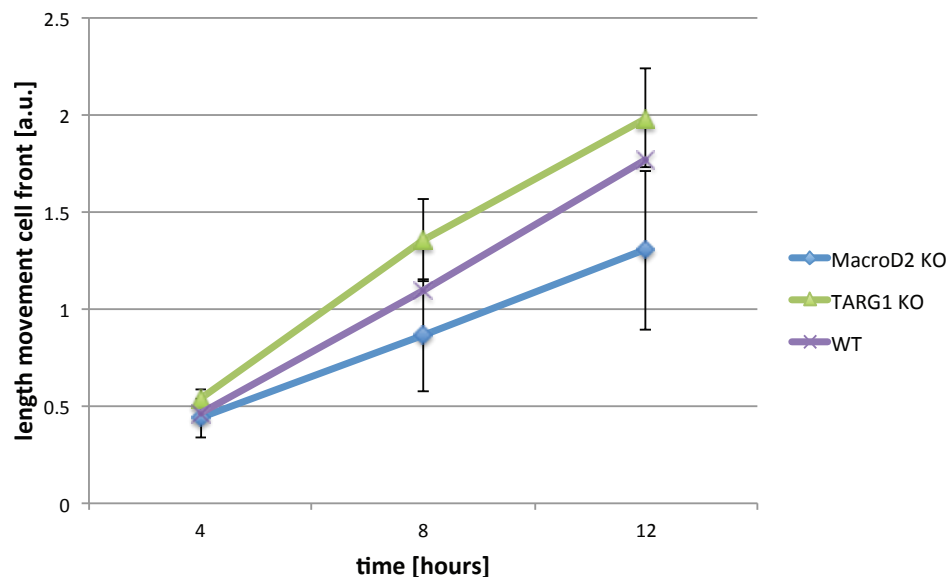


Figure 3.18: MacroD2 knockout cell migrate slower than wild-type cells in a scratch assay. Confluent cells are scratched from plate and washed off. Cell migration was monitored in 10 minute intervals over 12 hours. Length of cell front movement (y-axis) is depicted over time (x-axis) in 4 hour intervals.

In scratch assays, cells were scratched off a confluent plate and their migration into the resulting cell-free area (scratch) was then monitored over time. Scratch assays are a reliable method to detect migration defects. They can however show false results if cell lines have different cellular doubling times (Liang et al., 2007). This is the case since cells with faster doubling times might fill in the scratch faster than slower proliferating cells, without having any defects in cell migration. Since all single cell lines and wild-type cell lines had similar cellular doubling times (see section 3.2.3, figure 3.13), I could investigate cell migration with a scratch assay. The scratch assay revealed that MacroD2 knockout cell

lines migrated significantly slower than TARG1 knockout or wild-type cells twelve hours after the scratch was performed (figure 3.18).

Since double knockout cell lines proliferate significantly slower than either of the single knockout cell lines (see section 3.2.3, figure 3.13), a scratch assay can not be used to compare double knockout cell lines to any other cell line. Therefore, I established a new migration assay in our laboratory where I track unlabeled, single cells in a thinly seeded 96-well plate for 24 hours (for the assay schematic refer to figure A.4). For the cell tracking, I was using CellTracker GUI, a MatLab plugin (<http://www.celltracker.website/index.html>). The length of overall cell migration was used as an output and box plots were generated using GraphPad Prism 7.0.

In this migration assay, TARG1 knockout cell lines migrated significantly slower than wild-type cell lines. This migration defect was, however, quite subtle compared to the migration defect observed in double knockout cell lines (figure 3.19). The severity of the migration defect observed for the double knockout cell line is much greater than the effect of both single knockout cell lines combined (synergistic effect). Together, these results indicate that MacroD2 and TARG1 might compensate for the loss of the other protein to some extent, and therefore perform redundant roles in cell migration. In the migration assay in 96-well plates, TARG1 knockout cells had significant but rather mild migration defects, whereas MacroD2 knockout cells had a significant but also rather mild migration defect in the scratch assay.

Scratch assays show cell migration upon cell contact loss and therefore show induced migration. Cell migration observed in scratch assays is regulated by a plethora of cell signaling pathways, some of which have general importance while others only influence some cancer cell lines. An important signaling pathway in scratch assays is EGFR signaling (Magi et al., 2012). The differences in the mild migration defects in the single knockout cells observed in the different migration assays might stem from the fact that MacroD2 does not react to stimulation sufficiently, while TARG1 knockout cell lines do react to stimulation (in the scratch assay) but have a minor migration defect in general.

In order to show that defects in cell migration in the double knockout cell lines are due to the loss of both enzymes, rescue experiments with full-length MacroD2 or TARG1 would be very helpful. Since cells need to be seeded scarcely for the migration assay, I was not able to transfect double knockout cells with MacroD2 or TARG1 for rescue experiments. Scarcely seeded cells cannot be transfected for technical reasons. More densely seeded cells can be transfected successfully but tend to clump together when reseeding in an appropriate density for the migration assay. Therefore, I set up an indirect rescue experiment. In cells lacking MacroD2 and/or TARG1 more proteins will be MARYlated. In order to decrease the number of MARYlated proteins in human cells, I performed NAD⁺ depletion experiments with the NAMPT inhibitor FK866. NAD⁺ depletion results in reduced activity of all PARP family members Cambronne et al. (2016). NAD⁺ depletion, however, not only diminishes the number of MARYlated proteins but the number of PARYlated proteins as well (as shown in the ADP-ribosylation cycle in figure 1.3).

NAD⁺ depletion resulted in decreased migration of wild-type cells as depicted in figure 3.20. This was to be expected since PARP and PARP9 were shown to regulate cell

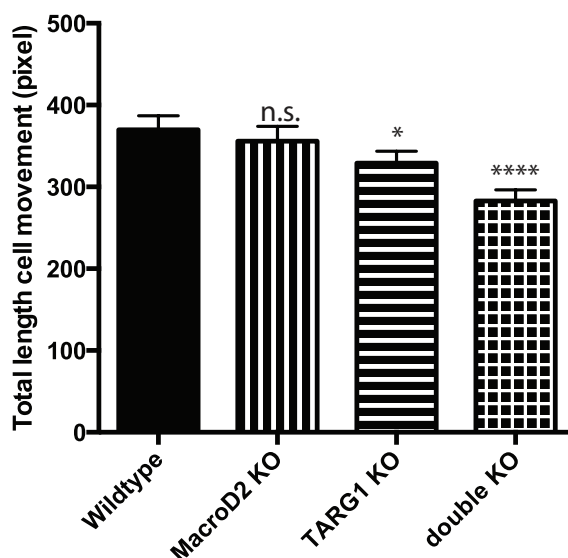


Figure 3.19: Double knockout cell migrate significantly slower than wildtype cells in a 96-well migration assay. Cell migration assay with cell tracking in 96-well plates. Cells were seeded thinly in 96-well plates, spun down and immediately imaged with live cell imaging over 24 hours with 15 minute intervals. Single cells were tracked semi-automatically with MatLab plugin CellTracker GUI. Bar graph was calculated in GraphPad Prism 7.0 from two MacroD2, two TARG1, three double knockout and three wild-type cell lines in three replicates. Mean with 95% confidence interval. Statistics with Kruskal-Wallis test.

migration (Aguiar et al., 2000; Cavone et al., 2011; Rodríguez et al., 2013; Ullrich et al., 2001). When each knockout cell line is compared in untreated conditions to the same cell line under NAD^+ depletion, it is evident that NAD^+ depletion results in faster migration of knockout cell lines (figure 3.20). The differences in migration between untreated and NAD^+ -depleted cells were not significant for any of the cell line types used. Nonetheless, this indicates that ADP-ribosylation changes resulting from NAD^+ depletion have an effect on cell migration in U2OS cells.

In summary, there were no significant changes in migration upon NAD^+ depletion, however all cell lines reacted to NAD^+ depletion in the expected manner, i.e. wild-type cells had decreased migration and all knockout cells had increased migration. This gives a first hint that the migration defect in all knockout cells might be regulated by ADP-ribosylation.

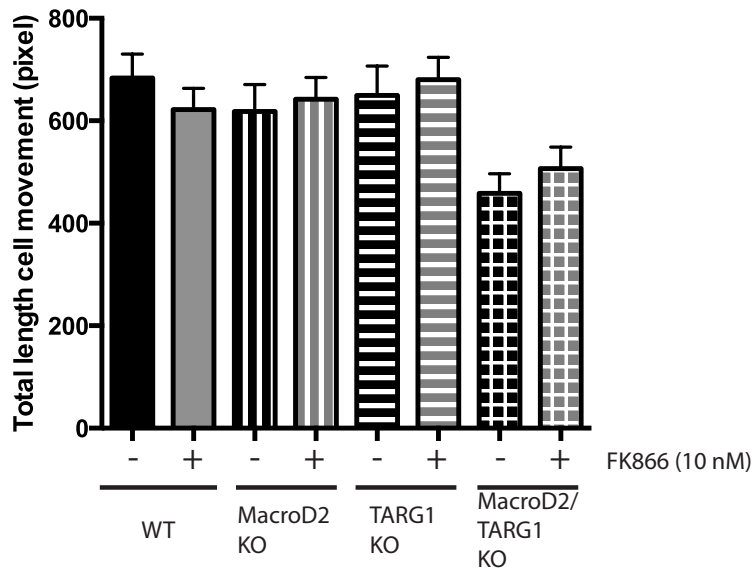


Figure 3.20: NAD⁺ depletion did not induce significantly faster migration in single or double knockout cells. Cells were seeded thinly and after attachment treated with FK866 (NAMPT inhibitor; NAD⁺ depletion) or untreated for 16 hours. Cells were imaged and analyzed as in fig. 3.19. Statistical differences to wild-type cells were assessed with Kruskal-Wallis test in GraphPad Prism 7.0.

3.2.5 Influence of MacroD2 and TARG1 on EGFR Signaling

EGF-stimulated Cell Migration

MacroD2 and TARG1 influence cell migration and attachment which are actin cytoskeleton regulated processes. It still remains to be investigated how both proteins influence these processes. Since the actin cytoskeleton and EGFR signaling are closely entwined, EGFR is a likely candidate to explain how MacroD2 and TARG1 influence the actin cytoskeleton. EGFR not only causes actin reorganization (Edwards et al., 1999; Papakonstanti and Stournaras, 2008; Rijken et al., 1991) but EGFR activity is regulated through the actin cytoskeleton as well (Lynch et al., 2003; Ohashi et al., 2011; Tang and Gross, 2003). Cell migration in scratch assays is regulated through EGFR signaling among many other pathways (Magi et al., 2012). *In vitro* data shows that F-actin interaction with EGFR strongly decreases EGFR phosphorylation (Tang and Gross, 2003). Actin cytoskeleton proteins are responsible for decreased diffusion of EGFR dimers (Low-Nam et al., 2011) and influence EGFR internalization (Fiori et al., 2009).

According to the BioID data, MacroD2 interacts with proteins involved in EGFR signaling (EPS15R, Crkl, CrkII, GAPVD1, Filamin A, and PAK2/3; as shown in table A.1). Of the MacroD2 interactors involved in EGFR signaling, the EGFR signaling transducers PAC2/3 and the skeletal protein Filamin A were shown to be involved in cell migration (Ye and Field, 2012; Yue et al., 2013). Therefore, I investigated if EGFR-induced cell migration is affected in any of the knockout cell lines. Treatment of cells with low amounts of EGF should result in increased migration speed compared to untreated cells due to the chemotactic effect of the growth factor (Roussos et al., 2011; Van Haastert and Devreotes, 2004; Wang, 2009).

Cell migration of wild-type cells increases significantly in EGF-treated cells over untreated wild-type cells. The increase in migration for EGF-treated TARG1 knockout cells over untreated cells is comparable and as significant as the increase in wild-type cells. For MacroD2 knockout and double knockout cells, however, this increased migration is less pronounced and less significant. This indicates that cells lacking MacroD2 do not increase migration sufficiently upon EGF treatment.

In summary, this experiment supports the hypothesis that the lack of MacroD2 decreases the ability of cells to increase migration upon stimulation and explains why MacroD2 knockout cells did not migrate slower than wild-type in untreated/unstimulated conditions. Double knockout cell lines exhibit decreased migration in unstimulated conditions and additionally do not react to stimulation sufficiently.

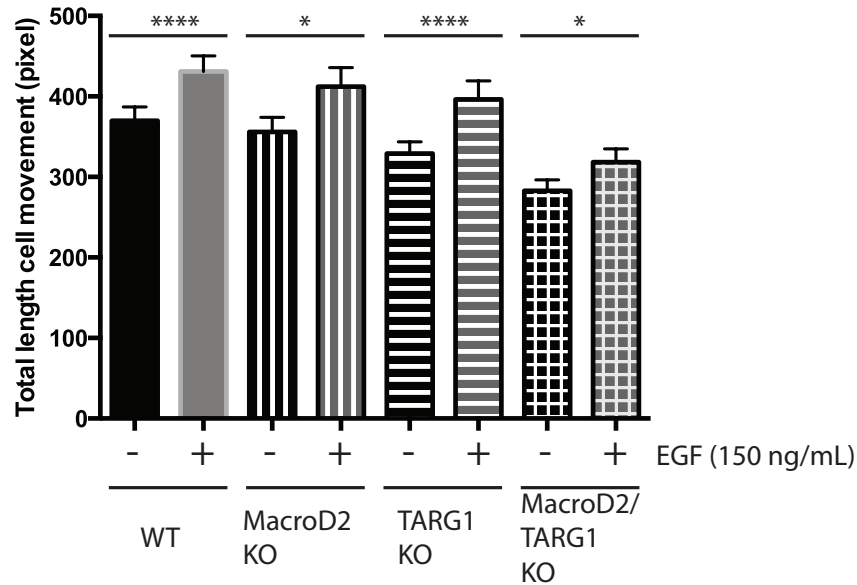


Figure 3.21: MacroD2 knockout and double knockout cells do not induce cell migration sufficiently upon EGF-stimulation. EGF-induced cell migration. Cell migration assay was performed as in fig. 3.19. Cells were seeded in Leibowitz medium containing 150 ng/mL EGF and imaged and analyzed as previously described and depicted in figure A.4. Statistics with GraphPad Prism 7.0 using a Kruskal-Wallis test.

MacroD2 and TARG1 influence EGF-stimulated internalization and nuclear localization of EGFR

Most of the interactors of MacroD2 identified with the BioID approach which were involved in EGFR signaling, i.e. EPS15R, Crkl, CrkII, GAPVD1, and Filamin A are connected to EGFR internalization in literature (Benmerah et al., 1995; Birge et al., 1992, 2009; Carbone et al., 1997; Fiori et al., 2009; Thalappilly et al., 2010). To investigate if EGFR internalization is changed in any of the cell lines lacking MacroD2 and/or TARG1, all cell lines were treated with EGF for various time frames and the localization of EGFR was visualized with immunofluorescence experiments. According to literature and as depicted in figure 1.7, EGF stimulation leads to activation of EGFR and subsequent internalization in clathrin-dependent or -independent endocytosis. EGFR can get recycled back to the plasma membrane or get degraded in lysosomes (for review see ref. (Haglund and Dikic, 2012)). Apart from recycling and degradation, EGFR can get transported through the Golgi and ER into the nucleus and function as a transcription co-factor for, e.g., Cyclin D (for review see refs. (Brand et al., 2011; Lo and Hung, 2006)).

Representative stainings for EGFR in untreated cells, after 30, and after 120 minute EGF treatment in all used cell lines are depicted in figure 3.22. Untreated wild-type cells show cytoplasmic and nuclear EGFR staining. Upon 30 minute EGF treatment, the EGFR staining is localized to cytoplasmic foci present throughout the cytoplasm. Similar staining

patterns were observed for HeLa and two bladder carcinoma cell lines (TCCSUP, 253J) in untreated and EGF/HF-EGF treated conditions (Kim et al., 2007; Villaseñor et al., 2015). After 2 hour treatment with EGF the staining pattern for EGFR closely resembles the staining pattern of untreated cells.

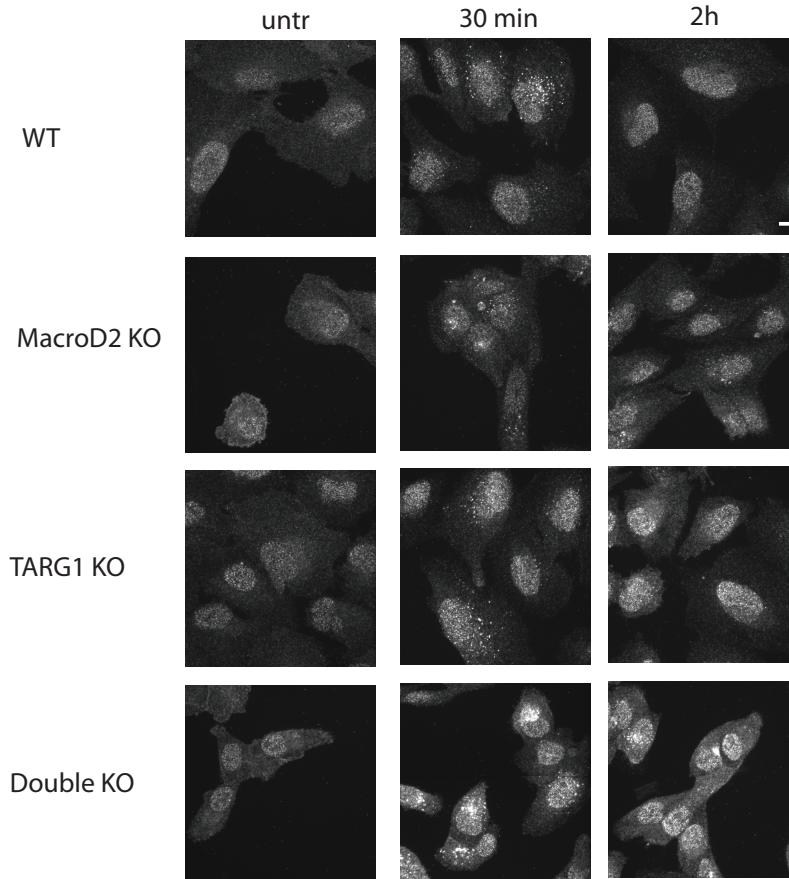


Figure 3.22: Double knockout cells show clusters of EGFR upon EGF-treatment in the peri-nuclear area. EGF-stimulated internalization of EGFR at 30 minute incubation, 2 hour incubation, and in untreated cells. Cells were treated for different time intervals with EGF ($2 \mu\text{g}/\text{mL}$). Cells were fixed in 4% paraformaldehyde and stained with anti-EGFR antibody and Hoechst. Representative images from each type of cell line were chosen from three biological replicates.

In both MacroD2 and TARG1 knockout cell lines the EGFR staining resembles the wild-type staining. They show similar nuclear and cytoplasmic staining in untreated conditions and show cytoplasmic foci after 30 minute EGF-treatment, which are not visible after 2 hour EGF treatment. In double knockout cell lines, untreated cells resemble wild-type cells. After a 30 minute EGF treatment they show increased perinuclear accumulation of EGFR foci. The number of perinuclear EGFR foci was quantified using CellProfiler (Carpenter

et al., 2006). In order to quantify perinuclear EGFR staining, I detected nuclei by their Hoechst staining and defined a 30 pixel ring round the nucleus as a proxy for the perinuclear region. I counted the foci in this ring with CellProfiler and plotted the result from three biological replicates as box plots with GraphPad Prism 7.0 (figure 3.23). Double knockout cell lines showed significantly increased numbers of perinuclear EGFR foci over wild-type and both single knockout cell types.

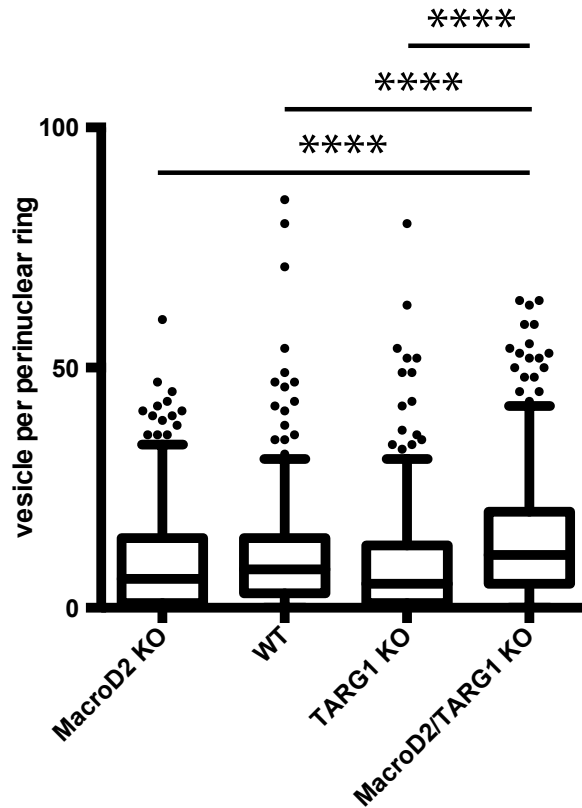


Figure 3.23: Perinuclear EGFR foci after 30 minute EGF treatment are significantly enriched in double knockout cell lines. Quantification of perinuclear EGFR foci after 30 minute EGF ($2 \mu\text{g}/\text{mL}$) treatment. Cells from three biological replicates were analyzed for their number of perinuclear EGFR foci with CellProfiler. Nuclei were detected with Hoechst staining. A ring around the nucleus was drawn with 30 pixel distance from the nucleus as a proxy for the perinuclear region. EGFR foci in the perinuclear ring were counted per cell. Results were plotted in box plot with Tukey error bars with GraphPad Prism 7.0. Statistics were calculated using the Kruskal-Wallis test.

To investigate whether the increased perinuclear EGFR accumulation impairs nuclear transport of EGFR, I measured the nuclear intensity of EGFR in untreated and 30 minute EGF-treated cell lines with CellProfiler. The increase in nuclear EGFR upon EGF

treatment compared to untreated cells is comparable in all types of cell lines (figure 3.24). This data collectively indicates that double knockout cells show deregulations in response to EGF treatment - they do not increase migration sufficiently and show increased perinuclear clumping of EGFR-containing vesicles. The increase in perinuclear EGFR does, however, not correlate with defects in nuclear translocation of EGFR.

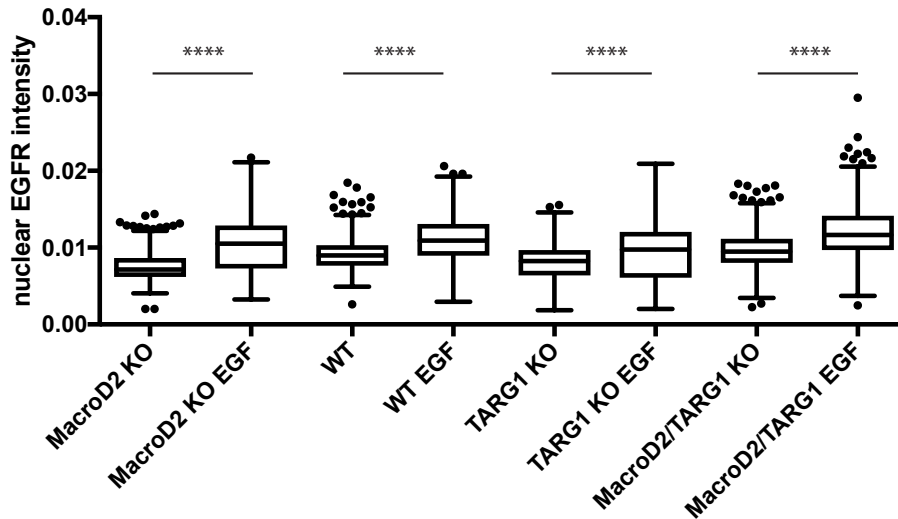


Figure 3.24: The increase in nuclear EGFR intensity upon 30 minute EGF-treatment is comparable in all wt and knockout cell lines. Quantification of nuclear EGFR intensity. Nuclear EGFR intensity was quantified with CellProfiler in untreated and 30 minute EGF-treated cells from three biological replicates. Results were plotted in box plot with Tukey error bars with GraphPad Prism 7.0. Statistics were calculated using the Kruskal-Wallis test.

Rescue experiments of perinuclear EGFR accumulation with MacroD2, a non-ADP-ribose binding mutant of MacroD2, and TARG1

To investigate if the observed increased perinuclear accumulation of EGFR in double knockout cell lines is indeed due to the lack of both proteins, I expressed either GFP-tagged MacroD2 or GFP-tagged TARG1 in all double knockout cell lines. After transfection I performed immunofluorescence experiments after 30 minute EGF treatment. I could show in a small scale experiment that the amount of perinuclear EGFR after a 30 minute EGF treatment is dramatically reduced in cells expressing GFP-MacroD2 while all untransfected (GFP-negative) cells still show perinuclear accumulation of EGFR, as depicted in figure 3.25. This shows that the accumulation of EGFR may be due to the lack of MacroD2.

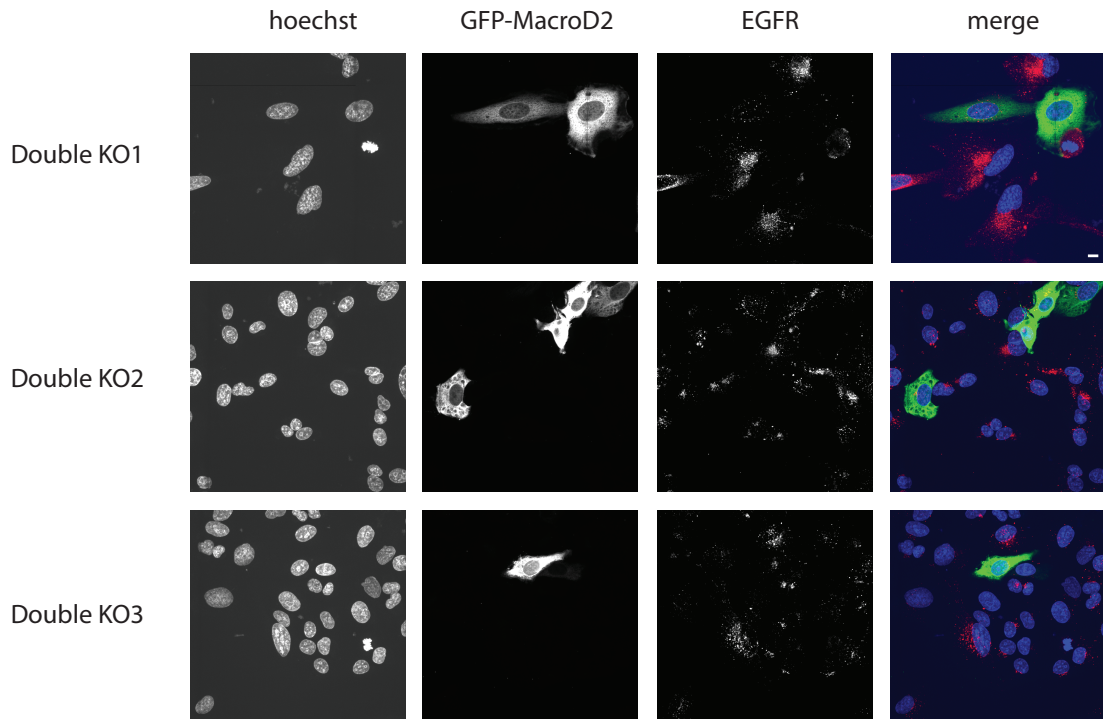


Figure 3.25: GFP-MacroD2 can reduce perinuclear EGFR accumulation upon EGF treatment in all double knockout cell lines. Re-expression of GFP-tagged MacroD2 in all three double knockout cell lines. All double knockout cell lines were transfected with GFP-MacroD2. The next day the cell lines were treated with EGF, fixed in methanol, and stained with antibodies against GFP and EGFR. Nuclei were Hoechst stained.

Since the expression of MacroD2 was able to decrease the perinuclear EGFR accumulation in double knockout cell lines, I wanted to investigate if may stems from the enzymatic activity of MacroD2. Therefore, I transfected a GFP-tagged mutant MacroD2 (G188E), which can not bind to ADP-ribose (Jankevicius et al., 2013), in a small scale experiment. In double KO1 and double KO2 cell lines, most GFP-positive cells still showed comparable

perinuclear EGFR staining to untransfected cells. In double KO3, however, the only transfected cell in the field does not show any perinuclear EGFR, while all untransfected cells do. Taken together this indicates that the enzymatic function of MacroD2 is important for EGFR internalization.

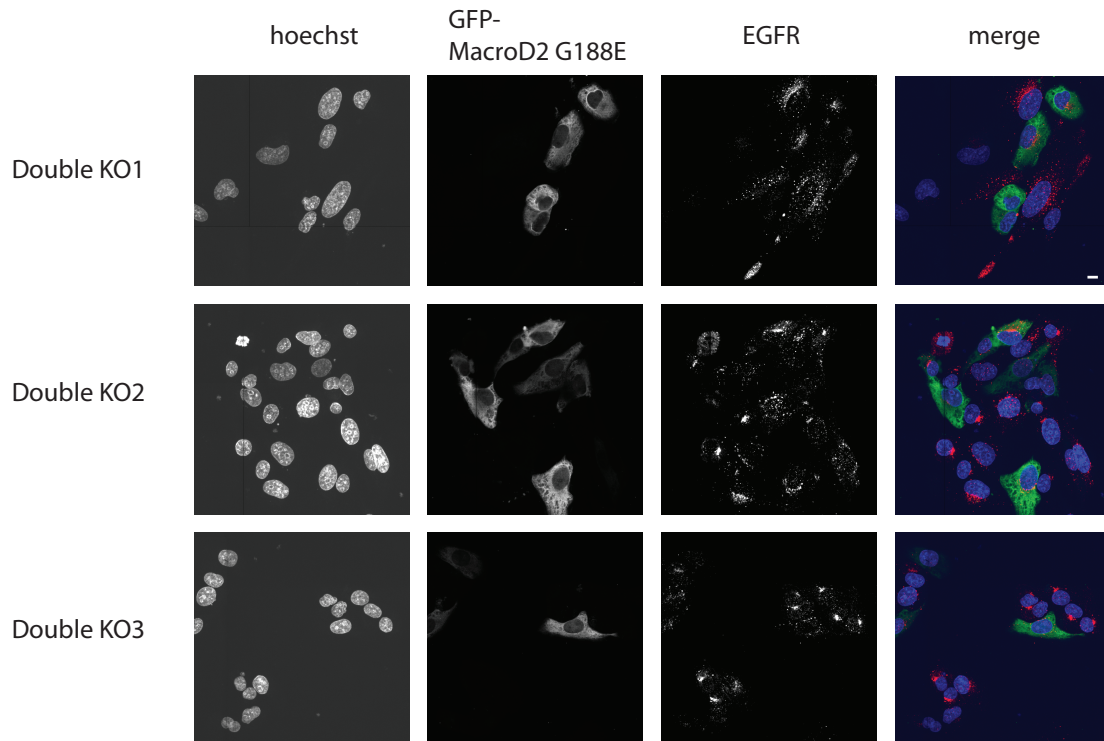


Figure 3.26: GFP-MacroD2 G188E, a non-ADP-ribose binding mutant, does not reduce perinuclear EGFR accumulation upon EGF treatment in all double knockout cell lines. Re-expression of none-ADP-ribose binding GFP-tagged MacroD2 G188E in all three double knockout cell lines. All double knockout cell lines were transfected with the non-binding mutant GFP-MacroD2 G188E. The next day the cell lines were treated with EGF, fixed in methanol, and stained with antibodies against GFP and EGFR. Nuclei were Hoechst stained.

In figure 3.27 I performed the same small scale experiments as in figure 3.25 but transfected GFP-TARG1 in all double KO cell lines. In this experiment the amount of perinuclear EGFR was drastically reduced in GFP-TARG1 transfected double knockout cell line 1 (double KO1) and double knockout cell line 3 (double KO3) cells, while all untransfected cells of these cell lines showed increased perinuclear EGFR accumulation. In double KO2 cells there was only a single, very weakly transfected cell present. A decrease of the observed phenotype of perinuclear accumulation of EGFR was not detectable in this cell. The results indicate that the expression of TARG1 in the double KO cells results in decreased perinuclear EGFR after a 30 minute EGF treatment.

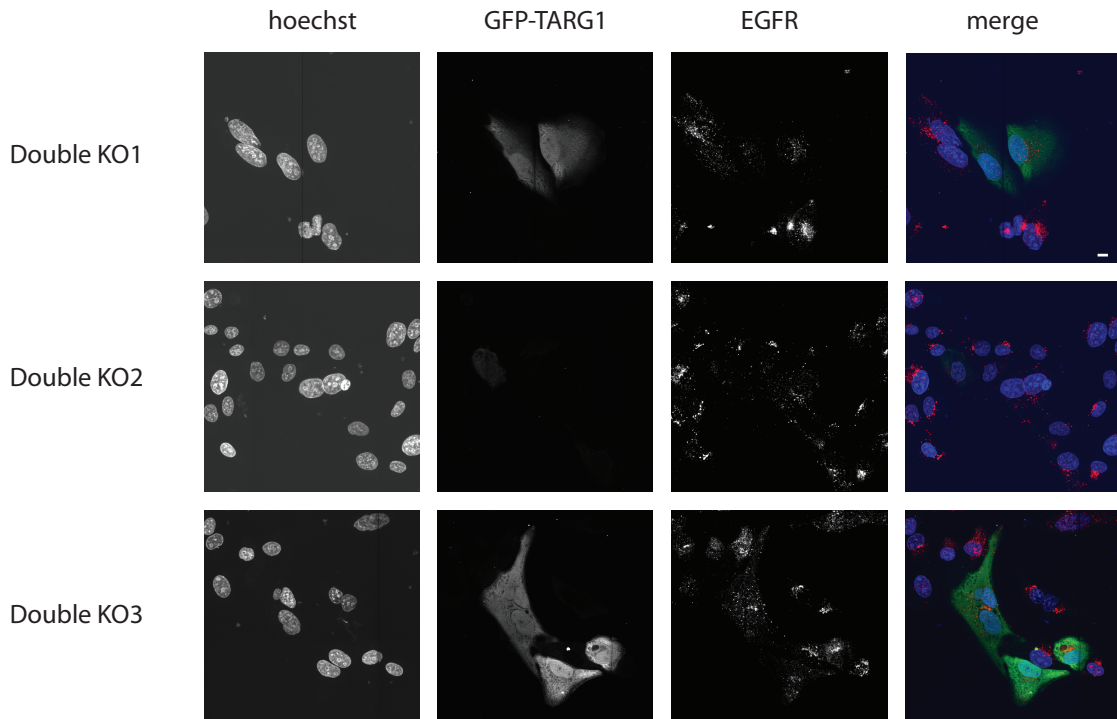


Figure 3.27: GFP-TARG1 does reduce perinuclear EGFR accumulation upon EGF treatment in double knockout cell lines. Re-expression of GFP-tagged TARG1 in all three double knockout cell lines. All double knockout cell lines were transfected with GFP-TARG1. The next day the cell lines were treated with EGF, fixed in methanol, and stained with antibodies against GFP and EGFR. Nuclei were Hoechst stained.

In summary, these small scale experiments indicate that the increased perinuclear accumulation of EGFR in all double knockout cell lines stems from the loss of both proteins. Additionally, this implies that MacroD2 and TARG1 perform redundant functions in the internalization of EGFR upon EGF treatment since the presence of a single protein can compensate for the loss of the other protein. Furthermore, the finding that a none-ADP-ribose binding mutant of MacroD2 was not able to decrease the perinuclear EGFR accumulation, suggests that this phenotype is dependent on MacroD2 binding and most likely removing ADP-ribose from target proteins.

Chapter 4

Discussion

So far not much is known about the cellular functions of MacroD2 and TARG1 in human cells, apart from a strong indication that both might be involved in the response to DNA damage (Golia et al., 2017; Jankevicius et al., 2013; Sharifi et al., 2013). Since both proteins are localized to the same cellular compartments and perform the same reaction (removing acidic amino acid linked mono-ADP-ribose from target proteins), it is unknown to which extent both enzymes are redundant.

The goal of my thesis was to identify cellular functions of MacroD2 and TARG1 in unstressed cells. To address the function of both enzymes, I used a two-pronged approach. I identified transient protein interaction partners of MacroD2 with the BioID system and investigated possible functions which arise due to interactions with proteins from specific gene ontology (GO) terms with their corresponding loss-of-function phenotypes in MacroD2, TARG1, and double knockout cell lines, i.e. if MacroD2 interacts with many proteins from one GO term I would screen in MacroD2 knockout cells if this cellular process was compromised.

4.1 MacroD2 and TARG1 possess redundant functions in regulating the actin cytoskeleton - most likely through modulating EGFR signaling

4.1.1 Summary

In order to investigate the function of both enzymes in unstressed cells, I identified interaction partners of MacroD2 with the BioID system. This approach allows the identification of weak and transient interactors. Proteins significantly enriched in cells expressing the MacroD2 fusion protein over both control cell lines (expressing the biotin ligase BirA only, and wildtype HEK Trex cells) were used to calculate gene ontology-term networks with the Cytoscape plugin ClueGO (Bindea et al., 2009). This network revealed that MacroD2 interacts, among others, with many proteins belonging to the actin cytoskeleton and focal

adhesions as depicted in figure 3.8.

In order to study if potential phenotypes hypothesized from the BioID data are present in cells lacking MacroD2 and/or TARG1, I generated cells lacking either one or both of the proteins with CRISPR/Cas9 and validated the absence of the corresponding gene at DNA and protein level.

Based on GO-terms from the BioID assay, I formulated the hypothesis that MacroD2 and possibly TARG1 regulate the actin cytoskeleton in human cells. With the use of xCelligence (description in figure A.3), which measures attachment and proliferation directly through impedance changes, I could show that MacroD2/TARG1 double knockout cells attach significantly slower than wild-type cells (figure 3.17). Both single knockout cells did not show an attachment defect. This was a first hint that MacroD2 and TARG1 might be redundant in their role in regulating the actin cytoskeleton, since either protein compensated for the loss of the other in cell attachment. To investigate additional potential functions of MacroD2 and TARG1 which depend on the actin cytoskeleton and actin dynamics, I investigated cell migration. I tracked single cells for one day and quantified the total length of cell movement for all knockout and wildtype cell lines. The quantification of the total length of cell movement is depicted as a box plot in figure 3.19 and shows that MacroD2 knockout cells migrate the same length as wild-type cells. TARG1 knockout cells showed a small but significant decrease in cell migration over wild-type cells. Double knockout cells had a very pronounced and significant cell migration defect.

Based on the experiments I performed, the question still remained how the actin cytoskeleton was deregulated in knockout cells. Epidermal Growth Factor Receptor (EGFR) was shown to influence migration in scratch assays and to generally regulate the actin cytoskeleton which is the basis for cell attachment and migration (Magi et al., 2012; Oda et al., 2005). Additionally, it was also shown that EGFR is regulated through actin cytoskeletal proteins indicating a tight and ever increasing link between EGFR signaling and the actin cytoskeleton (Ohashi et al., 2011; Tang and Gross, 2003). The hypothesis that MacroD2 influences the actin cytoskeleton through EGFR signaling is further supported by the BioID results, since MacroD2 - apart from interacting with a multitude of actin binding proteins - was shown to interact with proteins involved in EGFR signaling (EPS15R, Crkl, CrkI, GAPVD1, filamin A) A.1.

Therefore I investigated if cells lacking MacroD2 and/or TARG1 would increase their migration upon Epidermal Growth Factor (EGF) stimulation in the previously described 96-well migration assay. As depicted in figure 3.21, wild-type cell lines as well as TARG1 knockout cell lines showed strongly and significantly increased migration upon stimulation compared to unstimulated cells. MacroD2 knockout cells, as well as double knockout cells to a higher extent, did not show increased migration to the same extent as wild-type cells upon stimulation with EGF. This shows that MacroD2 is important for EGF-stimulated cell migration and leads to the question if and how EGFR signaling is deregulated in cells lacking MacroD2 alone or in double knockout cell lines.

EGF stimulation activates the EGF receptor which is internalized and either recycled back to the plasma membrane, degraded or transported into the nucleus (schematic representation in figure ??; (Brand et al., 2011; Haglund and Dikic, 2012; Lo and Hung, 2006;

Madshus and Stang, 2009)). Therefore, I investigated how EGFR localization would change in all cell lines upon EGF treatment with immunofluorescence experiments. In untreated wild-type cells I saw strong cytoplasmic and nuclear signal for EGFR. Upon 30 minute treatment most signal is present in foci in the cytoplasm which are no longer visible after 2 hour treatment. This staining pattern is very similar to staining patterns of other cancer cell lines e.g. HeLa (Villaseñor et al., 2015). TARG1 knockout cell lines showed a very similar staining pattern to wild-type cell lines. In MacroD2 knockout cells and to a much stronger extent in double knockout cells, these foci are all clustered close to the nucleus, in the perinuclear region, 30 minutes after EGF treatment (figure 3.22). The number of EGFR foci was quantified in a perinuclear ring using CellProfiler (Carpenter et al., 2006) for all cell lines. The quantification shows a significant increase of perinuclear EGFR foci in double knockout cells compared to all other cell lines after 30 minute EGF treatment. This indicates that the internalization of EGFR is somehow deregulated in cells lacking both MacroD2 and TARG1. The conclusion that the observed EGFR internalization defect in double knockout cells stems from the lack of both proteins needs to be validated with further experiments. To this end, I set up a small scale rescue experiment where I expressed either GFP-tagged MacroD2 or GFP-tagged TARG1 in all three double knockout cell lines. When I expressed GFP-MacroD2 in all cell lines, I could show that the perinuclear EGFR accumulation after 30 minute EGF treatment was not present in transfected cells but still very pronounced in all untransfected cells (figure 3.25). The same was true when I expressed GFP-TARG1 in all three cell lines (figure 3.27). These findings need to be repeated in large scale experiments in order to ensure their validity and to be able to quantify the decreased perinuclear EGFR accumulation.

In summary, these experiments indicate that the lack of MacroD2 and TARG1 simultaneously result in deregulated EGFR internalization. This loss-of-function phenotype can be alleviated if either of the proteins is expressed in the cells. This indicates two things: firstly, the lack of both proteins and not possible defects in the cells induced with the CRISPR/Cas method is the reason for EGFR deregulation. Secondly, both proteins can alleviate the observed phenotype and are therefore redundant in their function in EGFR internalization.

With the indication that the lack of MacroD2 and TARG1 results in EGFR internalization defects, it is still unknown how their lack induces this phenotype. Therefore, I wanted to address if the deregulation of EGFR internalization was due to the enzymatic function of MacroD2 and TARG1 - de-ADP-ribosylating target proteins. To this end, I expressed the non-ADP-ribose binding mutant of MacroD2 (G188E) (Jankevicius et al., 2013) in all three double knockout cell lines. In figure 3.26 it becomes clear that transfected cells show undistinguishable amounts of perinuclear EGFR from untransfected cells. This indicates that the enzymatic activity of MacroD2 is essential for the reversal of the phenotype. Same as for the rescue experiments with MacroD2 and TARG1, this assay needs to be repeated in a large scale in order to validate the experiments and to enable quantification of perinuclear EGFR.

In summary, cells lacking both MacroD2 and TARG1 have defects in cell migration and attachment. Both functions depend on the reorganization of the actin cytoskeleton.

Furthermore, double knockout cell lines do not increase migration sufficiently upon EGF stimulation. These findings indicate that MacroD2 and TARG1 have important functions in actin organization and might influence the actin cytoskeleton through EGFR signaling. To investigate which step of the EGFR signaling pathway is deregulated in double knockout cell lines, I addressed the localization of EGFR upon stimulation. I observed an increase in perinuclear EGFR after 30 minute EGF treatment (summarized in figure 4.1). This indicates that double knockout cells have a defect in EGFR internalization. The lack of a single protein either had no or very mild defects in actin regulated functions as well as EGFR signaling, indicating that both enzymes can compensate for each other to a certain degree.

4.1.2 Outlook

Future avenues to find the molecular mechanism behind the EGFR-mediated actin defects in double knockout cells

Even though I was able to show that MacroD2 and TARG1 have redundant functions in actin regulated processes, the response to EGFR, and EGFR internalization, there are still many unaddressed questions. Cells lacking both MacroD2 and TARG1 have defects in cell migration and attachment and do not increase migration sufficiently after EGF stimulation. However, I was not able to show that this is due to the lack of both enzymes. This has technical reasons. Firstly, xCelligence, which was used to measure cell attachment and proliferation directly based on impedance changes, is a method which is very sensitive to changes in cell number and cell health. For this reason I decided against re-transfecting MacroD2 or TARG1 in the knockout cells in this assay, as well as using a knockdown of e.g., filamin A (FLNA, for review see (Yue et al., 2013)) as a positive control in xCelligence measurements. Secondly, migration assays necessitate the plating of very few, un-clumped cells. Cells in this cell density cannot be transfected directly (trial transfections with Xfect (clontech) and FuGene (Promega)). To circumvent this problem, I transfected cells at a higher density and tried to re-plate them in low density. This trial failed due to much increased cellular clumping leading to no or very few single cells. For this reason, I used PiggyBac Transposon system vectors (systembio) to express MacroD2 or TARG1 inducibly and titratably as well as GFP from an IRES site. However, due to increased vulnerability stemming most likely from severe attachment defects I was so far not able to generate stable double knockout cell lines expressing either MacroD2 or TARG1 from integrated PiggyBac vectors, since no cell survived the strain of FACS sorting. If the cell lines can be generated, it will be important to show that the attachment, migration, and EGF-stimulation defects stem from the lack of the knocked out proteins and not from potentially present off-target effects. The rescue experiment of the internalization assay of EGFR was performed in a small scale and should be repeated in a big scale to ensure quantification of perinuclear EGFR.

The hypothesis that MacroD2 and TARG1 regulate the dynamic actin cytoskeleton also needs further investigation. The finding that double knockout cells attach worse and

4.1 MacroD2 and TARG1 possess redundant functions in regulating the actin cytoskeleton - most likely through modulating EGFR signaling 71

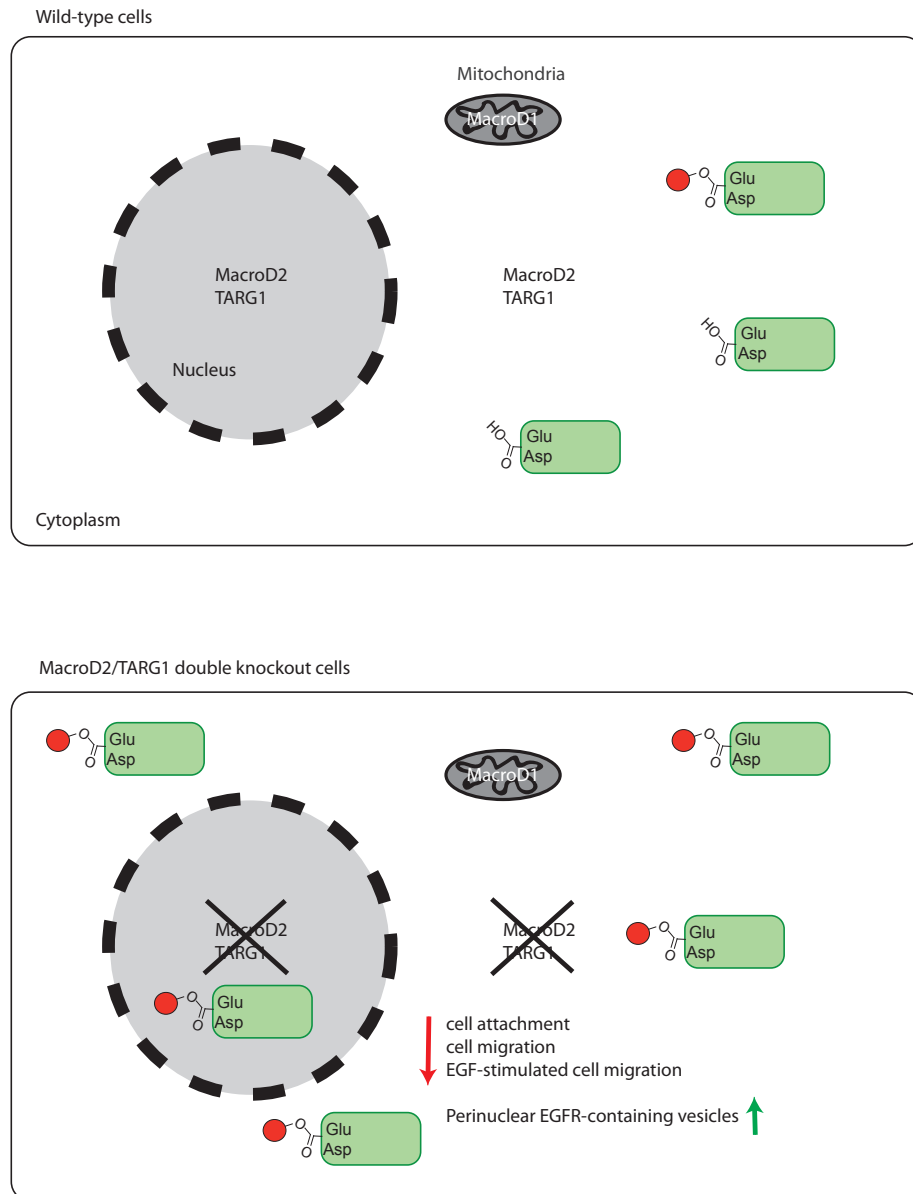


Figure 4.1: Double knockout cell lines exhibit decreased cell attachment, migration and EGF-stimulated cell migration accompanied by an increase in perinuclear EGFR. MacroD2 and TARG1 are localized to the nucleus and cytoplasm while MacroD1 is expressed exclusively in mitochondria. MacroD1, MacroD2, and TARG1 remove mono-ADP-ribose proteins only when ADP-ribose is linked to the protein via acidic amino acids. In double knockout cells the amount of mono(ADP-ribosyl)ated target proteins is increased. Double knockout cells have decreased cell attachment, migration and EGF-stimulated migration. Furthermore, the show increased perinuclear EGFR containing vesicles.

migrate slower would indicate that the focal adhesions necessary for both processes might be weakened. However, in immunofluorescence staining of already attached, fixed cells I could not see any defects in focal adhesion location or size. In order to address if this issue is only present in attaching and actively migrating cells, cells need to be transfected with either fluorophore-coupled liveact (an actin binding peptide) or actin together with a tagged focal adhesion protein such as vinculin or zyxin. This would show if there are defects in focal adhesion maturation necessary for proper cell attachment in live cells. With transfection with the same plasmids it would be possible to image migrating cells and to assess the size and location of focal adhesions and the reorganization of the actin cytoskeleton. With both assays the presence of lamellipodia (small membrane protrusions) and filopodia (finger-like big membrane protrusions) could be investigated and quantified. Both structures can be differentiated by their morphology and how their actin components are organized (lamellipodia have branched actin networks, filopodia have parallel actin fibers). For further investigation of these structures, we could further test for possible defects with additional immunofluorescence experiments with structure specific component analysis, e.g. quantify the expression of cofilin and filamins in lamellipodia (Blanchoin et al., 2014; Revenu et al., 2004).

Additionally, we do not know if the defects in cell migration and attachment stem from the enzymatic function of both enzymes. If the defects result from hindered removal of ADP-ribose from proteins, it is important to prove that their enzymatic functions are necessary and to additionally investigate which enzyme adds those moieties to target proteins to gain a deeper knowledge of the whole signaling cascade. A simple solution to the question which identified interactors of MacroD2 interact with MacroD2 due to the fact that those are target proteins that MacroD2 de-ADP-ribosylates is to repeat the BioID experiments with a non-ADP-ribose binding mutant of MacroD2 (G188E). Proteins interacting with MacroD2 due to its enzymatic function should not be present in pulldowns with the non-binding mutant. To address which enzyme might add ADP-ribose to MacroD2s target proteins, it is necessary to see which ADP-ribose polymerase works in the same pathways as MacroD2. A possible candidate protein which might add ADP-ribose to MacroD2s target proteins is PARP14. It was shown that PARP14, a MARylating PARP, co-localizes with identified targets of MacroD2: focal adhesion proteins (vinculin, vasp, and paxillin) (Vyas et al., 2013). Vinculin itself is an identified interactor of MacroD2, involved in cell migration (Hotulainen and Lappalainen, 2006) and ADP-ribosylated according to the ADPrigoDB (Vivelo et al., 2017). I would therefore suggest to knock down PARP14 in the double knockout cells and to investigate if both the attachment and migration defects diminish once the polymerase adding MAR is removed. As an alternative approach one could overexpress PARP14 in wild-type cells and observe if migration and attachment are affected in the same manner as in the double knockout cells. This would support the hypothesis that an excess of MAR on target proteins involved in actin regulated processes results in a deregulation of those.

So far I was able to show that in double knockout cells not only actin regulated processes are deregulated but the response to EGF is changed, too. It is, however, not clear how the response to EGF is altered. I showed that the response to EGF in migration is diminished

and EGFR internalization is altered. To strengthen these results further, filamin A could be used as a positive control in both assays and will be used by my supervisor Gyula Timinszky in further work on the project. Cells' migratory response to EGF stimulation is reduced in FLNA's absence and FLNA is an important factor in EGFR internalization (Fiori et al., 2009). The reduced migration in response to EGF in double knockout cells, however, might stem from many steps in the vast signaling network surrounding EGFR. Firstly, it would be important to know what number of receptors are present in knockout cells in unstimulated and EGF-stimulated conditions and compare the results to wild-type cells in the same conditions. Overexpression of EGFR is a common cause for various cancer types such as colon, brain and breast (Brand et al., 2013; Scaltriti and Baselga, 2006) and is therefore an interesting avenue to pursue. These findings might also shed light on the yet unidentified reason behind the correlation between MacroD2 and cancer (breast (Mohseni et al., 2014) and colon (Briffa et al., 2015; Rajaram et al., 2013; van den Broek et al., 2015)). Apart from the number of EGFR receptors, it needs to be investigated if the ratio of receptors on the plasma membrane to internalized receptors is changed. This could be investigated with FACS analysis of permeabilized and unpermeabilized cells, as performed in previous publications (Brockhoff et al., 1994; Grøvdal et al., 2004). In this analysis, cells are fixed with or without activation with EGF and stained with EGFR-antibody with or without permeabilization. Without permeabilization only plasma-membrane bound receptors will be detected, with permeabilization both external and internal EGFR will be detected.

Additionally to receptor location and abundance, it would be important to assess if the receptor activation by autophosphorylation and the activated receptor localization is altered. This can be done with the previously described FACS assay with the distinction of the use of a phospho-specific EGFR-antibody. Analysing how many receptors are activated and where activated receptors are localized in cells lacking MacroD2 and/or TARG1 would give us insight into the question if the removal of ADP-ribose from target proteins involved in EGFR activation or localization causes the defects in the response to EGFR in cell migration observed in this thesis. Aberrant activity of EGFR is a long known key player in the development and growth of tumor cells and might explain the correlation between MacroD2 mutations and cancer (Briffa et al., 2015; Mohseni et al., 2014; Rajaram et al., 2013; van den Broek et al., 2015).

Apart from defects in the number or activity and location of EGFR it is very important to address if downstream signaling of EGFR is affected in double knockout cells. Therefore, it would be important to address if the classical signal cascade of EGFR signaling through adaptor proteins to a multitude of pathways such as the MAPK pathway and Akt signaling is deregulated. This can be done with western blots of total downstream proteins and their activated, phosphorylated form, such as MEK1/pMEK1, Akt/pAkt, and PKC/pPKC (Oda et al., 2005). Many downstream signaling pathways of EGFR are very important for cell proliferation and migration and could explain why MacroD2 interacts with proteins connected to actin/focal adhesions and microtubules.

The immunofluorescence assays in all cell lines showed that double knockout cells show clusters of perinuclear EGFR after a 30 minute EGF treatment (figure 3.22). This could not be observed for wild-type cells at any of the chosen time points (untreated, 30, and

120 minute treatment). This raises the question if wild-type cells show perinuclear EGFR clustering at any time point or if this is a specific phenotype only observable in double knockout cell lines. I would suggest to follow EGFR localization in live-cell imaging experiments by using either fluorophore-coupled EGF or fluorescent EGFR with EGF treatment in wild-type cells and double knockout cells. This would show if wild-type cells show perinuclear EGFR clustering at all and if they do so, how this time point compares to double knockout cells, i.e. is EGFR internalization and clustering faster or slower than in wild-type cells. Additionally, it would be interesting to know at which cellular compartments clustered perinuclear EGFR co-localizes. Possible candidates would be endosomes and lysosomes which would indicate a classical internalization defect with increased or decreased receptor degradation which was also observed for filamin A (Fiori et al., 2009), one of the most significant MacroD2 interactors in the BioID screen. Additionally, some proteins involved in EGFR signaling identified with the BioID screen were already shown to be ADP-ribosylated (PAK3, CRK, CTTN, VCL) (Vivelo et al., 2017). Another possibility would be that EGFR is stuck in one of the compartments involved in nuclear transport - the Golgi apparatus or the endoplasmic reticulum. Since I could not observe any changes in the amount of nuclear EGFR in the double knockout cell lines (figure 3.24) this is less likely than the possibility that EGFR accumulates in the perinuclear region in the degradation pathway.

Possible MacroD2 interactors and their ADP-ribosylation status

To address the connection between identified MacroD2 interactors and the observed phenotypes, we need to validate promising interactor candidates of MacroD2. We decided to investigate which pathways are deregulated in the generated knockout cells first, in order to narrow down the list of likely and interesting interactors. Validating the interaction between MacroD2 and interesting candidates could be addressed with pulldown experiments. Good candidate proteins for this type of validation are filamin A - one of the strongest interactors according to BioID data - as well as focal adhesion and EGFR signaling proteins identified in this study. These are very promising candidates since filamin A (Gagné et al., 2008, 2012), some focal adhesion proteins (AHNAK (Gagné et al., 2012), DST (Gagné et al., 2012), MDC1 (Gagné et al., 2012), PRUNE (Feijs et al., 2013b), SRP68 (Carter-O'Connell et al., 2014), TLN1 (Gagné et al., 2012), VIM (Gagné et al., 2012)), and EGFR signaling proteins (PAK3, CTTN (Feijs et al., 2013b), VCL (Gagné et al., 2012)) were reported to be ADP-ribosylated in the ADPriboDB (Vivelo et al., 2017). Pulldown experiments of endogenous MacroD2 would have the advantage that we could exclude overexpression artifacts. Additionally, all pulldown experiments could be performed with endogenous MacroD2, TARG1 and compared to pulldowns from MacroD1 or any PARP family member. This assay would validate the BioID data and address if the observed compensation from MacroD2 and TARG1 stems from interactions with the same set of proteins or from interaction with distinct proteins which are involved in the same cellular pathways.

In case no interactions can be validated with conventional pulldowns of MacroD2 or TARG1 due to the very transient nature of ADP-ribosylation signaling, cross-linking in-

teracting complexes is a possible path to circumvent this caveat. Apart from performing pulldown experiments, the interactions to MacroD2 could be validated with bimolecular fluorescence complementation (BIFC) or fluorescence resonance energy transfer experiments (FRET), both methods are very fast and time resolved and should therefore detect transient interactions.

Apart from validating the interaction between MacroD2 and promising target candidates, it would be very helpful to understand the nature of their interaction. With the use of the BioID system I was able to identify MacroD2 interaction partners. It, however, remains elusive to what extent these interactions stem from the interaction of the macrodomain of MacroD2 with ADP-ribosylated target proteins or if they are independent from its enzymatic function, such as the interaction between ATM and MacroD2 which results in nuclear export of MacroD2 (Golia et al., 2017). This question would be very important to address, however until now there is no method available that detects MARylated proteins in an unbiased approach. This is mainly due to the chemistry of ADP-ribose which is highly charged, heterogenous (true only for PAR chains) and labile. Additionally, ADP-ribose can be attached to multiple amino acids and is a very transient modification (Daniels et al., 2015). Due to the chemistry of ADP-ribose no MAR-specific antibody or detection probe exists. So far, many studies have been performed to identify the human ADP-ribosylome. However, these studies were either PAR specific or did not differentiate between MAR and PAR, and additionally most of the studies were performed in DNA-damaging conditions (Daniels et al., 2015). All studies either used the PAR-specific antibody 10H or ADP-ribose digest product binding chemicals (e.g. boronate affinity capture of hydroxylamine digested ADP-ribosylated proteins) or ADP-ribose binding proteins (e.g. Af151) and did not select for which proteins are PARylated and which are MARylated. These studies show that ADP-ribosylated proteins perform many important cellular functions such as translation, cellular macromolecular complex assembly and DNA damage response (for review see refs. (Daniels et al., 2015; Gupte et al., 2017; Martello et al., 2016)). Serine was recently identified as a new ADP-ribose anchor with a new approach. Instead of enriching ADP-ribosylated proteins with the previously mentioned approaches, the researchers isolated histones to identify ADP-ribosylation sites with a new peptide digestion method - based on filter-aided sample preparation (FASP) - coupled with a phospho-proteomic approach for ADP-ribosylation enrichment and a new peptide detection method to preserve ADP-ribosylated sites (UHPLC-MS/MS with an alternative fragmentation mode (electron transfer dissociation ETD) (Leidecker et al., 2016)).

Apart from studies on the whole ribosylome, new methods were developed to detect target proteins of specific PARPs with a chemical engineering approach. The chemically engineered MARylating PARPs (PARP10 and PARP11) were using a NAD-analog to tag target proteins (Carter-O'Connell et al., 2016).

Due to the lack of MAR-specific antibodies or detection methods, the cellular levels and locations of MAR are still largely unknown. A systematic approach in HeLa cells to identify PARP functions showed with PARP-specific antibodies that while all PARylating PARPs except for the TANKyrases are localized exclusively to the nucleus during the interphase, most MARylating PARPs show both nuclear and cytoplasmic staining with

increased cytoplasmic staining. The only exceptions are PARP3 and PARP11 which are mainly nuclear (Vyas et al., 2013) (for review see ref. (Hottiger, 2015b)). The literature suggests that MARYlated proteins should be present in the cytoplasm as well as the nucleus in unstressed cells.

A possible way to differentiate MARYlated interactors from interactors independent of MacroD2s enzymatic function would be to repeat the BioID experiments with a non-ADP-ribose binding mutant. Proteins which interact with MacroD2 and the non-binding mutant do not depend on ADP-ribosylation, while proteins whose interaction is not present with the non-binding mutant are likely ADP-ribosylated. Candidates identified to be most ADP-ribosylated through their lack of interaction with non-binding MacroD2 should be further investigated.

A study showed that the second and third macrodomain of PARP14 specifically binds to MARYlated target proteins of PARP10 and auto-MARYlated PARP10 *in vivo* and *in vitro* (Forst et al., 2013). In order to formally show that cells lacking MacroD2, TARG1 or both enzymes have increased numbers of MARYlated target proteins, I would suggest detection with GFP-tagged macrodomain two or three from PARP14. In order to perform this assay the GFP-PARP14-macrodomain construct needs to be cloned, expressed in bacteria and purified. With this detection probe MARYlated target proteins of MacroD2 and TARG1 could be observed in immunofluorescence assays. Since this has never been done before, this assay would need to be set up with different cell permeabilization times and solutions to ensure that the detection probes reached the target proteins in the cells. If this assay works out in immunofluorescence assays, I would suggest to address if there are detectable changes in MARYlated proteins upon EGF treatment, e.g. do they co-localize with perinuclear EGFR clusters, actin structures or focal adhesions. This approach could show general MARYlation levels and might indicate what structures are potential targets for MacroD2 or TARG1 but will not show which proteins are MARYlated interactors. With the data gained from BioID experiments I could test specific potential target proteins such as filamin A, EPS15R, vinculin, zyxin with an assay called far-western blot. In far-western blots, protein lysates are separated on PAGE-gels, transferred to nitrocellulose and detected with MAR-binding proteins such as macrodomain three of PARP14. This protein is then detected with antibodies as in western blots. The size of the bands stemming from the MAR-binder could be compared to the size of the protein of interest with reprobing the membrane with a specific antibody. If direct detection of MARYlated proteins yields too many bands for proper analysis, pull-downs with the BioID systems before detection could help decrease band number. With this method the MARYlation status of the interacting proteins could be probed.

4.2 Interesting pathways which MacroD2 and TARG1 might influence

4.2.1 MacroD2 and TARG1 in neuronal function

Both MacroD2 and TARG1 are connected to neurological disorders and proper neuronal function in the literature, as discussed in the introduction in detail. A homozygous mutant of TARG1 was found in patients with severe neurodegeneration (Sharifi et al., 2013) and MacroD2 is connected to neuronal function through its involvement in Kabuki syndrome (Maas et al., 2007), familial schizophrenia (Xu et al., 2009), autism-like disorder (Anney et al., 2010; Frye et al., 2016; Jones et al., 2014), and genetic generalized epilepsy (Mefford, 2016), stroke (Debette et al., 2010), multiple sclerosis (Baranzini et al., 2009), and was shown to influence temporal lobe volume (Kohannim et al., 2012). In the BioID assay, I found GO-terms connecting MacroD2 with neuronal function such as “postsynaptic specialization”, “postsynaptic development”, “dendritic development”, “neuron projection extension”, “axon extension”, and “regulation of axonogenesis”. Because they were not significant they do however not appear in the GO-term network of significant GO-terms (figure 3.8). Proteins belonging to neuronal GO-terms are Shootin1 (SHTN1), Synaptojanin-1 (SYNJ1), Afadin (AFDN), Dystonin (DST), Caldesmon (CALD), neuroblast differentiation-associated protein AHNAK (AHNAK), Cortactin (CTTN), dihydropyrimidinase-related protein 2 (DPYSL2), Drebrin (DBN), CD2-associated protein (CD2AP), serine/threonine-protein kinase PAK2 (PAK2) and PAK3 (see table A.1). In this section I will show how all MacroD2 interactors are connected to neuronal function and how these proteins relate to known functions of MacroD2, TARG1 and ADP-ribosylation.

The analysis of MacroD2s interactors involved in neuronal function shows a high number of proteins to be actin binding proteins - Afadin, Dystonin, Caldesmon, AHNAK, Cortactin, Drebrin, CD2AP. This correlation most likely stems from the fact that the actin cytoskeleton performs important functions in neurons (Cingolani and Goda, 2008; Cooper, 2013; Hotulainen and Hoogenraad, 2010). In the following, I will take a closer look at each actin-binding MacroD2 interactor and its relation to neuronal functions.

Afadin, an actin-binding protein, is best known for its function in cell-cell junctions in polarized epithelia during embryogenesis (Ikeda et al., 1999). Apart from its function in epithelial cells it regulates neuronal function. It was shown to regulate presynaptic differentiation, presynaptic function and puncta adherentia junctions - mechanical adhesion sites between axons and their target dendrites - in hippocampal neurons of mice (Toyoshima et al., 2014). Afadin was further implicated in regulating adherens junction integrity, cell polarity, and mitotic spindle orientation of radial glial cells and thus prevents premature exit from the neurogenic niche (Rakotomamonjy et al., 2017). Additionally, it was shown to maintain the dendritic field, i.e. its architecture and synaptic strength throughout a cell’s lifetime. Perturbations in dendritic fields might be correlated with psychiatric disorders (Srivastava et al., 2012). Two papers mention a possible involvement of Afadin in

schizophrenia (Srivastava et al., 2012; Toyoshima et al., 2014). Schizophrenia is one of the diseases where MacroD2 involvement is under discussion (Xu et al., 2009). An interaction between MacroD2 and Afadin could entail one route to explain its published connections to neuronal disorders.

Dystonin, another actin binding protein, is present in different compartments of neurons, i.e. cell bodies, dendrites, and axons, all of which are rich in F-actin, neurofilaments, and microtubules. It was shown that Dystonin can be trapped with a inactive PARG mutant and should therefore be ADP-ribosylated under genomic stress conditions (Gagné et al., 2012). It was shown that Dystonin is essential for maintaining neuronal cytoskeletal integrity without being required for neuronal morphology (Dalpé et al., 1998). In mice a phenotype with severe movement disorder and neuron degeneration was observed due to Dystonin mutation (Young and Kothary, 2007). These phenotypes resemble phenotypes of patients with Kabuki syndrome which entails skeletal anomalies and mental retardation. A 250 kb *de novo* microdeletion of MacroD2 was observed in a patient with Kabuki syndrome (Maas et al., 2007). Additionally, a case report was published in which a boy with mild-to-moderate autism spectrum disorder - autism spectrum disorder refers to a group of neurodevelopment disorders - was diagnosed due to speech and fine motor delays and repetitive behavior. The boy had a 633 kb deletion in the MacroD2 gene without showing any other causes for autism spectrum disorder such as neurologic, metabolic or nutritional disorders (Frye et al., 2016). This study claimed for the first time that MacroD2 is not merely associated with autism like traits but might be causative for autism spectrum disorder.

Caldesmon, a calmodulin binding protein, regulates the actin cytoskeleton by inhibiting myosin ATPase activity (Pritchard and Moody, 1986). Caldesmon and a tropomyosin isoform were identified in rat neuronal growth cones which were previously shown to be regulated by intracellular calcium ions (Kira et al., 1995). These findings and the possible interaction with MacroD2 tie neuronal function to actin deregulation.

AHNAK or Desmoyokin is a giant (700 kDa) scaffolding nucleoprotein with many identified but very diverse functions including but not limited to its involvement in the formation of the blood-brain barrier, cell contact zones, cell migration, DNA repair, and muscle membrane repair. It is involved in actin cytoskeleton remodeling. AHNAK was identified to be ADP-ribosylated under genotoxic stress conditions (Gagné et al., 2012). A study from 2015 connects AHNAK for the first time with neurogenesis *in vivo*. In this study, AHNAK deficient mice showed both increased cell proliferation through increased BrdU and PCNA staining and adult hippocampal neurogenesis (Shin et al., 2015). AHNAKs function in neurogenesis and its role in actin remodeling further support the emerging theme that actin reorganization is important for neuronal function.

Cortactin is an F-actin binding protein and a Src substrate connecting actin rearrangement with tyrosine kinase signaling. Cortactin is involved in filopodium and lamellipodium formation in response to growth factor receptor activation and was shown to be involved in receptor mediated endocytosis of EGFR. It is an actin nucleation factor whose function is regulated by phosphorylation and acetylation. Cortactin is phosphorylated by PAK, another MacroD2 interactor (see table A.1) and deacetylated by sirtuins (Daly,

2004; MacGrath and Koleske, 2012; Schnoor et al., 2018) which are intricately involved in ADP-ribosylation signaling. Cortactin interacts with PAK in a phospho-dependent manner and their interaction is involved in human platelet lamellipodia spreading (Vidal et al., 2002). Cortactin was identified to be a substrate of PARP14 in a protein microarray experiment. Since PARP14 MARylates its target proteins, Cortactin is likely MARylated (Feijs et al., 2013b). Current publications connect Cortactin to neuronal defects. Alzheimer disease correlates with decreased synaptic plasticity due to impaired modification and turnover of the actin cytoskeleton which in turn is regulated by Cortactin (Mota et al., 2014). Additionally, in mice Sirt1 is necessary for Cortactin deacetylation. Deficient mice show hypogonadotropic hypogonadism due to impaired migration of specific gonadotropin-releasing hormone expressing neurons (Di Sante et al., 2015). Furthermore, the interaction between Cortactin and core components of the postsynaptic density Shank scaffold proteins permits dynamic regulation of synapse morphology and function via remodeling of the actin cytoskeleton (MacGillavry et al., 2016). Cortactin as well as Synaptojanin 1, another identified MacroD2 interactor, is involved in neuronal function and was also implicated in EGFR endocytosis. Cortactin not only connects MacroD2 with neuronal functions but with EGFR endocytosis as well, providing a potential route to explain the observed connection between neuronal function and EGFR signaling and actin remodeling found in this thesis.

Drebrin (developmentally regulated brain protein), an actin-binding protein, is important for axon and dendrite growth cones, synaptogenesis, as well as neuron migration through its modulation of F-actin properties (changes in helical pitch of F-actin, slower treadmilling and decreased depolymerization). In the brain of Alzheimer's disease patients Drebrin disappears from dendritic spines. Apart from Drebrin's function in the brain, it was connected with actin-regulated processes such as cell migration and spermatogenesis (for review see ref. (Shirao et al., 2017)).

CD2AP (Cortactin-CD2-associated protein or Cas ligand with multiple Src homology 3 domains (CMS)) is an adaptor protein connecting membrane proteins, e.g. focal adhesion proteins, with the actin cytoskeleton and is involved in the regulation of the actin cytoskeleton (Kirsch et al., 1999). It further connects actin rearrangements with EGFR receptor internalization which improves our understanding of how growth factors regulate rearrangements of the actin cytoskeleton at the protein level (Lynch et al., 2003). Polymorphisms of the protein are associated with late-onset Alzheimer's disease which might stem from its interacting neurotrophin signaling proteins which control growth of non-injured axons and long-range signaling endosomes. Furthermore, CD2AP was increased in neurons during collated sprouting and decreased in injured neurons (Harrison et al., 2016). It was further shown that it polarizes endosomes in dendrites and axons (i.e. it keeps amyloid precursor protein (APP) and beta-site APP cleaving enzyme 1 (BACE1) apart) which is involved in the generation of beta-amyloid, the main trigger of Alzheimer's disease (Ubelmann et al., 2017). CD2AP directly interacts with Cortactin which was shown to regulate synaptic plasticity and therefore influence Alzheimer's disease (Mota et al., 2014). Beta-amyloid peptides are generated through sequential cleavage of APP by BACE1 and gamma-secretase in early endosomes. The small GTPase ADP-ribosylation factor 6 (ARF6) and its activity control the sorting of BACE1 into endosomes and thereby

influence beta-amyloid production (Sannerud et al., 2011). ARF6 is an ADP-ribosylation factor involved in the activation of cholera toxin (O’Neal et al., 2005), indirectly linking ADP-ribosylation to Alzheimer’s disease. Additional support for this hypothesis stems from the fact that the enhancement of PARP1 activity was demonstrated in the brain of Alzheimer’s patients (Strosznajder et al., 2012). PARP1 expression was shown in neurons of Alzheimer’s patients which were in close proximity to neurons with increased beta-amyloid proteins (Love et al., 1999). Since PARP1 generated PAR is a transient protein modification degraded through a MAR-containing intermediate state, MacroD2 and TARG1 might be involved in Alzheimer’s disease as well. In summary CD2AP regulates multi-protein complexes and connects distinct cellular functions such as neuron growth and endosomal biology. Furthermore, it is directly involved in Alzheimer’s disease through its involvement in beta-amyloid protein generation which is also connected to ADP-ribosylation.

An emerging theme from all MacroD2 interactors involved in neuronal function is that many proteins are expressed and perform functions in the hippocampus - Shootin-1, Afadin, AHNAK, and DPYSL2. Additionally, ADP-ribosylation seems to influence the hippocampus in rats. PARP6, a neuronal enriched MARylating PARP, was shown to be a regulator of hippocampal dendritic morphogenesis (Huang et al., 2016) and PARP1 activation with the DNA damage inducer MNNG results in neuronal cell death in the hippocampus of rats resembling phenotypes occurring in neurodegenerative disorders (Gerace et al., 2014). The hippocampus is a brain region with huge capacity for structural reorganization which is present after development. It is connected to many important functions such as learning, memory, anxiety, and stress regulation (Leuner and Gould, 2010). This highlights that a possible influence of MacroD2 on the hippocampus might be a fruitful avenue to pursue. Furthermore, patients with MacroD2 mutations might harbor yet unknown hippocampal defects which need further investigation. Additionally, neuronal reorganization might depend on actin cytoskeletal reorganizations which were shown to be regulated by MacroD2 and TARG1 in this study. The function of the actin-binding proteins Afadin and AHNAK were described in detail due to their function in actin binding above.

Shootin-1 is involved in neuronal polarization in hippocampal neurons (Toriyama et al., 2006). It interacts with a kinesin KIF20B and was proposed to mediate the interaction of Shootin-1 with microtubules to ensure its mobilization to the developing neuron (Sapir et al., 2013). It was further published that Shootin-1 interacts with CDKL5, a gene associated with epileptic encephalopathies, and their interaction correlated with Shootin-1 phosphorylation (Nawaz et al., 2016). This raises the question if the potential interaction of MacroD2 and Shootin-1 is due to yet unknown MARylation of Shootin-1. These findings strengthen the proposed connection between MacroD2 and epilepsy (Mefford, 2016).

DPYSL2 (dihydropyrimidinase-like 2), is a cytosolic protein expressed in regions of the central and peripheral nervous system. DPYSL2 and DPYSL3 are phosphorylated by cyclin-dependent kinase 5 (Cdk5) and dual specificity tyrosine-phosphorylated and regulated kinase 2 (DYRK2) which allows further phosphorylation by glycogen synthetase kinase 3 (GSK3). GSK3 is activated by MacroD2 *in vitro* by removing inhibitory MARylation (Rosenthal et al., 2013). These phosphorylation effects were shown to be necessary for the positioning of Rohon-Beard primary sensory neurons and neural crest cells in develo-

ping zebrafish (Tanaka et al., 2012). DPYSL2 is supposed to be necessary for the correct position of caudal primary motor neurons in the spinal cord of zebrafish (Morimura et al., 2013). It was published by Lee et al. that in rats which were prenatally stressed the expression of DPYSL2 in the prefrontal cortex and hippocampus was downregulated and that small nucleotide polymorphisms in DPYSL2 were associated with schizophrenia susceptibility (Lee et al., 2015). Aberrant expression of DPYSL2 in the brain of schizophrenic patients was found in previous proteomics studies. In a study from 2016, a schizophrenia associated polymorphic CT dinucleotide repeat in DPYSL2 was shown to react in a dose-dependent manner to the mTOR inhibitor rapamycin. It was proposed that the translation of DPYSL2 is regulated by mTOR (Pham et al., 2016). These studies connect DPYSL2 which is strongly regulated by phosphorylation with neurodevelopment and schizophrenia to cell metabolism. These findings support the hypothesis that MacroD2 and ADP-ribosylation which is intricately involved in metabolism are involved in neuronal function. This further supports the finding that MacroD2 is involved in schizophrenia (Xu et al., 2009).

Another arising theme is that three MacroD2 interactors involved in neuronal function (Cortactin, CD2AP, and Synaptojanin 1, PAK2/3) are involved in EGFR signaling and endocytosis. In respect to the observed phenotypes of MacroD2/TARG1 double knockout cells it remains to be tested if deregulation in EGFR signaling result in differences in cell migration which in turn impairs neuronal function. The functions of Cortactin and CD2AP were described above in respect to their actin-binding nature.

Synaptojanin 1, an inositol 5-phosphatase, regulates the turnover of phosphatidylinositol 4,5-bisphosphate at the synapse whose activity is negatively regulated by phosphorylation through cyclin-dependent kinase 5 (Cdk5) and activated by dephosphorylation through calcineurin (Lee et al., 2004). Synaptojanin 1 was shown to localize to clathrin-coated endoplasmatic intermediates in presynaptic nerve terminals and is implicated in post-endocytotic uncoating of vesicles influencing availability of synaptic vesicles at nerve terminals (Haffner et al., 1997; Mani et al., 2007). A splice isoform of Synaptojanin 1 interacts with EPS15 (Haffner et al., 1997), a homolog of an EGFR substrate involved in receptor endocytosis (Benmerah et al., 1998) identified as a MacroD2 interactor in this study. These findings link Synaptojanin 1 not only to proper neuronal function but also establish a connection between neuronal function through regulation of synaptic vesicles and EGFR endocytosis. The interaction between MacroD2 and Synaptojanin 1 might indicate that MacroD2 regulates neuronal function through its influence on EGFR endocytosis.

p21-activated kinase 2 (PAK2) and PAK3 are two of six isoforms of a serine/threonine protein kinase which are well characterized key effectors of the small GTPase Rac and Cdc42. PAK regulates cell survival, motility, proliferation and has anti-apoptotic effects, all of which are signals required for malignant transformation. PAKs are overexpressed and/or overactivated in several human cancer types such as breast, colon, and lung cancer (for review see ref. (Ye and Field, 2012)). PAK3 was identified as a substrate of PARP14 and is likely MARYlated (Feijs et al., 2013b). PAK2/3 are expressed in the brain and are important for neuronal cell fate, axon guidance, neuronal polarization and migration. Several studies link PAK3 to Alzheimer's disease and mental retardation (for review see ref. (Kreis and Barnier, 2009)). MacroD2 and PAK2/3 show some similar phenotypes, such

as their involvement in colon cancer, neuronal defects, and cell migration. Studying the interaction of MacroD2 with PAKs further might prove a fruitful avenue to explain how MacroD2 regulates such diverse phenotypes.

In summary, the molecular mechanism by which MacroD2 and TARG1 might influence neuronal functions remains a very intriguing subject for further research.

4.2.2 MacroD2's and TARG1's role in DNA damage response in unstressed cells

MacroD2 and TARG1 were shown to recruit to sites of DNA damage (Jankevicius et al., 2013; Sharifi et al., 2013). Furthermore, MacroD2 is phosphorylated by ATM in its C-terminal domain and subsequently exported from the nucleus. The interaction with ATM, a major factor in the repair of double strand breaks, as well as the finding that MacroD2 recruitment to DNA damage depends on the presence of double strand breaks leads to the hypothesis that MacroD2 is involved in the repair of double strand breaks (Golia et al., 2017). The focus of my thesis was to identify the function of MacroD2 and TARG1 in unstressed cells, without any induction of DNA damage. However, even within unstressed cells a background level of damaged DNA exists since DNA integrity is challenged in all mammalian cells with estimated 10^5 DNA lesions per day due to internal and external sources such as cell metabolism, replication errors, and oxidative stress (Wei 2016, Herceg 2001). This might be the reason why MacroD2 interacts with various proteins involved in GO-terms from “cell cycle checkpoint”, “DNA integrity checkpoint”, and “DNA damage checkpoint” according to the BioID study performed on unstressed cells in this thesis. Proteins from the non-significantly enriched GO-terms “DNA integrity checkpoint”, and “DNA damage checkpoint” are Fanconi anemia group J protein (BRIP1), cell cycle and apoptosis regulator protein 2 (CCAR2), DEP domain-containing protein 1B (DEPDC1B), GRB10-interacting GYF protein 2 (GIGYF2), mediator of DNA damage checkpoint protein 1 (MDC1), double-strand break repair protein MRE11 (MRE11A), 26S proteasome non-ATPase regulatory subunit 1 (PSMD1), 26S proteasome non-ATPase regulatory subunit 8 (PSMD8), and TIP41-like protein (TIPRL).

The connection between MacroD2 and DNA damage even in unstressed cells is not surprising due to the fact that the response to DNA damage is highly connected to ADP-ribosylation signaling. PARPs (mainly PARP1/2) recognize DNA damage and recruit further DNA repair proteins to sites of DNA damage. PARP1 as the founding and best studied member of the PARP family is involved in the response to single and double strand breaks (for review see refs. (Herceg and Wang, 2001; Wei and Yu, 2016)). Several DNA damage checkpoint proteins, such as p53, p21, DNA ligase III, XRCC1, and DNA-PK were shown to contain PAR binding sites which are localized to a 20 amino acid motif, the so called PAR-binding motif (Pleschke et al., 2000). MRE11 was shown to contain a putative PAR-binding domain (Haince et al., 2008) (for review see refs. (Teloni and Altmeyer, 2016; Wei and Yu, 2016)).

Interestingly, a connection between DNA repair disorders and neurodegeneration is

emerging, e.g., defects in non-homologous end-joining manifests in microcephaly and defects in single strand break repair are associated with neurodegeneration. Additionally, it was shown in several studies that oxidative damage accumulates in aging brains and oxidative DNA damage was found in neurodegenerative diseases including Alzheimer, Parkinson, and Huntington (for review see ref. (Coon and Benarroch, 2018)). PARP1 was shown to be involved in neurodegenerative diseases including Alzheimer's and Parkinson's (for review see ref. (Martire et al., 2015)). Additionally, AHNAK, a potential MacroD2 interactor identified in this thesis, is connected to neuronal function and interacts with the DNA repair factor XRCC4 (Davis et al., 2014).

In summary, MacroD2's and TARG1's involvement in the DNA integrity checkpoint could be an avenue to explain the yet unknown mechanism why both enzymes are involved in cancer and neurological disorders.

Chapter 5

Materials and Methods

5.1 Reagents

Biotinylated Protein Ladder (7727; Sigma)
DMSO (Dimethylsulfoxide) (D2438; Sigma)
Dulbecco's PBS (Dulbecco's Phosphate Buffered Saline) (D8537; Sigma)
Etoposide (E1383; Sigma)
FK866 hydrochloride hydrate (NAD synthesis/NAMPT inhibitor) (F8557; Sigma)
hEGF (human Epidermal Growth Factor) (E9644; Sigma)
Hoechst 33342 (H3570; Sigma)
Hygromycin B (10687; Thermo Fisher)
Oligos (Metabion)
Proteinase Inhibitor (Complete EDTA free protease inhibitor) (05056489001; Sigma)
Streptavidin-HRP (405210; Biolegend)
Streptavidin-Alexa-568 (S11226; Life Technologies) Streptavidin magnetic beads (DB MyOne Streptavidin C1) (65001, Life Technologies)
Page Ruler Prestained Plus (26620; Life Technologies)
Propidium Iodide (P4170; Sigma)
Puromycin (Puromycin dihydrochloride solution) (P9620; Sigma)
DMEM - high glucose (#5671; Sigma)
10% FBS (Charge 42G3261K; 10270106; Life Technologies)
2 mM L-Glutamine (25030081; Life Technologies)
Pen/Strep (Penicillin/Streptomycin) (15140-122; Life Technologies)
Leibovitz's L-15 Medium, no phenol red (21083027; Life Technologies)
Trypsine (Trypsin-EDTA solution) (T3924; Sigma)
Poly-D-Lysine (P7280; Sigma)
Doxycycline (D9891; Sigma)
Biotin (B4501; Sigma)

5.2 Antibodies

Table 5.1: Used antibodies

Antigene	Company/Homemade	Article Number	Species	WB Dilution	IF Dilution
actin	Abcam	ab6276	mouse	-	1:1000
tubulin	Sigma	T9026	mouse	1:10000	-
MacroD2 poly-clonal purified (G2)	home made	-	rabbit	1:1000	1:500
TARG1	Homemade	-	rabbit	1:2000	-
Vinculin	abcam	ab73412	rabbit	-	1:500
EGFR	abcam	ab52894	rabbit	1:1000	1:500
Zyxin	abcam	ab109316	rabbit	-	1:500
Filamin A	abcam	ab11074	goat	-	1:500
myc	Home-made	-	mouse	1:50	1:500
GFP (purified)	Home-made	-	goat	1:1000	1:700
anti-mouse HRP	BioRad	170-6516	goat anti-mouse	1:10000	-
anti rabbit HRP	BioRad	170-6515	goat anti-rabbit	1:10000	-
anti rabbit HRP	Agilent	PO39901-2	swine anti-rabbit	1:3000	-
anti goat HRP	Abcam	ab97110	donkey anti-goat	1:10000	-
secondary Antibodies	Thermo Fisher	-	-	-	1:1000
Streptavidin Alexa-568	Thermo Fisher	S11226	-	-	1:1000

5.3 Buffers

RIPA

50 mM Tris-HCl
0.15 M NaCl
0.1% Sodium Deoxycholate
1 mM EDTA
1 % NP-40
pH 7.5

SDS loading buffer 6x

250 mM Tris-HCl
10% DTT
5% SDS
40% glycerol
0.005% Bromphenol Blue

SDS-PAGE Stacking Buffer

0.5 M Tris-HCl
0.4% SDS
pH 6.8

SDS-PAGE Resolving Buffer

1.5 M Tris-HCl
0.4% SDS
pH 8.8

SDS-PAGE Running Buffer 10x

250 mM Trizma
1.92 M Glycine
1% SDS

Transfer Buffer

25 mM Trizma Base
192 mM Glycine
20% Methanol

Ponceau

0.1% Ponceau S
1% Acetic Acid

TBS 10x

500 mM Trizma
1.5 M NaCl
pH 7.6

Mild Stripping Buffer

200 mM Glycine
0.1 % SDS
1 % Tween 20

BioID pulldown Buffers**Lysis Buffer**

50 mM Tris-HCl
500 mM NaCl
0.2 % SDS
pH 7.4
add Proteinase Inhibitor and 1 mM DTT fresh

Wash Buffer 1

2 % SDS

Wash Buffer 2

0.1 % desoxycholate acid
1 % Triton-X-100
1 mM EDTA
500 mM NaCl
50 mM HEPES
pH 7.5

Wash Buffer 3

0.5 % desoxycholate acid
0.5 % NP-40
1 mM EDTA
250 mM LiCl
10 mM Tris-HCl
pH 7.4

Proteomics Buffer

20 mM Trizma
100 mM NaCl
1 mM EDTA
pH 7.4

5.4 Kits

Pierce ECL Plus Western Blotting Substrate (32132; Thermo Fisher)
Miniprep Kit (mi-PMN250; metabion)
Midi Prep Kit (A2496; Promega)
Gel-Extraction Kit (mi-GEL250; Metabion)
PCR- Purification Kit (mi-PCR250; Metabion)
Relia Prep gDNA Tissue Miniprep System (A5051; Promega)

5.5 Cloning

When generating new plasmids, the gene of interest was PCR amplified from cDNA or existing plasmids with primers adding the desired restriction sites, if necessary. The reaction was run on a 1% agarose gel (1 % agarose in TAE buffer), cut with a scalpel and the DNA

was extracted with the gel extraction kit.

The PCR fragment and desired plasmid were digested with 10-20 u of restriction enzyme at the indicated temperature (usually 37C) for 2-4 hours. Digested inserts and vectors were ligated in a molecular ratio of (3:1) at 16 C over night.

Ligated plasmids were transformed in chemically competent XL10 cells with 30 seconds heatshock at 42C. Cells were plated in LB plates with appropriate selection (Ampicillin or Kanamycin). Bacteria from single colonies were placed into LB with appropriate selection for 8-16 hours. Plasmids were isolated with a mini-prep kit. Plasmids were sanger sequenced. Sequence verified plasmids were amplified according to the midi prep kits manual.

5.6 Plasmids

Plasmid	Location	Glycerol stock
BioID01 (myc-BirA-MacroD2FL)		yes
BioID05 (myc-BirA-MacroD2MD)		yes
BioID08 (myc-BirA-MacroD2i2)		yes
BioID11 (myc-BirA; EVC)		yes
BioID12 (MacroD2FL-BirA-HA)		yes
BioID15 (MacroD2MD-BirA-HA)		yes
BioID21 (MacroD2i2-BirA-HA)		yes
BioID31 (BirA-HA; EVC)		yes
GFP-TARG1	GJ122	yes
GFP-MacroD2	CL2155	no
GFP-MacroD2 G188E	CL3521	no

Table 5.2: Used plasmids with database location and glycerol stock availability

5.7 Cell Culture

Media

DMEM complete

DMEM - high glucose

10% FBS

2 mM L-Glutamine

100 U/mL Penicillin + 100 g/mL Streptomycin

DMEM without FBS

DMEM - high glucose
2 mM L-Glutamine
100 U/mL Penicillin + 100 g/mL Streptomycin

Imaging Media

Leibovitz's L-15 Medium
10% FBS
100 U/mL Penicillin + 100 g/mL Streptomycin

Freezing Media for Human Cells

FBS
10% DMSO

Used Cell Lines

Table 5.3: Used cell lines. Cell line name, content and selection

Name	Contains	Antibiotics for Culturing
U2OS	Osteosarcome cell line	none
GM05/MD2KO1	U2OS based MacroD2-KO (Target MacroD2 full)	none
GM09/MD2KO2	U2OS based MacroD2-KO (Target MacroD2 Md2-KO-67)	none
TARGET2c6/TARG1KO1	U2OS based TARG1-KO (Target T2)	none
TARGET2c15/TARG1KO2	U2OS based TARG1-KO (Target T2)	none
GM24/cU2OS1	clonal U2OS	none
GM26/cU2OS2	clonal U2OS	none
GM05TKOc6/DKO1	U2OS based MacroD2- and TARG1-KO (Nickase)	none
GM09TKOc19/DKO2	U2OS based MacroD2- and TARG1-KO (Nickase)	none
GM09TKOc21/DKO3	U2OS based MacroD2- and TARG1-KO (Nickase)	none
HEK Trex	Human Embryonic Kidney cells with Flip-in inducible expression system	Blastidine and Zeocin
BioID01/MD2FL-1	HEK Trex expressing MacroD2 full length	Hygromycin and Blastidine
BioID05/MD2MD-1	HEK Trex expressing MacroD2 Macrodomain-only	Hygromycin and Blastidine
BioID07/MD2i2-1	HEK Trex expressing MacroD2 full length	Hygromycin and Blastidine
BioID11/EVC-1	HEK Trex expressing MacroD2 full length	Hygromycin and Blastidine

Thawing cell

Vial of cells was collected from the liquid nitrogen tank and quickly warmed in a 37°C water bath. Thawed cells were transferred to 5 mL complete DMEM. The cells were pelleted at 700 rpm for 3 minutes. Supernatant was removed and pellet was resuspended in 10 mL complete DMEM and transferred to a T75 flask and placed in a 37°C humidified incubator with 5 % CO₂.

Passaging cell

Cells were passaged when they reached 80-90% confluency. U2OS and HEK Trex cells were split in a ratio of 1:6-1:8 (clonal U2OS, MacroD2 knockout and TARG1 knockout cells). MacroD2/TARG1 double knockout cells were split in a ratio of 1:3-1:5. Cells were passaged twice per week. For passaging, media was aspirated from the cells, wells were washed in PBS, PBS was aspirated. Three mL of trypsin was added to each flask and cells were incubated for 3 minutes at room temperature with gentle tapping to release cells. At least 6 mL complete DMEM were added to the trypsinized cells to stop the reaction and flask was washed with the cell suspension by pipetting the cell suspension up and down. Portion of cells, according to split ratio, was transferred to new flask with 10 mL complete DMEM.

Freezing cell

Cells were grown to 60-80% confluency in a T75 or T150 flask. Cells were removed from flask as for discarded for cell passaging. Cells were washed with PBS, trypsinized for 3 minutes, complete DMEM was added and cell suspension was pelleted at 700 rpm for 3 minutes. The Supernatant was removed and 1 mL freezing media was added per cryovial (V7884; Sigma) to the cells resuspended. From T25 flask one vial was frozen down, from one T75 flask 2-3 vials were made and from one T150 flask 5 vials were frozen down. 1 mL cell solution was aliquoted into one vial, vials were placed in a CoolCell (BCS-405; BioCision) and put in the -80 °C freezer over night. The next day vials were transferred to the liquid nitrogen tank.

Generating stable cell lines

Cells were seeded at a density of 500000 cells/mL into two wells of a 6-well plate (1 mL cell suspension per well). Cells were centrifuged at 300 rpm/1 minute to allow homogenous attachment. 6-well plate was placed in the 37 °C humidified incubator with 5 % CO₂ over night. Cells were transfected according to manufacturer's protocol with Xfect (631318; Clontech for U2OS) or with Lipofectamine 3000 (L3000001; Thermo Fisher for HEK Trex). Cells were clonally selected either with FACS sorting (FACS Aria II or FACS Fusion; GE) or picked by hand with sterile cloning cylinders (Pyrex cloning cylinders; CLS31668; Sigma) For FACS sorting, cells were trypsinized, resuspended in PBS, FACS tube (#352235; Corning) strained and kept in a styrofoam box until sorting into 96-well plates containing 150-200 µL

complete DMEM per well. When colonies had formed the plates were controlled for single colonies and double colonies were excluded. Single colonies were transferred to 24-well plates. For cloning cylinder method, transfected cells were trypsinized and transferred in different volumes to 15 cm petri dishes (e.g. 100 μ L, 200 μ L, 400 μ L, 800 μ L, 1600 μ L cell suspension to 15 mL complete DMEM with selection (e.g. Puromycin). Plates were placed in the 37 °C humidified incubator with 5 % CO₂ and allowed to grow until large colonies were formed. Plates where cells had formed big, sparse colonies were used. Plates were PBS washed, cylinders were put over colonies and 100-200 μ L trypsinase was added to each cone. When cells have detached from the petri dish (observed with the microscope) 200 μ L of complete DMEM were added, cells were pipetted up and down and added to 2 mL complete DMEM with selection in 24-well plates. For both methods when cells reached 50% confluency in 24-well plates they were transferred to T25 flasks with appropriate selection media.

5.8 Transfections

The day before transfection, cells were seeded according to manufacturers protocol and depending on cell lines and plating surface. U2OS cells were transfected with Xfect (631318; Clontech) according to manufacturer's protocol and HEK Trex cell were transfected with Lipofectamine 3000 (L3000001; Thermo Fisher) according to manufacturer's protocol. For Xfect transfected cells, medium was changed after 4 hours. Cells were used for downstream applications one to two days post transfection.

5.9 Knockdowns

For siRNA knockdowns cells were seeded one day prior to knockdown according to manufacturers protocol and depending on cell lines and plating surface. Cells were treated with Lipofectamine RNAiMax (13778075; Life Technologies) according to manufacturers protocol. Cells were used two to three days post siRNA transfection.

5.10 Drug and Antibiotic treatments

Table 5.4: Drug Treatments

Drug	Company	Ordering Number	Working Dilution	Incubation Time
FK866	Sigma	F8557	10 nM	16 hours
hEGF	Sigma	E9644	150 ng/mL or 2 μ g/mL	-
Doxycycline	Sigma	D9891	5 μ g/mL	at least 24 hours
Biotin	Sigma	B4501	50 μ M	24 hours

Table 5.5: Antibiotic Treatments

Antibiotic	Company	Ordering Number	Working Dilution
Hygromycine	Thermo Fisher	10687-010	200 $\mu\text{g}/\text{mL}$
Blasticidine	Thermo Fisher	R210-01	15 $\mu\text{g}/\text{mL}$
Zeocin	Thermo Fisher	R25001	100 $\mu\text{g}/\text{mL}$

5.11 Generation of CRISPR Knockout Cell Lines

5.11.1 Classic CRISPR

Generation and validation of CRISPR knockout cell lines generated with classical Cas9 was performed according to the nature protocols paper from the Zhang laboratory (Ran et al., 2013).

Table 5.6: CRISPR Target Sequences

Gene Knockout	Target	Forward Primer; top Reverse Primer; bottom
MacroD2	MD2-KO-67	caccgATAAATGCCTGTTGAGATGC aaacGCATCTCAACAGGCATTTATc
	full	caccgATACTGTAGGGCCAATAGCC aaacGGCTATTGGCCCTACAGTATc
TARG1	T1	caccgATCAGTGAGGATTGTTCGCAT aaacATGCGACAATCCTCACTGATc
	T2	caccgAGGATTGTTCGCATGGGCGCT aaacAGCGCCCATGCGACAATCCTc
MacroD1	Md1-1	caccgTCCGGCACTCGTCGGTAAGCAGG aaacCCGATAGCCGCCGGTGATCTTGGc
	Md1-2	caccgCCAAGATCACCGGCGGCTATCGG aaacCCGATAGCCGCCGGTGATCTTGGc

Primers were designed using <http://crispr.mit.edu> to find appropriate target sequences.

Primers were phosphorylated and annealed with T7 PNK, according to (Ran et al., 2013). Annealed primers were cloned into pSpCas9(BB)-2A-GFP (Addgene plasmid ID: 48138). Colonies were sequence verified using U6- fwd primer (GAGGGCCTATTTCC-CATGATTCC).

Verified plasmids were transfected into human cancer cell lines U2OS. 2 wells of a 6-well plate were transfected with pSpCas9(BB)-2A-GFP containing the target sequence per construct.

1-2 days post transfection GFP-positive cells were sorted with FACsAria II into 5 96-well plates per construct. Surviving, proliferative cells were raised and tested.

5.11.2 Nickase CRISPR

Nickase Cas9 introduce single strand breaks, so in order to generate a double strand break 2 nickase enzymes targeting opposite strands have to be used. Targeting sequences can have a small offset of optimally 0-20 bp. The double-nickase approach generates double strand breaks with similar frequency to classical Cas9 but should minimize off-target effects (Ran et al., 2013). Nickase CRISPR knockout generation and validation was performed with plasmids containing CRISPR nickase (pX335A-Cas9(D10A)) and 2 targets for TARG1 targeting intron 2 and two targets targeting intron 5 were received from Mareike Bütepage (AK Lüscher, Uniklinik RWTH Aachen). Using these constructs a approximately 2.8 kb fragment of TARG1 gDNA should be deleted. It was shown that deleting fragments up to 10 kb is efficiently possible using two double strand breaks targeted with CRISPR/Cas9 (Zheng et al., 2014).

All four sequence verified plasmids were transfected into two wells of a 6-well plate of MacroD2 KO cell lines (GM05 and GM09) simultaneously. Transfected cells were put on Puromycin selection media ($2 \mu\text{g}/\text{mL}$) and selected with the cloning cylinder method (5.7).

5.12 Genotyping of CRISPR Knockout Cell Lines

5.12.1 Classic CRISPR

Genomic DNA of clonal CRISPR cell lines was extracted using Relia Prep gDNA Tissue Miniprep System. A 1 kb fragment surrounding the Cas9 cutsite was PCR amplified with primers introducing EcoRI and HindIII restriction sites. The DNA was purified with the PCR clean-up kit. The PCR fragment and the vector pBluescript II KS(+) were digested at 37°C for 4 hours. The desired fragments of the PCR product and the vector were run on a 1% gel, extracted from the gel with a clean scalpel and extracted from the gel with a gel-extraction kit. The PCR fragment was ligated into the 3 kb vector pBluescript II KS(+) (molar ratio 3:1). Multiple single colonies were picked and plasmids were purified with a Miniprep Kit. Several Plasmids from each cell line were Sanger sequenced with primers PUC fwd and PUC18 rev. For all used cell lines, 3 Alleles with mutations introducing premature stop-codons were identified.

5.12.2 Nickase CRISPR

Genomic DNA of clonal CRISPR cell lines was extracted using Relia Prep gDNA Tissue Miniprep System. Primers amplifying a 500 bp fragment of Exon 4 were used as a negative control and primers amplifying a fragment of about 1 kb with successful removal of the fragment between all target sites were used as a positive control. Primers were received from Lüscher laboratory. Fragments were run on 1% agarose gels for genotyping.

5.13 Western blotting

Lysates for Western Blotting were prepared in RIPA buffer with Proteinase Inhibitor tablets (approximately 100 L RIPA per pellet from a T75 flask). Cells were sonified with a Branson Sonifier (5-10 pulses at 30 % duty cycle and output level of 3) in cycles until all lysates became clear. Lysates were spun at 20000g for 15 minutes. Supernatant was transferred to new tube. Protein concentration was determined with according to manufacturers protocol with Protein Assay Kit (BioRad; 5000001).

30-50 μ g protein lysate was separated using SDS-PAGE (30-50 V, time depending on protein of interest) with appropriate amount of loading dye on either 5% stacking gel 15% resolving gel or on gradient gels (NP0323BOX; Thermo Fisher). Proteins were transferred to a nitrocellulose membrane for 90 minutes at 50 V at 4 °C or for 4 hours at and 150 mA at 4 °C. As a control of successful transfer, the membrane was stained with Ponceau S solution to show transferred proteins. The membrane was destained with TBS-T (0.05 % Tween 20). The membrane was blocked in 5% milk or 5% BSA for 1 hour at room temperature and incubated overnight with primary antibodies (for dilution see 5.2) diluted in blocking buffer at 4 °C.

The following day, the membrane was washed three times in TBS-T, then incubated with HRP-conjugated secondary antibodies diluted in blocking solution for 1 hour at room temperature. After another three washing steps, the membrane was incubated with Pierce ECL Plus Western blotting reagents. Signal was detected using chemoluminescence reader (Fusion FX; Vilber Lourmat) or with film (Fuji Super RX; 41070; BEMA BWPlus) development.

5.14 Immunofluorescence

Immunofluorescence experiments were performed in COV-covered, black 96-well plates (655866; Greiner) or 8-well Lab-Teks (155411; Thermo Fisher). Cell number varied depending on assay. Plates were washed once with cold PBS and fixed with either 4% PFA 10 minutes at room temperature or ice-cold, freshly made Methanol for 10 minutes at -20 deg C. Plates were washed once in PBS-T (0.05 % Tween 20) and permeabilized with PBS with 0.25% Triton X for 10 minutes after PFA fixation. Plates were washed three times for five minutes at room temperature with PBS-T. Plates were blocked with 3% BSA or milk for one hour at room temperature. Plates were incubated over night with primary antibody diluted in blocking solution in the coldroom while shaking gently. Plates were washed three times for five minutes at room temperature with PBS-T. Plates were incubated with Alexa-fluorophore coupled secondaries raised against the species of the primary antibody (e.g. MacroD2 antibody G2 (rabbit) with goat anti-rabbit Alexa-488; 1:1000 dilution) for two hours at room temperature. If necessary, cell nuclei were stained for 10 minutes with hoechst 33352 (200 ng/mL) in PBS. Plates were washed three times five minutes at room temperature with PBS-T.

5.15 Microscopy

Microscopy was performed on a Zeiss AxioObserver Z1 confocal spinning-disk microscope equipped with an AxioCam HRm CCD camera (Zeiss) or a sCMOS ORCA Flash 4.0 camera (Hamamatsu) through a Zeiss Pln Apo 10x/0.3 DICII (1.11 μm pixel resolution) or a Zeiss Pln Apo 20x/0.8 DICII (0.42 μm pixel resolution) or a Zeiss Pln Apo 40x/0.95 DICIII (0.35 μm pixel resolution) or a Zeiss C-Apochromat 40x/1.2 water-immersion objective (0.28 μm pixel resolution).

5.16 BioID Pulldowns

Four 10-cm petri dishes per cell line and replicate were grown to 80% confluency in complete DMEM containing Hygromycin and Blasticidin (concentration in table 5.5). Medium was exchanged to complete DMEM containing Doxycyclin and Biotin for 24 hours (concentrations in table 5.4). Cells from all four plates were trypsinized, collected and pelleted in one 15 mL falcon tubes per cell line, washed in cold PBS and flash frozen in liquid nitrogen. Pellets were stored in $-80\text{ }^{\circ}\text{C}$ freezer until use. Pellets were thawed on ice and resuspended in 2.4 mL Lysis buffer. 240 μL 20 % Triton-X-100 were added and mixed by trituration. Samples were sonified twice with a Branson Sonifier 250 (30 pulses at 30 % duty cycle and output level of 3). 2.16 mL pre-chilled 50 mM Tris-HCl (pH 7.4) was added to each lysate and mixed by inverting the falcon tube. Samples were sonified one more with previous settings. Samples were aliquoted evenly into three pre-chilled low-binding tubes (Corning Costar low binding microcentrifuge tubes; CLS3207; Corning). Samples were spun 10 minutes at 16500 g at $4\text{ }^{\circ}\text{C}$. During centrifugation three new low-binding tubes were placed in a magnetic rack and 750 μL lysis buffer and 750 μL 50 mM Tris-HCl (pH 7.4) were added to each tube. Streptavidin magnetic beads were mixed and 100 μL were added to each tube on the magnetic rack.

After sample centrifugation 20 μL of supernatant was collected in a new tube (Input). Supernatant from magnetic beads was removed and supernatant of lysates was added to magnetic beads without disturbing the insoluble pellet on the tube wall. Beads were resuspended with gentle pipetting. Tubes were incubated on a rotor at $4\text{ }^{\circ}\text{C}$ over night.

The next day tubes were placed on a magnetic rack for 3 minutes to allow beads to accumulate on one side of the tube. 20 μL of the supernatant was transferred to a new tube (Unbound). The supernatant on the beads was removed and beads were resuspended in 1.5 mL Wash Buffer 1. Tubes were incubated on a rotor at room temperature for 8 minutes. Beads were collected as previously described (20 μL of supernatant was collected in new tube as W1) and supernatant of three tubes per cell line was removed. 1.5 mL Wash Buffer 1 was added to one tube, beads were resuspended and transferred to second tube, resuspended and put into the third tube. Tubes were incubated on a rotor for 8 minutes at room temperature. Beads were washed in Wash Buffer 2 (Sample W2 was put to new tube) and Wash Buffer 3 (Sample W3 added to new tube). Beads were resuspended in 50 mM Tris-HCl (pH 7.4) . 150 μL were transferred to a new tube (Sample Pulldown). The

remaining beads were washed three times with Proteomics Buffer. In the last wash step beads were transferred to a new low-binding tube. The supernatant was removed completely and beads were stored in the -80°C freezer until needed.

Beads from Pulldown sample were collected, supernatant was removed and beads were re-suspended in $100\ \mu\text{L}$ loading dye. All previously collected samples were mixed with loading dye. Samples were boiled for 5 minutes at 98°C . $20\ \mu\text{L}$ of samples were loaded in SDS-PAGE, transferred to a nitrocellulose membrane. Membrane was blocked in 5% biotin-free BSA (Roth; 0163) over night in the cold room. Membrane was incubated with streptavidin-HRP (1:2000) for 1 hour.

5.17 Mass Spectrometry

5.17.1 On-bead tryptic digest

$50\ \mu\text{L}$ buffer containing 100 mM Trizma (pH 7.5), 15 mM DTT, 4 M Urea and 100 mM Iodacetamide were added per sample of pulldown beads, and samples were incubated at 28°C for 50 minutes while shaking vigorously (1300 rpm) in the dark. Samples were diluted to $400\ \mu\text{L}$ with 100 mM Tris (pH 7.5). $1\ \mu\text{g}$ of trypsin was added to each sample for protein digestion. Samples were incubated for 12 hours at 28°C and 1300 rpm. The next day each sample was acidified using $2\ \mu\text{L}$ TFA and $6\ \mu\text{L}$ FA. Sample pH was determined with pH strips. All samples had a pH below 2.

5.17.2 Whole cell Proteome

Cell Lysis

Cells from a T75 flask that were at 80% confluency were pelleted. Pellets were washed with PBS once, flash frozen in liquid nitrogen and stored in the -80°C freezer for later use. $50\ \mu\text{L}$ SDT buffer (2% SDS, 50 mM DTT, 100 mM Tris pH 7.4, Proteinase Inhibitor) were added to all pellets. Samples were resuspended and transferred to Covaris Sonicator vials. Samples were strongly sonified with Covaris. Samples were transferred to eppendorf tubes and spun at full speed for 5 minutes. Samples were incubated at 50°C for 60 minutes to reduce disulfide bonds. Afterwards samples were cooled to room temperature.

FASP buffer exchange

$400\ \mu\text{L}$ Iodacetamide solution (8M Urea, 100 mM Tris pH 8.2, 30 mM Iodacetamide, 1 mM MgCl_2 , 25 u/mL benzonase, phosphatase inhibitor) were added to all samples. All samples were incubated at 25°C , 500 rpm for 45 minutes in the dark. Samples were transferred to filter membranes (cut-off 10 kDa) and washed twice with $300\ \mu\text{L}$ 8 M Urea and three times with $300\ \mu\text{L}$ 4 M Urea.

Digestion

500 ng LysC was added to all samples for predigestion at 25 °C for 4 hours. Urea was diluted with 350 μ L 100 mM Tris, pH 8.2 per sample. 0.1 μ g trypsin was added to each sample, samples were incubated to 27 °C for 12 hours while shaking. The next morning 0.1 μ g trypsin was added to all samples and samples were digested for 6 hours. Peptides were eluted from filter membrane by centrifugation. Remaining supernatant was mixed with 350 μ L 100 mM Tris (pH 8.2) and eluted completely as a second fraction into the first fraction. All samples were acidified with 300 μ L 100% FA. All samples had a pH below 3.

5.17.3 Sample desalting

C18 stage tips were prepared for all samples with 3 discs of C18 filter material in one P200 tip. C18 stage tips were washed twice in a centrifuge (1500 rpm, 3-5 minutes per spin) with 50 μ L 100% Methanol each, twice with 50 μ L Elution Solvent (30% Methanol, 40 % ACN, 0.1 % FA) and three times with 65 μ L 0.1 % TFA in water.

Samples were desalted in a centrifuge at 20 °C. The samples (max. 200 μ L) were transferred onto the discs and centrifuged at 800 rpm for 15 minutes until sample was almost completely filtered. If necessary, the second half of the sample was loaded and filtered through (Flowthrough).

C18 tips were placed into a new tube and washed three times with 80 μ L 0.1 % FA (1200 rpm, 10 minutes) (Wash).

The C18 tips were placed in a new tube. Peptides were eluted twice with 70 μ L Elution Solvent at 1000 rpm for 10 minutes each.

Samples were dried in speed vacuum centrifuge (2000 rpm/30 °C/ approximately 3 hours).

5.17.4 Mass Spectrometry Measurements

Mass Spectrometry measurement was performed by Dr. Andreas Schmidt (ZfP, BioMedical Center). Samples were analyzed via nanoRP-C18-HPLC MS/MS on a QExactive HF mass spectrometer online coupled to an Ultimate 3000 nano-chromatography system in direct injection mode. 5 μ L of the sample were applied to the separation column in 0.1% FA. First, samples were washed for 5 min at 4% B (80% ACN, 0.1% FA) before applying the separation gradient from 4 to 50% B in 50 min. The gradient was followed by a high organic wash and column reconstitution at 4% B for 35 min. The column outlet was directly coupled to the mass spectrometer for on line detection of eluting peptides. During the entire LC program, MS data were acquired in positive ionization mode using a data-dependent acquisition method consisting of 1 survey scan and up to 10 HCD-MS/MS experiments. Survey scan data were acquired from 375 to 1600 m/z with a maximal resolution of 60,000 and AGC gain of 3×10^6 ions. Each survey scan was followed by up to 10 MS/MS experiments on precursor ions with charge states 2+ to 5+. Other charge states and undefined precursors were excluded from MS/MS experiments. For MS/MS data a resolution of 15,000 and a AGC of 1×10^5 (underfill ratio 4%) was enabled. Precursor ions were isolated by the quadrupol

applying a symmetrical within a 2 Da window around the precursor ion, and fragmented in the HCD-cell at normalized collision energy of 27. Previously selected precursors were excluded from repeated analysis for 20 seconds within a 12 ppm accuracy window. Fragment ions were acquired in separate MS/MS spectra for each precursor (MSX count: 1). Peptide-related isotope distribution was preferred, but not required for precursor selection.

5.18 Mass Spec Data Analysis

Peptide identification was performed in MaxQuant with the Andromeda search engine by Dr. Andreas Schmidt (Cox and Mann, 2008; Cox et al., 2011). Acquired iBAQ values (signal intensity calculated as sum of all identified peptide intensities over the sum of all theoretical possible peptides) from MaxQuant were used in Perseus (Tyanova et al., 2016). Data was uploaded with generic matrix upload. Name of columns were changed to more descriptive names with categorical annotation. Missing values were replaced for each column separately (width 0.3, downshift 0.8). Heatmaps, intensity plots and volcano plots were generated in Perseus. Venn Diagramms were generated with Venny2.1 (<http://bioinfogp.cnb.csic.es/tools/venny/>) and results were redrawn with proper proportions with adobe illustrator. GO-term networks were calculated and drawn with ClueGo, a Cytoscape plugin (Bindea et al., 2009).

5.19 Cell Cycle Profiling

Cells were seeded in a T150 cm flask, when they reached about 80 % confluency they were trypsinized, resuspended in DMEM and counted (Vi-Cell; Bscckmann-Coulter). Cells were adjusted to 10^6 cells, washed in PBS and pelleted. Pellet was vortexed and 1 mL 70% Ethanol was added drop-wise to the pellet. Cells were incubated on ice for 30 minutes for fixation.

Cells were pelleted at 1000 g for 5 minutes and the supernatant was removed with a P200 tip. Cells were washed in 1 mL PBS twice. Cells were resuspended in 50 μ L RNase A solution (100 μ g/mL) to remove RNA. 400 μ L propidium iodide (PI) solution (50 μ g/mL) was added directly to cells in RNase A solution and mixed by pipetting slowly. Cells were incubated 10 minutes in the dark at room temperature and 10000 cells were analysed with FACS Canto at a flow rate below 400 events/second. Control samples without PI staining were used to ensure proper gating. forward scatter (FSC) versus side scatter (SSC) were used to identify cells. Doublets were excluded with FSC-A (area of FSC) versus FSC-W (width of FSC). Single cells were displayed in a PI histogram which was used for cell cycle analysis. Percentage of cells in G1-, S- and G2-phase were calculated in PI histogram.

5.20 xCelligence

The xCelligence method measures changes in impedance and can be used to determine attachment speed and cell proliferation.

Cells were trypsinized, collected and counted with the automatic cell counter (Vi-Cell; Bscckmann-Coulter). Cell number was adjusted to obtain 1 mL of 50 cells/ μL . E-plate with 16-wells was incubated at least 30 minutes with 100 μL complete DMEM. Plates were place in xCelligence machine. Background was measured in step one.

After background measurement 100 μL cell solution were added to four wells of a E-plate per cell line (four technical replicates). Impedance was measured for at least three days (measurment timing described below).

Sequence	Step	Sweep	Intervall (min)
1	1	1	1
2	1	70	2
2	2	100	15
2	3	100	60

Cell Attachment was analysed from start of experiment until cells were attached as slope (1/hour). Cell Proliferation was analysed from cell attachment until the log-phase of cell doubling as doubling time (hours).

5.21 Scratch Assay

35000 cells were seeded per well of a 8-well LabTek, spun at 300 rpm, 1 minute and placed in the 37°C humified incubator with 5 % CO₂. The next day, cells were scratch with a P200 tip off the plate. Cells were washed twice with 250 μL complete DMEM. Medium was removed and Imaging Medium was added to cells. Cells were imaged on the confocal microscope with 10x objective every 20 minutes for 16 hours. For each biological replicate 4 image fields along the scratched area were imaged.

Cell migration into the scratch area was analysed using Fiji. Length of cell movement vertical to cell boundary at time point zero was measured.

5.22 Cell Migration Assay

5.22.1 Migration with and without EGF stimulation

Cells were trypsinized and counted with the automated cell counter (Vi-Cell; Bscckmann-Coulter). Cells were adjusted to 10 cells/L, placed in a 15 mL falcon, spun at 700 rom for 3 minutes. Medium was removed and cells were resuspended in either complete Leibovitz or complete Leibovitz supplemented with 150 ng/mL EGF.

200 μL cell suspension was seeded per well of a black cycloolefin-covered 96-well plate. 3 wells were seeded per treatment and cell line. Cells were centrifuged at 300 rpm for one minute and imaged with the confocal microscope. Two tiles per well were imaged with 15

minute intervals for 24 hours with the 10x objective. Single cell migration was tracked with MatLab plugin CellTracker in semiautomated mode. Total length of cell movement was calculated.

5.22.2 Migration with and without FK866 treatment

Cells were plated onto 96-well plates as described above in 5.22.1 at a density of 1000 cells per well. Cells were spun at 300 rpm for one minute and allowed to attach for six hours. The medium was exchanged to Imaging Medium with and without 10 nM FK866 and incubated over night for 16 hours. Cells were imaged and analysed as in 5.22.1.

5.23 EGFR Internalization Assay

10000 cells were seeded per well in a black cycloolefin-covered 96-well plate. Per cell line seven wells were seeded in 200 μ L complete DMEM medium. The next day cells were treated with 2 μ g/mL EGF for 2, 1, 0.5, 0.25 hours (and untreated). Cells were fixed in PFA as in 5.14. Cells were stained in 1:500 anti-EGFR antibody (see table5.2). Secondary was anti-rabbit Alexa-488. Cells were imaged on the confocal with the 40x air objective. Per tile 15 z-stacks with 1 μ m distance were imaged through the center of the cells over the whole cells. Maximim Z-Projections were generated in Zeiss software for the 8 middle z-stacks.

5.24 EGFR Internalization Rescue

7000 cells were seeded per well in a black cycloolefin-covered 96-well plate. Per cell line seven wells were seeded in 200 μ L complete DMEM medium. The next day the medium was exchanged to 75 new complete DMEM μ L per well. Cells were transfected with 250 ng plasmid DNA of GFP-MacroD2, GFP-MacroD2 G188E and GFP-TARG1 with Xfect. Medium was exchanged to 200 μ L complete DMEM medium per well after 4-5 hours. The next day cells were treated with 2 μ g/mL EGF for 10, 20, 30, 40, 50 and 60 minutes (and untreated). Cells were fixed in ice-cold methanol for 10 minute at -20C as in 5.14. Cells were stained in 1:500 anti-EGFR antibody and 1:700 with anti-GFP (see table5.2). Secondary was anti-goat Alexa-488 and anti-rabbit Alexa-568. Cells were hoechst treated. Cells were imaged on the confocal with the 40x air objective. Per tile 15 z-stacks with 1 μ m distance were imaged through the center of the cells over the whole cells. Maximum Z-Projections were generated in Zeiss software for the 8 middle z-stacks.

Anhang A

Appendix

A.1 BioID validation

Table A.1: MacroD2 significant interactors

Protein Name	Uniprot Accession
Shootin-1	A0MZ66
MacroD2	A1Z1Q3
PDZ and LIM domain protein 1	O00151
Syntenin-1	O00560
Segment polarity protein dishevelled homolog DVL-2	O14641
Programmed cell death protein 5	O14737
Protein phosphatase 1G	O15355
Cytoplasmic dynein 1 light intermediate chain 2	O43237
Synaptojanin-1	O43426
Band 4.1-like protein 2	O43491
Lipoyl synthase, mitochondrial	O43766
Putative adenosylhomocysteinase 2;Putative adenosylhomocysteinase 3	O43865;Q96HN2
C-Jun-amino-terminal kinase-interacting protein 4	O60271
Glycylpeptide N-tetradecanoyltransferase 1;Glycylpeptide N-tetradecanoyltransferase 2	P30419;O60551
Mitotic checkpoint serine/threonine-protein kinase BUB1 beta	O60566
Eukaryotic translation initiation factor 5B	O60841
Ankyrin repeat domain-containing protein 17	O75179
Peroxisomal membrane protein PEX14	O75381
Splicing factor 3B subunit 1	O75533
Cold shock domain-containing protein E1	O75534
GTPase Era, mitochondrial	O75616

TIP41-like protein	O75663
Cyclin-K	O75909
TOX high mobility group box family member 4	O94842
Acyl-protein thioesterase 2	O95372
Pericentrin	O95613
Mitogen-activated protein kinase kinase kinase kinase 4;Misshapen-like kinase 1;TRAF2 and NCK-interacting protein kinase	O95819;Q8N4C8;Q9UKE5
Protein SGT1	O95905
Vimentin	P08670
Putative uncharacterized protein encoded by LINC00869	P0C866
Protein 4.1	P11171
Nucleoprotein TPR	P12270
Vinculin	P18206
Eukaryotic translation initiation factor 2 subunit 2	P20042
Calpastatin	P20810
Filamin-A	P21333
Tryptophan-tRNA ligase, cytoplasmic;T1-TrpRS;T2-TrpRS	P23381
Eukaryotic translation initiation factor 4B	P23588
Microtubule-associated protein 4	P27816
Kinesin-1 heavy chain	P33176
Acidic leucine-rich nuclear phosphoprotein 32 family member A;Acidic leucine-rich nuclear phosphoprotein 32 family member B	P39687;Q92688
Signal transducer and activator of transcription 1-alpha/beta	P42224
Ran GTPase-activating protein 1	P46060
Adapter molecule crk	P46108
Crk-like protein	P46109
Microtubule-associated protein 1B;MAP1B heavy chain;MAP1 light chain LC1	P46821
F-actin-capping protein subunit beta	P47756
26S proteasome non-ATPase regulatory subunit 8	P48556
Nuclear autoantigenic sperm protein	P49321
Fatty acid synthase;[Acyl-carrier-protein] S-acetyltransferase;[Acyl-carrier-protein]	
S-malonyltransferase;3-oxoacyl-[acyl-carrier-protein] synthase;3-oxoacyl-[acyl-carrier-protein] reductase;3-hydroxyacyl-[acyl-carrier-protein] dehydratase;Enoyl-[acyl-carrier-protein] reductase;Oleoyl-[acyl-carrier-protein] hydrolase	P49327
E3 SUMO-protein ligase RanBP2	P49792
Double-strand break repair protein MRE11A	P49959
Lipopolysaccharide-responsive and beige-like anchor protein	P50851
T-complex protein 1 subunit theta	P50990
Arf-GAP domain and FG repeat-containing protein 1	P52594

Transcription initiation factor IIA subunit 1;Transcription initiation factor IIA alpha chain;Transcription initiation factor IIA beta chain	P52655
Arginine-tRNA ligase, cytoplasmic	P54136
Ubiquitin carboxyl-terminal hydrolase 14	P54578
Eukaryotic translation initiation factor 5	P55010
Afadin	P55196
Splicing regulator RBM11	P57052
Small nuclear ribonucleoprotein E	P62304
ADP-ribosylation factor 5	P84085
Vigilin	Q00341
Exosome component 10	Q01780
A-kinase anchor protein 12	Q02952
Dystonin	Q03001
Caldesmon	Q05682
Neuroblast differentiation-associated protein AHNAK	Q09666
Nucleosome-remodeling factor subunit BPTF	Q12830
Serine/threonine-protein kinase PAK 2;PAK-2p27;PAK-2p34;Serine/threonine-protein kinase PAK 3	Q13177;O75914
Interferon-induced protein with tetratricopeptide repeats 5	Q13325
Metastasis-associated protein MTA1	Q13330
Splicing factor 3B subunit 2	Q13435
Golgin subfamily A member 4	Q13439
28 kDa heat- and acid-stable phosphoprotein	Q13442
Cullin-4B	Q13620
Cytoskeleton-associated protein 5	Q14008
Kelch-like ECH-associated protein 1	Q14145
Ubiquitin-associated protein 2-like	Q14157
Src substrate cortactin	Q14247
E3 ubiquitin/ISG15 ligase TRIM25	Q14258
Mediator of DNA damage checkpoint protein 1	Q14676
GTPase-activating protein and VPS9 domain-containing protein 1	Q14C86
Pericentriolar material 1 protein	Q15154
Serine/threonine-protein kinase 38	Q15208
Calponin-3	Q15417
Probable JmjC domain-containing histone demethylation protein 2C	Q15652
Zyxin	Q15942
Serine/threonine-protein kinase N1	Q16512
Dihydropyrimidinase-related protein 2	Q16555
Drebrin	Q16643
Serine/threonine-protein phosphatase 6 regulatory subunit 3	Q5H9R7
WD repeat-containing protein 44	Q5JSH3
Centrosomal protein of 170 kDa	Q5SW79

Ubiquitin-associated protein 2	Q5T6F2
WASH complex subunit FAM21C;WASH complex subunit FAM21A	Q9Y4E1;Q641Q2
Protein FAM91A1	Q658Y4
Very large A-kinase anchor protein	Q68DQ2
Anamorsin	Q6FI81
La-related protein 1	Q6PKG0
PERQ amino acid-rich with GYF domain-containing protein 2	Q6Y7W6
Uncharacterized protein FLJ45252	Q6ZSR9
Zinc finger CCCH-type antiviral protein 1	Q7Z2W4
Nuclear fragile X mental retardation-interacting protein 2	Q7Z417
ATP-dependent RNA helicase DHX29	Q7Z478
HAUS augmin-like complex subunit 6	Q7Z4H7
Transcriptional regulator Kaiso	Q86T24
Protein prune homolog	Q86TP1
Leucine zipper protein 1	Q86V48
ELKS/Rab6-interacting/CAST family member 1	Q8IUD2
Spindle and kinetochore-associated protein 3	Q8IX90
5-3 exoribonuclease 1	Q8IZH2
Spartin	Q8N0X7
Cell cycle and apoptosis regulator protein 2	Q8N163
ADP-ribosylation factor GTPase-activating protein 1	Q8N6T3
Plasminogen activator inhibitor 1 RNA-binding protein	Q8NC51
EH domain-binding protein 1	Q8NDI1
Protein CASC5	Q8NG31
WD repeat-containing protein 36	Q8NI36
TBC1 domain family member 15	Q8TC07
Protein CIP2A	Q8TCG1
Gem-associated protein 5	Q8TEQ6
DEP domain-containing protein 1B	Q8WUY9
PEST proteolytic signal-containing nuclear protein	Q8WW12
Cytoskeleton-associated protein 2	Q8WWK9
Protein NDRG1	Q92597
Heat shock protein 105 kDa	Q92598
Tetratricopeptide repeat protein 28	Q96AY4
Autophagy-related protein 2 homolog B	Q96BY7
EF-hand domain-containing protein D2	Q96C19
Elongator complex protein 4	Q96EB1
PDZ and LIM domain protein 5	Q96HC4
Deubiquitinating protein VCIP135	Q96JH7
Kinesin-like protein KIF20B	Q96Q89
Tubulin-folding cofactor B	Q99426
26S proteasome non-ATPase regulatory subunit 1	Q99460
Endophilin-A2	Q99961

Condensin complex subunit 3	Q9BPX3
Coronin-1B	Q9BR76
G patch domain-containing protein 1	Q9BRR8
Fanconi anemia group J protein	Q9BX63
Oxysterol-binding protein-related protein 11	Q9BXB4
STE20-like serine/threonine-protein kinase	Q9H2G2
Activity-dependent neuroprotector homeobox protein	Q9H2P0
Protein unc-45 homolog A	Q9H3U1
Serine/threonine-protein kinase WNK1	Q9H4A3
UPF0428 protein CXorf56	Q9H5V9
UPF0705 protein C11orf49	Q9H6J7
Probable ATP-dependent RNA helicase YTHDC2	Q9H6S0
RNA polymerase II-associated protein 3	Q9H6T3
Phosphorylated adapter RNA export protein	Q9H814
L-aminoadipate-semialdehyde dehydrogenase-phosphopantetheinyl transferase	Q9NRN7
Protein FAM114A2	Q9NRY5
COMM domain-containing protein 8	Q9NX08
WW domain-containing oxidoreductase	Q9NZC7
Spliceosome-associated protein CWC15 homolog	Q9P013
Vesicle-associated membrane protein-associated protein A	Q9P0L0
RNA-binding protein 27;RNA-binding protein 26	Q9P2N5;Q5T8P6
Epidermal growth factor receptor substrate 15-like 1	Q9UBC2
Coatomer subunit gamma-2	Q9UBF2
Testin	Q9UGI8
LIM domain and actin-binding protein 1	Q9UHB6
Signal recognition particle subunit SRP68	Q9UHB9
Septin-9	Q9UHD8
SAP30-binding protein	Q9UHR5
Tyrosine-protein kinase BAZ1B	Q9UIG0
Drebrin-like protein	Q9UJU6
ADP-sugar pyrophosphatase	Q9UKK9
Apoptotic chromatin condensation inducer in the nucleus	Q9UKV3
MKL/myocardin-like protein 2	Q9ULH7
Endoribonuclease Dicer	Q9UPY3
Charged multivesicular body protein 2b	Q9UQN3
Sex comb on midleg-like protein 2	Q9UQR0
RuvB-like 1	Q9Y265
Band 4.1-like protein 3;Band 4.1-like protein 3, N-terminally processed	Q9Y2J2
Thyroid hormone receptor-associated protein 3	Q9Y2W1
Suppressor of G2 allele of SKP1 homolog	Q9Y2Z0
Serine-threonine kinase receptor-associated protein	Q9Y3F4
Talin-1	Q9Y490

Ubiquitin carboxyl-terminal hydrolase 15	Q9Y4E8
WD repeat domain phosphoinositide-interacting protein 2	Q9Y4P8
Protein PRRC2C	Q9Y520
CD2-associated protein	Q9Y5K6

A.2 Validation of knockout cell lines

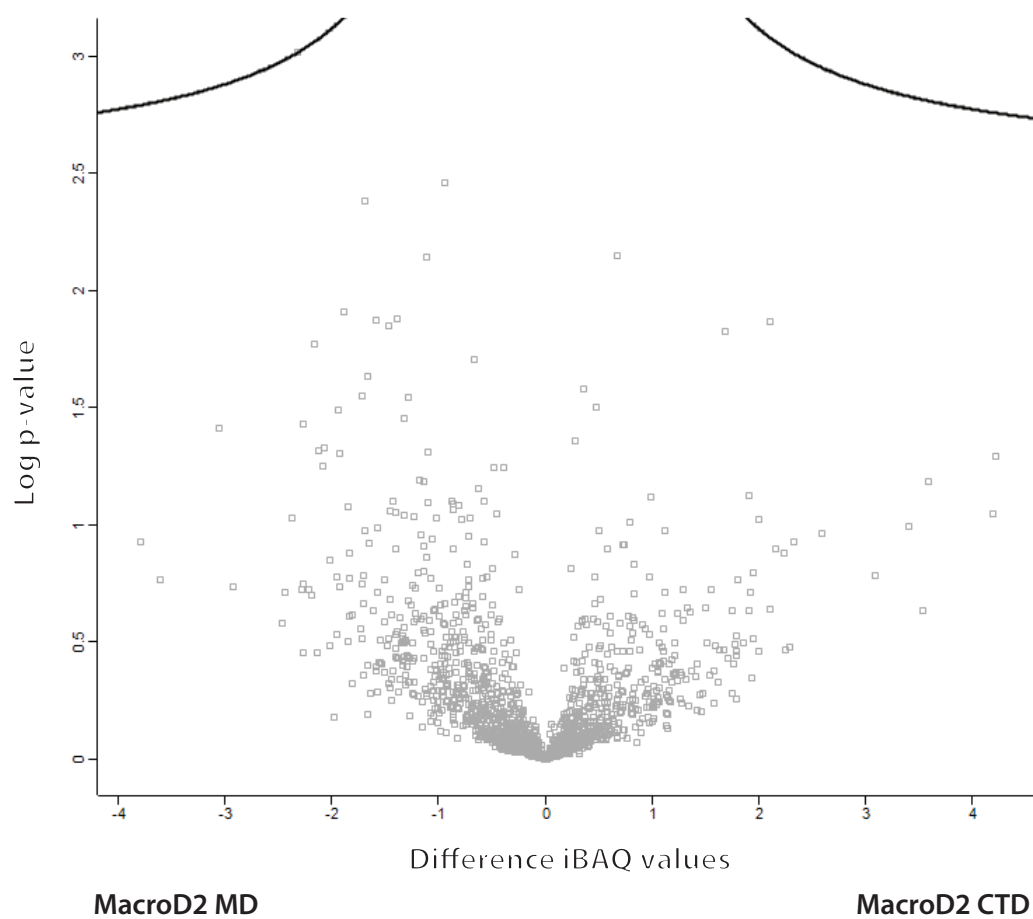


Figure A.1: Volcano plot of MacroD2 macrodomain and C-terminal domain interactors.iBAQ value intensity differences of individual detected are plotted against their p-value. No significantly changed proteins are on top of the cutoff line ($s_0=0.1$, FDR 0.05). Generated in Perseus

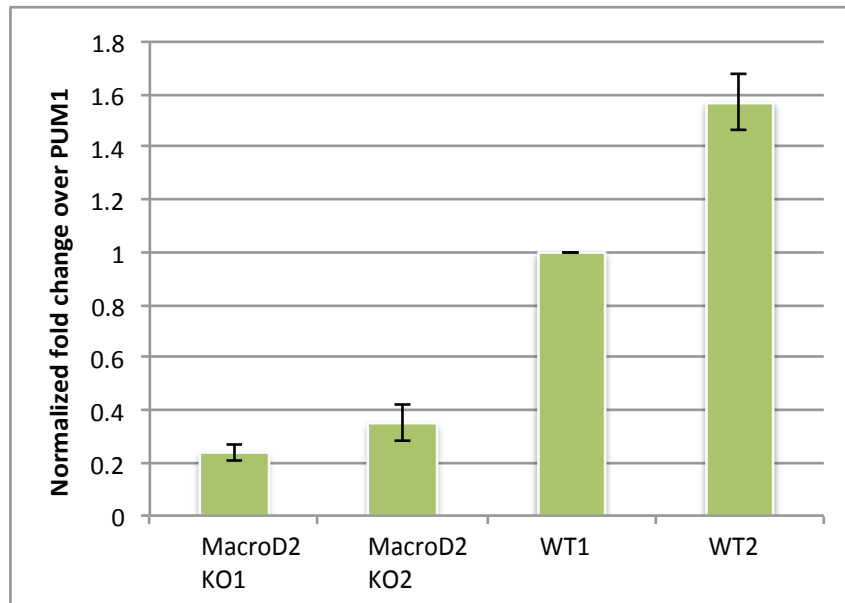


Figure A.2: RT-qPCR results of MacroD2 KO cell lines vs WT cell lines. Fold change over PUM1. Normalized to clonal WT1. Performed with Irene Chen (DAAD summer student)

Table A.2: Percent of cells in different cell cycle phases. PI stained cells were FACS sorted. Percentage of cells in G1-, S-, G2-phase. More than 10000 cells sorted. 2 Replicates per cell lines. Mean +/- Standard deviation

Cell Line	G1-phase	S-phase	G2-phase
MacroD2 KO1	48.2 +/- 6.9	9.7 +/- 1.0	33,7 +/- 0.4
MacroD2 KO2	51.6 +/- 7.4	9.5 +/- 2.3	33,9 +/- 4.0
WT1	53.7 +/- 0.1	9.5 +/- 0.9	23.2 +/- 3.3
WT2	53.6 +/- 7.9	11.0 +/- 4.1	29.0 +/- 4.5
TARG1 KO1	52.6 +/- 14.0	11.6 +/- 4.2	29.9 +/- 12.2
TARG1 KO2	53.0 +/- 2.3	13.4 +/- 4.2	27.8 +/- 1.1

A.3 Actin-regulated processes regulated by MacroD2 and/or TARG1

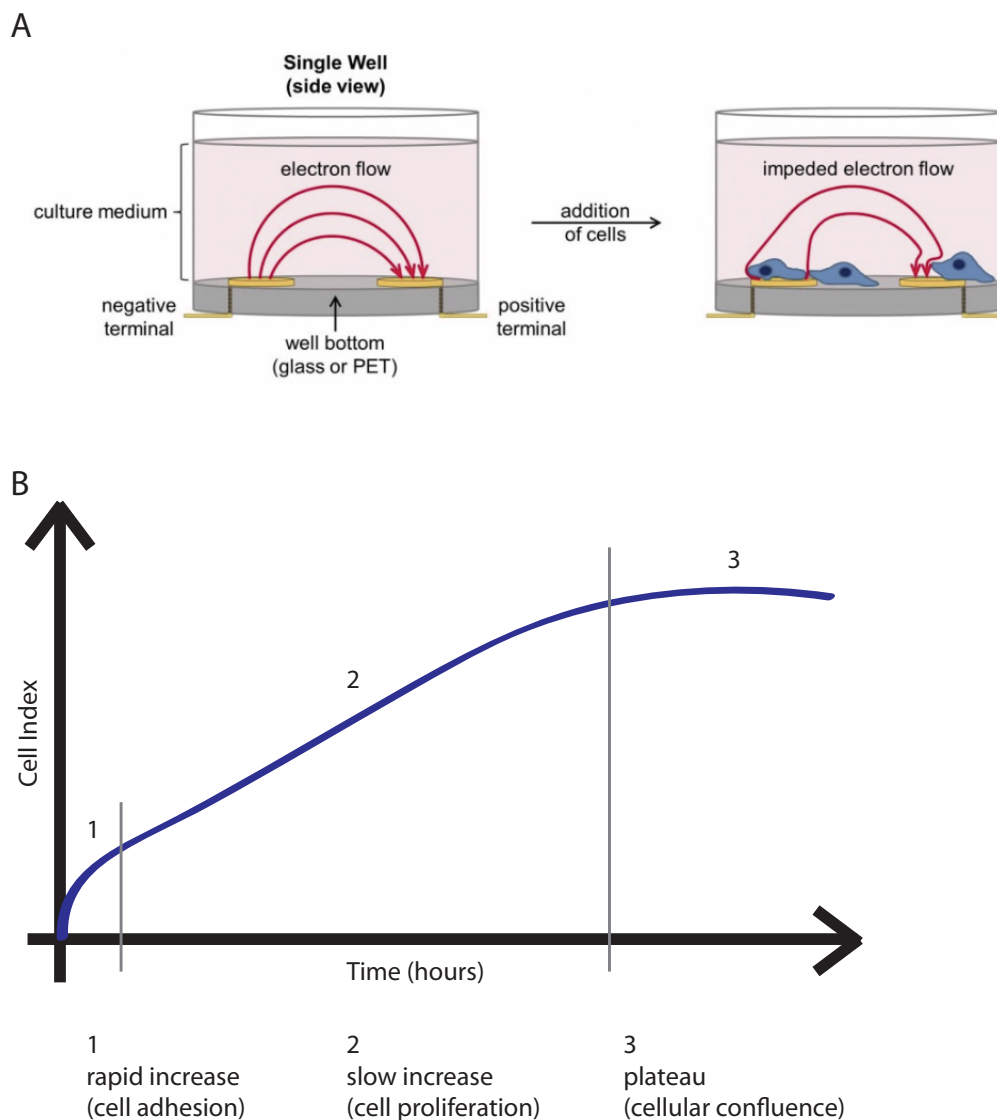


Figure A.3: xCelligence measurements. A) Schematic representation of xCelligence chamber and measurement. Electric flow in cells is measured. Upon attachment or proliferation of cells, electric flow is hindered/impeded. Impedance correlates directly with cell proliferation. B) Schematic xCelligence plot of cell attachment and proliferation. Cell attachment results in rapid increase in impedance, proliferation in slow increase and confluence results in plateau phase of the plot. From <https://www.aceabio.com/product/rtca-dp>

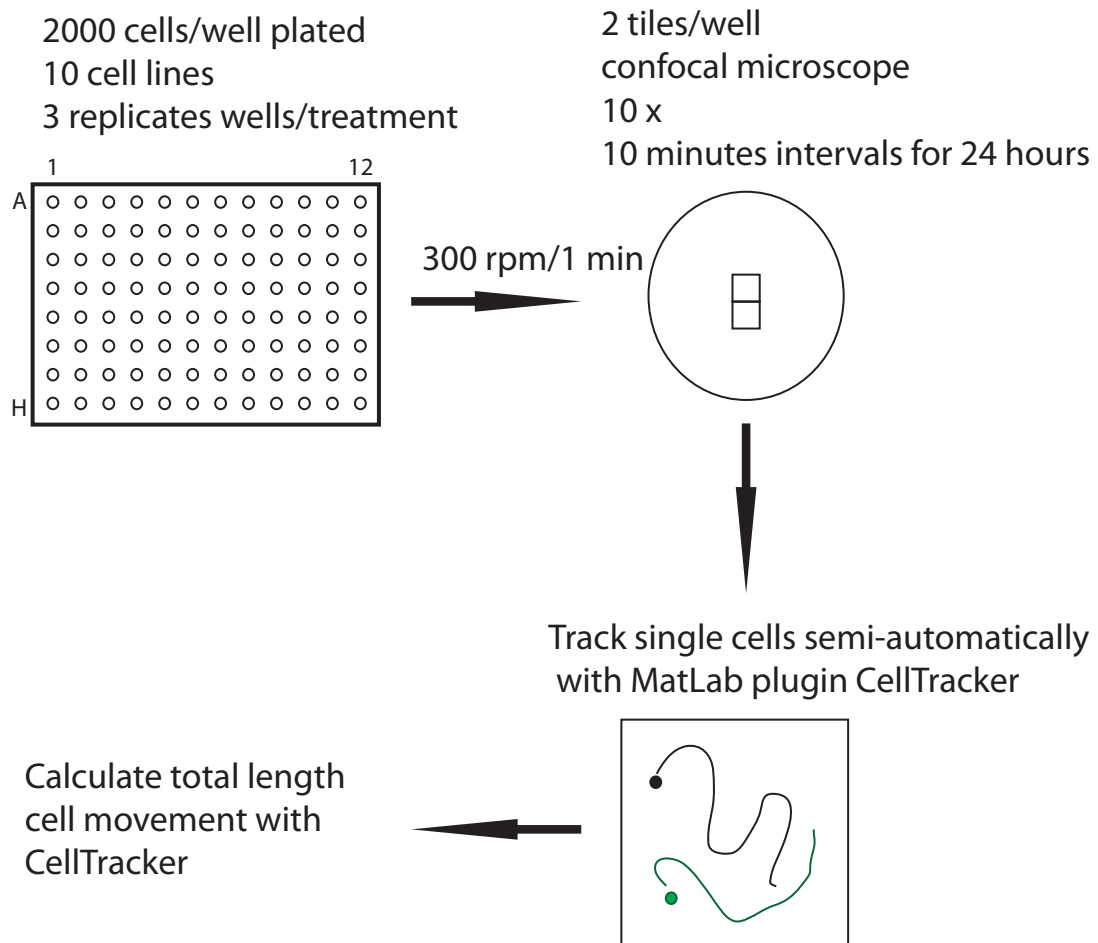


Figure A.4: Cells are seeded sparsely in a 96-well plate. Single cell migration is monitored semi-automatically with MatLab plugin CellTracker.GUI. Total length of migration is calculated by Matlab and plotted with Prism

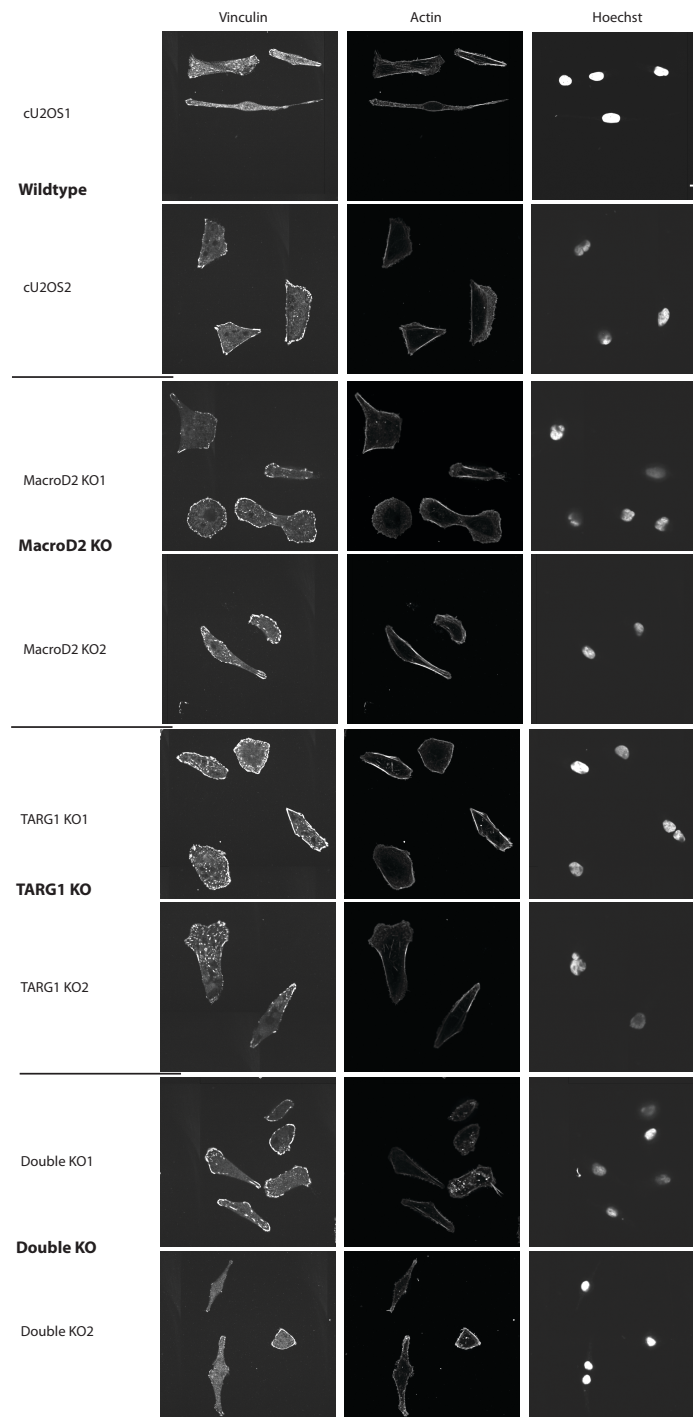


Figure A.5: Immunofluorescence images of all cell lines with actin and vinculin co-staining. Images of cells were taken at the cell attachment sites on the plate surface. Nuclei were stained with hoechst. Representative images were chosen. Experiment was repeated three times.

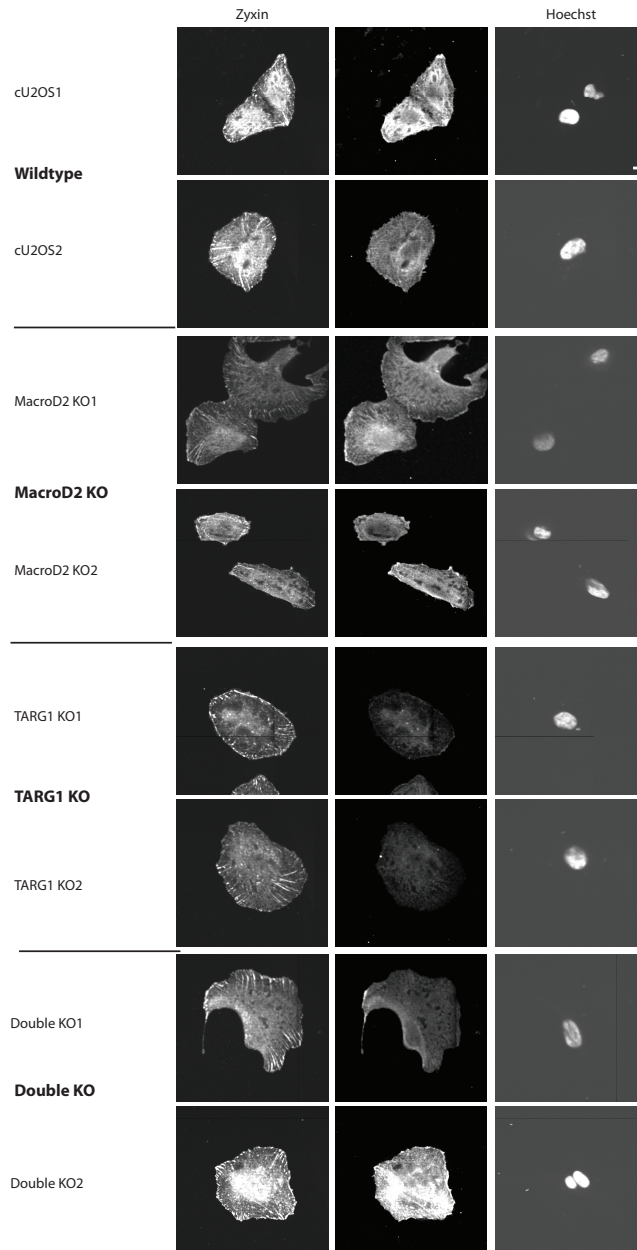


Figure A.6: Immunofluorescence images of all cell lines with Zyxin and Filamin A co-staining. Images of cells were taken at the cell attachment sites on the plate surface. Nuclei were stained with hoechst. Representative images were chosen. Experiment was repeated two times.

References

- R. C. T. Aguiar, Y. Yakushijin, S. Kharbanda, R. Salgia, J. A. Fletcher, and M. A. Shipp. BAL is a novel risk-related gene in diffuse large B-cell lymphomas that enhances cellular migration. *Blood*, 96(13):4328–4334, 2000.
- R. C. T. Aguiar, K. Takeyama, C. He, K. Kreinbrink, and M. A. Shipp. B-aggressive lymphoma family proteins have unique domains that modulate transcription and exhibit poly(ADP-ribose) polymerase activity. *Journal of Biological Chemistry*, 280(40):33756–33765, 2005.
- I. Ahel, D. Ahel, T. Matsusaka, A. J. Clark, J. Pines, S. J. Boulton, and S. C. West. Poly(ADP-ribose)-binding zinc finger motifs in DNA repair/checkpoint proteins. *Nature*, 451:81–85, 2008.
- P. Akan, A. Alexeyenko, P. I. Costea, L. Hedberg, B. W. Solnestam, S. Lundin, J. Hällman, E. Lundberg, M. Uhlén, and J. Lundeberg. Comprehensive analysis of the genome transcriptome and proteome landscapes of three tumor cell lines. *Genome Medicine*, 4(11):86, 2012.
- R. Anney, L. Klei, D. Pinto, R. Regan, J. Conroy, T. R. Magalhaes, C. Correia, B. S. Abrahams, N. Sykes, A. T. Pagnamenta, J. Almeida, E. Bacchelli, A. J. Bailey, G. Baird, A. Battaglia, T. Berney, N. Bolshakova, S. Bölte, P. F. Bolton, T. Bourgeron, S. Brennan, J. Brian, A. R. Carson, G. Casallo, J. Casey, S. H. Chu, L. Cochrane, C. Corsello, E. L. Crawford, A. Crossett, G. Dawson, M. de Jonge, R. Delorme, I. Drmic, E. Duketis, F. Duque, A. Estes, P. Farrar, B. A. Fernandez, S. E. Folstein, E. Fombonne, C. M. Freitag, J. Gilbert, C. Gillberg, J. T. Glessner, J. Goldberg, J. Green, S. J. Guter, H. Hakonarson, E. A. Heron, M. Hill, R. Holt, J. L. Howe, G. Hughes, V. Hus, R. Iglizzi, C. Kim, S. M. Klauck, A. Klevzon, O. Korvatska, V. Kustanovich, C. M. Lajonchere, J. A. Lamb, M. Laskawiec, M. Leboyer, A. Le Couteur, B. L. Leventhal, A. C. Lionel, X.-Q. Liu, C. Lord, L. Lotspeich, S. C. Lund, E. Maestrini, W. Mahoney, C. Mantoulan, C. R. Marshall, H. McConachie, C. J. McDougle, J. McGrath, W. M. McMahon, N. M. Melhem, A. Merikangas, O. Migita, N. J. Minshew, G. K. Mirza, J. Munson, S. F. Nelson, C. Noakes, A. Noor, G. Nygren, G. Oliveira, K. Papanikolaou, J. R. Parr, B. Parrini, T. Paton, A. Pickles, J. Piven, D. J. Posey, A. Poustka, F. Poustka, A. Prasad, J. Ragousis, K. Renshaw, J. Rickaby, W. Roberts, K. Roeder, B. Roge, M. L. Rutter, L. J. Bierut, J. P. Rice, J. Salt, K. Sansom, D. Sato, R. Segurado, L. Senman, N. Shah, V. C. Sheffield,

- L. Soorya, I. Sousa, V. Stoppioni, C. Strawbridge, R. Tancredi, K. Tansey, B. Thiruvahindrapduram, A. P. Thompson, S. Thomson, A. Tryfon, J. Tsiantis, H. Van Engeland, J. B. Vincent, F. Volkmar, S. Wallace, K. Wang, Z. Wang, T. H. Wassink, K. Wing, K. Wittmeyer, S. Wood, B. L. Yaspan, D. Zurawiecki, L. Zwaigenbaum, C. Betancur, J. D. Buxbaum, R. M. Cantor, E. H. Cook, H. Coon, M. L. Cuccaro, L. Gallagher, D. H. Geschwind, M. Gill, J. L. Haines, J. Miller, A. P. Monaco, J. I. Nurnberger Jr., A. D. Paterson, M. A. Pericak-Vance, G. D. Schellenberg, S. W. Scherer, J. S. Sutcliffe, P. Szatmari, A. M. Vicente, V. J. Vieland, E. M. Wijsman, B. Devlin, S. Ennis, and J. Hallmayer. A genome-wide scan for common alleles affecting risk for autism. *Human Molecular Genetics*, 19(20):4072–4082, 2010.
- K. Austen, P. Ringer, A. Mehlich, A. Chrostek-Grashoff, C. Kluger, C. Klingner, B. Sabass, R. Zent, M. Rief, and C. Grashoff. Extracellular rigidity sensing by talin isoform-specific mechanical linkages. *Nature Cell Biology*, 17(12):1597–1606, 2015.
- L. A. Baker, C. D. Allis, and G. G. Wang. Phd fingers in human diseases: Disorders arising from misinterpreting epigenetic marks. *Mutation Research/Fundamental and Molecular Mechanisms of Mutagenesis*, 647(1):3–12, 2008.
- S. E. Baranzini, J. Wang, R. A. Gibson, N. Galwey, Y. Naegelin, F. Barkhof, E.-W. Radue, R. L. P. Lindberg, B. M. G. Uitdehaag, M. R. Johnson, A. Angelakopoulou, L. Hall, J. C. Richardson, R. K. Prinjha, A. Gass, J. J. G. Geurts, J. Kragt, M. Sombekke, H. Vrenken, P. Qualley, R. R. Lincoln, R. Gomez, S. J. Caillier, M. F. George, H. Mousavi, R. Guerrero, D. T. Okuda, B. A. C. Cree, A. J. Green, E. Waubant, D. S. Goodin, D. Pelletier, P. M. Matthews, S. L. Hauser, L. Kappos, C. H. Polman, and J. R. Oksenberg. Genome-wide association analysis of susceptibility and clinical phenotype in multiple sclerosis. *Human Molecular Genetics*, 18(4):767–778, 2009.
- E. Barkauskaite, G. Jankevicius, A. G. Ladurner, I. Ahel, and G. Timinszky. The recognition and removal of cellular poly(ADP-ribose) signals. *The FEBS Journal*, 280(15):3491–3507, 2013.
- M. Beck, A. Schmidt, J. Malmstroem, M. Claassen, A. Ori, A. Szymborska, F. Herzog, O. Rinner, J. Ellenberg, and R. Aebersold. The quantitative proteome of a human cell line. *Molecular Systems Biology*, 7(1):549, 2011.
- B. J. Belin, T. Lee, and R. D. Mullins. DNA damage induces nuclear actin filament assembly by Formin-2 and Spire-1/2 that promotes efficient DNA repair. *eLife*, 4:e07735, 2015.
- A. Benmerah, J. Gagnon, B. Bègue, B. Mégarbané, A. Dautry-Varsat, and N. Cerf-Bensussan. The tyrosine kinase substrate eps15 is constitutively associated with the plasma membrane adaptor AP-2. *The Journal of Cell Biology*, 131(6):1831–1838, 1995.

-
- A. Benmerah, C. Lamaze, B. Bègue, S. L. Schmid, A. Dautry-Varsat, and N. Cerf-Bensussan. AP-2/Eps15 interaction is required for receptor-mediated endocytosis. *The Journal of Cell Biology*, 140(5):1055–1062, 1998.
- A. Bhardwaj, Y. Yang, B. Ueberheide, and S. Smith. Whole proteome analysis of human tankyrase knockout cells reveals targets of tankyrase-mediated degradation. *Nature Communications*, 8:2214, 2017.
- G. Bindea, B. Mlecnik, H. Hackl, P. Charoentong, M. Tosolini, A. Kirilovsky, W.-H. Fridman, F. Pagès, Z. Trajanoski, and J. Galon. ClueGO: A Cytoscape plug-in to decipher functionally grouped gene ontology and pathway annotation networks. *Bioinformatics*, 25(8):1091–1093, 2009.
- R. B. Birge, J. E. Fajardo, B. J. Mayer, and H. Hanafusa. Tyrosine-phosphorylated epidermal growth factor receptor and cellular p130 provide high affinity binding substrates to analyze Crk-phosphotyrosine-dependent interactions *in vitro*. *Journal of Biological Chemistry*, 267(15):10588–10595, 1992.
- R. B. Birge, C. Kalodimos, F. Inagaki, and S. Tanaka. Crk and CrkL adaptor proteins: networks for physiological and pathological signaling. *Cell Communication and Signaling*, 7(1):13, 2009.
- L. Blanchoin, R. Boujemaa-Paterski, C. Sykes, and J. Plastino. Actin dynamics, architecture, and mechanics in cell motility. *Physiological Reviews*, 94(1):235–263, 2014.
- J. J. Bonfiglio, P. Fontana, Q. Zhang, T. Colby, I. Gibbs-Seymour, I. Atanassov, E. Bartlett, R. Zaja, I. Ahel, and I. Matic. Serine ADP-ribosylation depends on HPF1. *Molecular Cell*, 65(5):932–940.e6, 2017.
- T. M. Brand, M. Iida, C. Li, and D. L. Wheeler. The nuclear epidermal growth factor receptor signaling network and its role in cancer. *Discovery Medicine*, 12(66):419–432, 2011.
- T. M. Brand, M. Iida, N. Luthar, M. M. Starr, E. J. Huppert, and D. L. Wheeler. Nuclear EGFR as a molecular target in cancer. *Radiotherapy and Oncology*, 108(3):370–377, 2013.
- R. Briffa, I. Um, D. Faratian, Y. Zhou, A. K. Turnbull, S. P. Langdon, and D. J. Harrison. Multi-scale genomic, transcriptomic and proteomic analysis of colorectal cancer cell lines to identify novel biomarkers. *PLOS ONE*, 10(12):e0144708, 2015.
- G. Brockhoff, F. Hofstaedter, and R. Knuechel. Flow cytometric detection and quantitation of the epidermal growth factor receptor in comparison to Scatchard analysis in human bladder carcinoma cell lines. *Cytometry*, 17(1):75–83, 1994.

- P. Burke, K. Schooler, and H. S. Wiley. Regulation of epidermal growth factor receptor signaling by endocytosis and intracellular trafficking. *Molecular Biology of the Cell*, 12(6):1897–1910, 2001.
- M. Bütepage, L. Eckeï, P. Verheugd, and B. Lüscher. Intracellular mono-ADP-ribosylation in signaling and disease. *Cells*, 4(4):569–595, 2015.
- M. G. Callow, H. Tran, L. Phu, T. Lau, J. Lee, W. N. Sandoval, P. S. Liu, S. Bheddah, J. Tao, J. R. Lill, J.-A. Hongo, D. Davis, D. S. Kirkpatrick, P. Polakis, and M. Costa. Ubiquitin ligase RNF146 regulates tankyrase and axin to promote Wnt signaling. *PLOS ONE*, 6(7):e22595, 2011.
- X. A. Cambronne, M. L. Stewart, D. Kim, A. M. Jones-Brunette, R. K. Morgan, D. L. Farrens, M. S. Cohen, and R. H. Goodman. Biosensor reveals multiple sources for mitochondrial NAD⁺. *Science*, 352(6292):1474–1477, 2016.
- R. Carbone, S. Fré, G. Iannolo, F. Belleudi, P. Mancini, P. G. Pelicci, M. R. Torrisi, and P. P. Di Fiore. eps15 and eps15R are essential components of the endocytic pathway. *Cancer Research*, 57(24):5498–5504, 1997.
- A. E. Carpenter, T. R. Jones, M. R. Lamprecht, C. Clarke, I. H. Kang, O. Friman, D. A. Guertin, J. H. Chang, R. A. Lindquist, J. Moffat, P. Golland, and D. M. Sabatini. CellProfiler: image analysis software for identifying and quantifying cell phenotypes. *Genome Biology*, 7(10):R100, 2006.
- I. Carter-O’Connell, H. Jin, R. K. Morgan, L. L. David, and M. S. Cohen. Engineering the substrate specificity of ADP-ribosyltransferases for identifying direct protein targets. *Journal of the American Chemical Society*, 136(14):5201–5204, 2014.
- I. Carter-O’Connell, H. Jin, R. K. Morgan, R. Zaja, L. L. David, I. Ahel, and M. S. Cohen. Identifying family-member-specific targets of mono-ARTDs by using a chemical genetics approach. *Cell Reports*, 14(3):621–631, 2016.
- L. Cavone, A. Aldinucci, C. Ballerini, T. Biagioli, F. Moroni, and A. Chiarugi. PARP-1 inhibition prevents CNS migration of dendritic cells during EAE, suppressing the encephalitogenic response and relapse severity. *Multiple Sclerosis Journal*, 17(7):794–807, 2011.
- P. Chambon, J. D. Weill, and P. Mandel. Nicotinamide mononucleotide activation of a new DNA-dependent polyadenylic acid synthesizing nuclear enzyme. *Biochemical and Biophysical Research Communications*, 11(1):39–43, 1963.
- J. D. Chapman, J.-P. Gagné, G. G. Poirier, and D. R. Goodlett. Mapping PARP-1 auto-ADP-ribosylation sites by liquid chromatography-tandem mass spectrometry. *Journal of Proteome Research*, 12(4):1868–1880, 2013.

-
- M.-M. Choi, J.-W. Huh, S.-J. Yang, E. H. Cho, S. Y. Choi, and S.-W. Cho. Identification of ADP-ribosylation site in human glutamate dehydrogenase isozymes. *FEBS Letters*, 579(19):4125–4130, 2005.
- L. A. Cingolani and Y. Goda. Actin in action: the interplay between the actin cytoskeleton and synaptic efficacy. *Nature Reviews Neuroscience*, 9(5):344–356, 2008.
- R. J. Coffey, C. J. Hawkey, L. Damstrup, R. Graves-Deal, V. C. Daniel, P. J. Dempsey, R. Chinery, S. C. Kirkland, R. N. DuBois, T. L. Jetton, and J. D. Morrow. Epidermal growth factor receptor activation induces nuclear targeting of cyclooxygenase-2, basolateral release of prostaglandins, and mitogenesis in polarizing colon cancer cells. *Proceedings of the National Academy of Sciences*, 94(2):657–662, 1997.
- E. A. Coon and E. E. Benarroch. DNA damage response: selected review and neurologic implications. *Neurology*, 90(8):367–376, 2018.
- J. A. Cooper. Mechanisms of cell migration in the nervous system. *The Journal of Cell Biology*, 202(5):725–734, 2013.
- J. Cox and M. Mann. MaxQuant enables high peptide identification rates, individualized p.p.b.-range mass accuracies and proteome-wide protein quantification. *Nature Biotechnology*, 26(12):1367–1372, 2008.
- J. Cox, N. Neuhauser, A. Michalski, R. A. Scheltema, J. V. Olsen, and M. Mann. Andromeda: a peptide search engine integrated into the MaxQuant environment. *Journal of Proteome Research*, 10(4):1794–1805, 2011.
- G. Dalpé, N. Leclerc, A. Vallée, A. Messer, M. Mathieu, Y. De Repentigny, and R. Kothary. Dystonin is essential for maintaining neuronal cytoskeleton organization. *Molecular and Cellular Neurosciences*, 10(5-6):243–257, 1998.
- R. Daly. Cortactin signalling and dynamic actin networks. *Biochemical Journal*, 382(1):13–25, 2004.
- C. Daniels, S.-E. Ong, and A. L. Leung. The promise of proteomics for the study of ADP-ribosylation. *Molecular Cell*, 58(6):911–924, 2015.
- M. D. Daugherty, J. M. Young, J. A. Kerns, and H. S. Malik. Rapid evolution of PARP genes suggests a broad role for ADP-ribosylation in host-virus conflicts. *PLOS Genetics*, 10(5):e1004403, 2014.
- T. A. Davis, B. Loos, and A. M. Engelbrecht. AHNAK: The giant jack of all trades. *Cellular Signalling*, 26(12):2683–2693, 2014.
- S. Debette, J. C. Bis, M. Fornage, H. Schmidt, M. A. Ikram, S. Sigurdsson, G. Heiss, M. Struchalin, A. V. Smith, A. van Der Lugt, C. DeCarli, T. Lumley, D. S. Knopman, C. Enzinger, G. Eiriksdottir, P. J. Koudstaal, A. L. DeStefano, B. M. Psaty, C. Dufouil,

- D. J. Catellier, F. Fazekas, T. Aspelund, Y. S. Aulchenko, A. Beiser, J. I. Rotter, C. Tzourio, D. K. Shibata, M. Tscherner, T. B. Harris, F. Rivadeneira, L. D. Atwood, K. Rice, R. F. Gottesman, M. A. van Buchem, A. G. Uitterlinden, M. Kelly-Hayes, M. Cushman, Y. Zhu, E. Boerwinkle, V. Gudnason, A. Hofman, J. R. Romero, O. Lopez, C. M. van Duijn, R. Au, S. R. Heckbert, P. A. Wolf, T. H. Mosley, S. Seshadri, M. M. B. Breteler, R. Schmidt, L. J. Launer, and W. T. Longstreth. Genome-wide association studies of MRI-defined brain infarcts: meta-analysis from the charge consortium. *Stroke*, 41(2): 210–217, 2010.
- A. Dereli-Öz, G. Versini, and T. D. Halazonetis. Studies of genomic copy number changes in human cancers reveal signatures of DNA replication stress. *Molecular Oncology*, 5(4): 308–314, 2011.
- Y. L. Deribe, T. Pawson, and I. Dikic. Post-translational modifications in signal integration. *Nature Structural & Molecular Biology*, 17(6):666–672, 2010.
- G. Di Sante, L. Wang, C. Wang, X. Jiao, M. C. Casimiro, K. Chen, T. G. Pestell, I. Yaman, A. Di Rocco, X. Sun, Y. Horio, M. J. Powell, X. He, M. W. McBurney, and R. G. Pestell. *Sirt1*-deficient mice have hypogonadotropic hypogonadism due to defective GnRH neuronal migration. *Molecular Endocrinology*, 29(2):200–212, 2015.
- K. Dittmann, C. Mayer, R. Kehlbach, and H. P. Rodemann. Radiation-induced caveolin-1 associated EGFR internalization is linked with nuclear EGFR transport and activation of DNA-PK. *Molecular Cancer*, 7(1):69, 2008.
- R. Dominguez and K. C. Holmes. Actin structure and function. *Annual Review of Biophysics*, 40(1):169–186, 2011.
- D. C. Edwards, L. C. Sanders, G. M. Bokoch, and G. N. Gill. Activation of LIM-kinase by Pak1 couples Rac/Cdc42 GTPase signalling to actin cytoskeletal dynamics. *Nature Cell Biology*, 1(5):253–259, 1999.
- K. L. H. Feijs, A. H. Forst, P. Verheugd, and B. Lüscher. Macrodomain-containing proteins: regulating new intracellular functions of mono(ADP-ribosyl)ation. *Nature Reviews Molecular Cell Biology*, 14(7):443–451, 2013a.
- K. L. H. Feijs, H. Kleine, A. Braczynski, A. H. Forst, N. Herzog, P. Verheugd, U. Linzen, E. Kremmer, and B. Lüscher. ARTD10 substrate identification on protein microarrays: Regulation of GSK3 β by mono-ADP-ribosylation. *Cell Communication & Signaling*, 11(1):5, 2013b.
- K. L. H. Feijs, P. Verheugd, and B. Lüscher. Expanding functions of intracellular resident mono-ADP-ribosylation in cell physiology. *The FEBS Journal*, 280(15):3519–3529, 2013c.

-
- Y. Feng and C. A. Walsh. The many faces of filamin: a versatile molecular scaffold for cell motility and signalling. *Nature Cell Biology*, 6(11):1034–1038, 2004.
- Y. Feng, M. H. Chen, I. P. Moskowitz, A. M. Mendonza, L. Vidali, F. Nakamura, D. J. Kwiatkowski, and C. A. Walsh. Filamin A (FLNA) is required for cell-cell contact in vascular development and cardiac morphogenesis. *Proceedings of the National Academy of Sciences*, 103(52):19836–19841, 2006.
- J. L. Fiori, T.-N. Zhu, M. P. O’Connell, K. S. Hoek, F. E. Indig, B. P. Frank, C. Morris, S. Kole, J. Hasskamp, G. Elias, A. T. Weeraratna, and M. Bernier. Filamin A modulates kinase activation and intracellular trafficking of epidermal growth factor receptors in human melanoma cells. *Endocrinology*, 150(6):2551–2560, 2009.
- P. Fontana, J. J. Bonfiglio, L. Palazzo, E. Bartlett, I. Matic, and I. Ahel. Serine ADP-ribosylation reversal by the hydrolase ARH3. *eLife*, 6:e28533, 2017.
- A. H. Forst, T. Karlberg, N. Herzog, A.-G. Thorsell, A. Gross, K. L. H. Feijs, P. Verheugd, P. Kursula, B. Nijmeijer, E. Kremmer, H. Kleine, A. G. Ladurner, H. Schüler, and B. Lüscher. Recognition of mono-ADP-ribosylated ARTD10 substrates by ARTD8 macrodomains. *Structure*, 21(3):462–475, 2013.
- R. E. Frye, M. Tippet, L. Delhey, and J. Slattery. Heterozygous deletion of macro domain containing 2 (MACROD2) is associated with autism spectrum disorder. *The North American Journal of Medicine and Science*, 9(1):35–37, 2016.
- J.-P. Gagné, J. M. Hunter, B. Labrecque, B. Chabot, and G. G. Poirier. A proteomic approach to the identification of heterogeneous nuclear ribonucleoproteins as a new family of poly(ADP-ribose)-binding proteins. *The Biochemical Journal*, 371(Pt 2):331–340, 2003.
- J.-P. Gagné, M. Isabelle, K. S. Lo, S. Bourassa, M. J. Hendzel, V. L. Dawson, T. M. Dawson, and G. G. Poirier. Proteome-wide identification of poly(ADP-ribose) binding proteins and poly(ADP-ribose)-associated protein complexes. *Nucleic Acids Research*, 36(22):6959–6976, 2008.
- J.-P. Gagné, É. Pic, M. Isabelle, J. Krietsch, C. Éthier, É. Paquet, I. Kelly, M. Boutin, K.-M. Moon, L. J. Foster, and G. G. Poirier. Quantitative proteomics profiling of the poly(ADP-ribose)-related response to genotoxic stress. *Nucleic Acids Research*, 40(16):7788–7805, 2012.
- M. L. Gardel, I. C. Schneider, Y. Aratyn-Schaus, and C. M. Waterman. Mechanical integration of actin and adhesion dynamics in cell migration. *Annual Review of Cell and Developmental Biology*, 26(1):315–333, 2010.

- E. Gerace, A. Masi, F. Resta, R. Felici, E. Landucci, T. Mello, D. E. Pellegrini-Giampietro, G. Mannaioni, and F. Moroni. PARP-1 activation causes neuronal death in the hippocampal CA1 region by increasing the expression of Ca²⁺-permeable AMPA receptors. *Neurobiology of Disease*, 70:43–52, 2014.
- I. Gibbs-Seymour, P. Fontana, J. G. M. Rack, and I. Ahel. HPF1/C4orf27 is a PARP-1-interacting protein that regulates PARP-1 ADP-ribosylation activity. *Molecular Cell*, 62(3):432–442, 2016.
- B. Golia, G. K. Moeller, G. Jankevicius, A. Schmidt, A. Hegele, J. Preißer, M. L. Tran, A. Imhof, and G. Timinszky. ATM induces MacroD2 nuclear export upon DNA damage. *Nucleic Acids Research*, 45(1):244–254, 2017.
- L. M. Grøvdal, E. Stang, A. Sorkin, and I. H. Madshus. Direct interaction of Cbl with pTyr 1045 of the EGF receptor (EGFR) is required to sort the EGFR to lysosomes for degradation. *Experimental Cell Research*, 300(2):388–395, 2004.
- R. Gupte, Z. Liu, and W. L. Kraus. PARPs and ADP-ribosylation: recent advances linking molecular functions to biological outcomes. *Genes & Development*, 31(2):101–126, 2017.
- C. Haffner, K. Takei, H. Chen, N. Ringstad, A. Hudson, M. H. Butler, A. E. Salcini, P. P. Di Fiore, and P. De Camilli. Synaptojanin 1: localization on coated endocytic intermediates in nerve terminals and interaction of its 170 kDa isoform with Eps15. *FEBS Letters*, 419(2-3):175–180, 1997.
- M. P. Hagan, A. Yacoub, and P. Dent. Radiation-induced PARP activation is enhanced through EGFR-ERK signaling. *Journal of Cellular Biochemistry*, 101(6):1384–1393, 2007.
- K. Haglund and I. Dikic. The role of ubiquitylation in receptor endocytosis and endosomal sorting. *Journal of Cell Science*, 125(2):265–275, 2012.
- J.-F. Haince, D. McDonald, A. Rodrigue, U. Déry, J.-Y. Masson, M. J. Hendzel, and G. G. Poirier. PARP1-dependent kinetics of recruitment of MRE11 and NBS1 proteins to multiple DNA damage sites. *Journal of Biological Chemistry*, 283(2):1197–1208, 2008.
- B. J. Harrison, G. Venkat, J. L. Lamb, T. H. Hutson, C. Drury, K. K. Rau, M. B. Bunge, L. M. Mendell, F. H. Gage, R. D. Johnson, C. E. Hill, E. C. Rouchka, L. D. F. Moon, and J. C. Petruska. The adaptor protein CD2AP is a coordinator of neurotrophin signaling-mediated axon arbor plasticity. *Journal of Neuroscience*, 36(15):4259–4275, 2016.
- K. Heine, S. Pust, S. Enzenmüller, and H. Barth. ADP-ribosylation of actin by the *clostridium botulinum* C2 toxin in mammalian cells results in delayed caspase-dependent. *Infection and Immunity*, 76(10):4600–4608, 2008.

-
- Z. Herceg and Z.-Q. Wang. Functions of poly(ADP-ribose) polymerase (PARP) in DNA repair, genomic integrity and cell death. *Mutation Research/Fundamental and Molecular Mechanisms of Mutagenesis*, 477(1-2):97–110, 2001.
- M. O. Hottiger. Nuclear ADP-ribosylation and its role in chromatin plasticity, cell differentiation, and epigenetics. *Annual Review of Biochemistry*, 84(1):227–263, 2015a.
- M. O. Hottiger. SnapShot: ADP-ribosylation signaling. *Molecular Cell*, 58(6):1134–1134.e1, 2015b.
- M. O. Hottiger, P. O. Hassa, B. Lüscher, H. Schüler, and F. Koch-Nolte. Toward a unified nomenclature for mammalian ADP-ribosyltransferases. *Trends in Biochemical Sciences*, 35(4):208–219, 2010.
- P. Hotulainen and C. C. Hoogenraad. Actin in dendritic spines: connecting dynamics to function. *The Journal of Cell Biology*, 189(4):619–629, 2010.
- P. Hotulainen and P. Lappalainen. Stress fibers are generated by two distinct actin assembly mechanisms in motile cells. *The Journal of Cell Biology*, 173(3):383–394, 2006.
- F. Huang, D. Kirkpatrick, X. Jiang, S. Gygi, and A. Sorkin. Differential regulation of EGF receptor internalization and degradation by multiubiquitination within the kinase domain. *Molecular Cell*, 21(6):737–748, 2006.
- J. Y. Huang, K. Wang, A. Vermehren-Schmaedick, J. P. Adelman, and M. S. Cohen. PARP6 is a regulator of hippocampal dendritic morphogenesis. *Scientific Reports*, 6:18512, 2016.
- J. Huelsken and J. Behrens. The Wnt signalling pathway. *Journal of Cell Science*, 115(21):3977–3978, 2002.
- L.-Y. Hung, J. T. Tseng, Y.-C. Lee, W. Xia, Y.-N. Wang, M.-L. Wu, Y.-H. Chuang, C.-H. Lai, and W.-C. Chang. Nuclear epidermal growth factor receptor (EGFR) interacts with signal transducer and activator of transcription 5 (STAT5) in activating Aurora-A gene expression. *Nucleic Acids Research*, 36(13):4337–4351, 2008.
- V. Iansante, P. M. Choy, S. W. Fung, Y. Liu, J.-G. Chai, J. Dyson, A. Del Rio, C. D’Santos, R. Williams, S. Chokshi, R. A. Anders, C. Bubici, and S. Papa. PARP14 promotes the Warburg effect in hepatocellular carcinoma by inhibiting JNK1-dependent PKM2 phosphorylation and activation. *Nature Communications*, 6:7882, 2015.
- W. Ikeda, H. Nakanishi, J. Miyoshi, K. Mandai, H. Ishizaki, M. Tanaka, A. Togawa, K. Takahashi, H. Nishioka, H. Yoshida, A. Mizoguchi, S.-I. Nishikawa, and Y. Takai. Afadin: A key molecule essential for structural organization of cell-cell junctions of polarized epithelia during embryogenesis. *The Journal of Cell Biology*, 146(5):1117–1131, 1999.

- M. Isabelle, J.-P. Gagné, I.-E. Gallouzi, and G. G. Poirier. Quantitative proteomics and dynamic imaging reveal that G3BP-mediated stress granule assembly is poly(ADP-ribose)-dependent following exposure to MNNG-induced DNA alkylation. *Journal of Cell Science*, 125(19):4555–4566, 2012.
- S. Jaganathan, P. Yue, D. C. Paladino, J. Bogdanovic, Q. Huo, and J. Turkson. A functional nuclear epidermal growth factor receptor, Src and Stat3 heteromeric complex in pancreatic cancer cells. *PLOS ONE*, 6(5):e19605, 2011.
- G. Jankevicius, M. Hassler, B. Golia, V. Rybin, M. Zacharias, G. Timinszky, and A. G. Ladurner. A family of macrodomain proteins reverses cellular mono-ADP-ribosylation. *Nature Structural & Molecular Biology*, 20(4):508–514, 2013.
- G. Jékely, H.-H. Sung, C. M. Luque, and P. Rørth. Regulators of endocytosis maintain localized receptor tyrosine kinase signaling in guided migration. *Developmental Cell*, 9(2):197–207, 2005.
- R. M. Jones, G. Cadby, J. Blangero, L. J. Abraham, A. J. O. Whitehouse, and E. K. Moses. *MACROD2* gene associated with autistic-like traits in a general population sample. *Psychiatric Genetics*, 24(6):241–248, 2014.
- M. Jwa and P. Chang. PARP16 is a tail-anchored endoplasmic reticulum protein required for the PERK- and IRE1 α -mediated unfolded protein response. *Nature Cell Biology*, 14(11):1223–1230, 2012.
- P. Kapoor and X. Shen. Mechanisms of nuclear actin in chromatin-remodeling complexes. *Trends in Cell Biology*, 24(4):238–246, 2014.
- D. I. Kim, B. KC, W. Zhu, K. Motamedchaboki, V. Doye, and K. J. Roux. Probing nuclear pore complex architecture with proximity-dependent biotinylation. *Proceedings of the National Academy of Sciences*, 111(24):E2453–E2461, 2014.
- H. Kim and C. A. McCulloch. Filamin A mediates interactions between cytoskeletal proteins that control cell adhesion. *FEBS Letters*, 585(1):18–22, 2011.
- J. Kim, W. J. Jahng, D. Di Vizio, J. S. Lee, R. Jhaveri, M. A. Rubin, A. Shisheva, and M. R. Freeman. The phosphoinositide kinase PIKfyve mediates epidermal growth factor receptor trafficking to the nucleus. *Cancer Research*, 67(19):9229–9237, 2007.
- M. Kira, J. Tanaka, and K. Sobue. Caldesmon and low Mr isoform of tropomyosin are localized in neuronal growth cones. *Journal of Neuroscience Research*, 40(3):294–305, 1995.
- K. H. Kirsch, M.-M. Georgescu, S. Ishimaru, and H. Hanafusa. CMS: an adapter molecule involved in cytoskeletal rearrangements. *Proceedings of the National Academy of Sciences*, 96(11):6211–6216, 1999.

-
- H. A. V. Kistemaker, A. P. Nardozza, H. S. Overkleeft, G. A. van der Marel, A. G. Ladurner, and D. V. Filippov. Synthesis and macrodomain binding of mono-ADP-ribosylated peptides. *Angewandte Chemie International Edition*, 55(36):10634–10638, 2016.
- O. Kohannim, D. P. Hibar, J. L. Stein, N. Jahanshad, X. Hua, P. Rajagopalan, A. W. Toga, C. R. Jack, M. W. Weiner, G. I. de Zubicaray, K. L. McMahon, N. K. Hansell, N. G. Martin, M. J. Wright, and P. M. Thompson. Discovery and replication of gene influences on brain structure using LASSO regression. *Frontiers in Neuroscience*, 6:115, 2012.
- P. Kreis and J.-V. Barnier. PAK signalling in neuronal physiology. *Cellular Signalling*, 21(3):384–393, 2009.
- C. Lauand, P. Rezende-Teixeira, B. A. Cortez, E. L. d. O. Niero, and G. M. Machado-Santelli. Independent of ErbB1 gene copy number, EGF stimulates migration but is not associated with cell proliferation in non-small cell lung cancer. *Cancer Cell International*, 13(1):38, 2013.
- H. Lee, J. Joo, S.-S. Nah, J. W. Kim, H.-K. Kim, J.-T. Kwon, H.-Y. Lee, Y. O. Kim, and H.-J. Kim. Changes in Dpysl2 expression are associated with prenatally stressed rat offspring and susceptibility to schizophrenia in humans. *International Journal of Molecular Medicine*, 35(6):1574–1586, 2015.
- S. Y. Lee, M. R. Wenk, Y. Kim, A. C. Nairn, and P. De Camilli. Regulation of synaptojanin 1 by cyclin-dependent kinase 5 at synapses. *Proceedings of the National Academy of Sciences*, 101(2):546–551, 2004.
- O. Leidecker, J. J. Bonfiglio, T. Colby, Q. Zhang, I. Atanassov, R. Zaja, L. Palazzo, A. Stockum, I. Ahel, and I. Matic. Serine is a new target residue for endogenous ADP-ribosylation on histones. *Nature Chemical Biology*, 12(12):998–1000, 2016.
- B. Leuner and E. Gould. Structural plasticity and hippocampal function. *Annual Review of Psychology*, 61(1):111–140, 2010.
- A. K. L. Leung, S. Vyas, J. E. Rood, A. Bhutkar, P. A. Sharp, and P. Chang. Poly(ADP-ribose) regulates stress responses and microRNA activity in the cytoplasm. *Molecular Cell*, 42(4):489–499, 2011.
- P. A. Levene and C. L. Alsborg. The cleavage products of vitellin. *Zeitschrift für physiologische Chemie*, (32):127–133, 1906.
- M. Li, L.-Y. Lu, C.-Y. Yang, S. Wang, and X. Yu. The FHA and BRCT domains recognize ADP-ribosylation during DNA damage response. *Genes & Development*, 27(16):1752–1768, 2013.
- N. Li and J. Chen. ADP-ribosylation: activation, recognition, and removal. *Molecules and Cells*, 37(1):9–16, 2014.

- N. Li, L. Feng, H. Liu, J. Wang, M. Kasembeli, M. K. Tran, D. J. Tweardy, S. H. Lin, and J. Chen. PARP inhibition suppresses growth of EGFR-mutant cancers by targeting nuclear PKM2. *Cell Reports*, 15(4):843–856, 2016.
- C.-C. Liang, A. Y. Park, and J.-L. Guan. *In vitro* scratch assay: a convenient and inexpensive method for analysis of cell migration *in vitro*. *Nature Protocols*, 2(2):329–333, 2007.
- H.-J. Liao and G. Carpenter. Role of the Sec61 translocon in EGF receptor trafficking to the nucleus and gene expression. *Molecular Biology of the Cell*, 18(3):1064–1072, 2007.
- S.-Y. Lin, K. Makino, W. Xia, A. Matin, Y. Wen, K. Y. Kwong, L. Bourguignon, and M.-C. Hung. Nuclear localization of EGF receptor and its potential new role as a transcription factor. *Nature Cell Biology*, 3(9):802–808, 2001.
- F. A. Lipmann and P. Levene. Serinephosphoric acid obtained on hydrolysis of vitellinic acid. *Journal of Biological Chemistry*, (98):109–114, 1932.
- R. Liu and J.-P. Jin. Calponin isoforms CNN1, CNN2 and CNN3: regulators for actin cytoskeleton functions in smooth muscle and non-muscle cells. *Gene*, 585(1):143–153, 2016.
- H.-W. Lo and M.-C. Hung. Nuclear EGFR signalling network in cancers: linking EGFR pathway to cell cycle progression, nitric oxide pathway and patient survival. *British Journal of Cancer*, 94(2):184–188, 2006.
- H.-W. Lo, S.-C. Hsu, M. Ali-Seyed, M. Gunduz, W. Xia, Y. Wei, G. Bartholomeusz, J.-Y. Shih, and M.-C. Hung. Nuclear interaction of EGFR and STAT3 in the activation of the iNOS/NO pathway. *Cancer Cell*, 7(6):575–589, 2005.
- H.-W. Lo, M. Ali-Seyed, Y. Wu, G. Bartholomeusz, S.-C. Hsu, and M.-C. Hung. Nuclear-cytoplasmic transport of EGFR involves receptor endocytosis, importin β 1 and CRM1. *Journal of Cellular Biochemistry*, 98(6):1570–1583, 2006.
- S. Love, R. Barber, and G. K. Wilcock. Increased poly(ADP-ribose) ation of nuclear proteins in Alzheimer’s disease. *Brain*, 122(2):247–253, 1999.
- S. T. Low-Nam, K. A. Lidke, P. J. Cutler, R. C. Roovers, P. M. P. van Bergen en Henegouwen, B. S. Wilson, and D. S. Lidke. ErbB1 dimerization is promoted by domain co-confinement and stabilized by ligand binding. *Nature Structural & Molecular Biology*, 18(11):1244–1249, 2011.
- X. Luo, K. W. Ryu, D.-S. Kim, T. Nandu, C. J. Medina, R. Gupte, B. A. Gibson, R. E. Soccio, Y. Yu, R. K. Gupta, and W. L. Kraus. PARP-1 controls the adipogenic transcriptional program by PARylating C/EBP β and modulating its transcriptional activity. *Molecular Cell*, 65(2):260–271, 2017.

-
- D. K. Lynch, S. C. Winata, R. J. Lyons, W. E. Hughes, G. M. Lehrbach, V. Wasinger, G. Corthals, S. Cordwell, and R. J. Daly. A cortactin-CD2-associated protein (CD2AP) complex provides a novel link between epidermal growth factor receptor endocytosis and the actin cytoskeleton. *Journal of Biological Chemistry*, 278(24):21805–21813, 2003.
- N. M. C. Maas, T. Van de Putte, C. Melotte, A. Francis, C. T. R. M. Schrandt-Stumpel, D. Sanlaville, D. Genevieve, S. Lyonnet, B. Dimitrov, K. Devriendt, J.-P. Fryns, and J. R. Vermeesch. The *C20orf133* gene is disrupted in a patient with Kabuki syndrome. *Journal of Medical Genetics*, 44(9):562–569, 2007.
- H. D. MacGillavry, J. M. Kerr, J. Kassner, N. A. Frost, and T. A. Blanpied. Shank-cortactin interactions control actin dynamics to maintain flexibility of neuronal spines and synapses. *European Journal of Neuroscience*, 43(2):179–193, 2016.
- S. M. MacGrath and A. J. Koleske. Cortactin in cell migration and cancer at a glance. *Journal of Cell Science*, 125(7):1621–1626, 2012.
- L. MacPherson, L. Tamblyn, S. Rajendra, F. Bralha, J. P. McPherson, and J. Matthews. 2,3,7,8-Tetrachlorodibenzo-*p*-dioxin poly(ADP-ribose) polymerase (TiPARP, ARTD14) is a mono-ADP-ribosyltransferase and repressor of aryl hydrocarbon receptor transactivation. *Nucleic Acids Research*, 41(3):1604–1621, 2013.
- I. H. Madshus and E. Stang. Internalization and intracellular sorting of the EGF receptor: a model for understanding the mechanisms of receptor trafficking. *Journal of Cell Science*, 122(19):3433–3439, 2009.
- S. Magi, E. Tashiro, and M. Imoto. A chemical genomic study identifying diversity in cell migration signaling in cancer cells. *Scientific Reports*, 2:823, 2012.
- M. Malanga, A. Czuby, A. Girstun, K. Staron, and F. R. Althaus. Poly(ADP-ribose) binds to the splicing factor ASF/SF2 and regulates its phosphorylation by DNA topoisomerase I. *Journal of Biological Chemistry*, 283(29):19991–19998, 2008.
- M. Mani, S. Y. Lee, L. Lucast, O. Cremona, G. Di Paolo, P. De Camilli, and T. A. Ryan. The dual phosphatase activity of Synaptojanin1 Is required for both efficient synaptic vesicle endocytosis and reavailability at nerve terminals. *Neuron*, 56(6):1004–1018, 2007.
- R. Martello, M. Leutert, S. Jungmichel, V. Bilan, S. C. Larsen, C. Young, M. O. Hottiger, and M. L. Nielsen. Proteome-wide identification of the endogenous ADP-ribosylome of mammalian cells and tissue. *Nature Communications*, 7:12917, 2016.
- S. Martire, L. Mosca, and M. D’Erme. PARP-1 involvement in neurodegeneration: a focus on Alzheimer’s and Parkinson’s diseases. *Mechanisms of Ageing and Development*, 146-148:53–64, 2015.

- M. Mashimo, J. Kato, and J. Moss. ADP-ribosyl-acceptor hydrolase 3 regulates poly (ADP-ribose) degradation and cell death during oxidative stress. *Proceedings of the National Academy of Sciences*, 110(47):18964–18969, 2013.
- M. Mashimo, J. Kato, and J. Moss. Structure and function of the ARH family of ADP-ribosyl-acceptor hydrolases. *DNA Repair*, 23:88–94, 2014.
- P. Mayer-Kuckuk, O. Ullrich, M. Ziegler, T. Grune, and M. Schweiger. Functional interaction of poly(ADP-ribose) with the 20S proteasome *in vitro*. *Biochemical and Biophysical Research Communications*, 259(3):576–581, 1999.
- H. C. Mefford. Finding the missing pieces: the microdeletion burden in GGE. *Epilepsy Currents*, 16(1):16–17, 2016.
- P. Mehrotra, J. P. Riley, R. Patel, F. Li, L. Voss, and S. Goenka. PARP-14 functions as a transcriptional switch for Stat6-dependent gene activation. *Journal of Biological Chemistry*, 286(3):1767–1776, 2011.
- R. Milo. What is the total number of protein molecules per cell volume? A call to rethink some published values. *BioEssays*, 35(12):1050–1055, 2013.
- G. K. Moeller and G. Timinszky. Reversing ADP-ribosylation. *eLife*, 6:e29942, 2017.
- M. Mohseni, J. Cidado, S. Croessmann, K. Cravero, A. Cimino-Mathews, H. Y. Wong, R. Scharpf, D. J. Zabransky, A. M. Abukhdeir, J. P. Garay, G. M. Wang, J. A. Beaver, R. L. Cochran, B. G. Blair, D. M. Rosen, B. Erlanger, P. Argani, P. J. Hurley, J. Lauring, and B. H. Park. *MACROD2* overexpression mediates estrogen independent growth and tamoxifen resistance in breast cancers. *Proceedings of the National Academy of Sciences*, 111(49):17606–17611, 2014.
- R. Morimura, K. Nozawa, H. Tanaka, and T. Ohshima. Phosphorylation of Dpsyl2 (CRMP2) and Dpsyl3 (CRMP4) is required for positioning of caudal primary motor neurons in the zebrafish spinal cord. *Developmental Neurobiology*, 73(12):911–920, 2013.
- S. I. Mota, I. L. Ferreira, J. Valero, E. Ferreira, A. L. Carvalho, C. R. Oliveira, and A. C. Rego. Impaired Src signaling and post-synaptic actin polymerization in Alzheimer’s disease mice hippocampus - Linking NMDA receptors and the reelin pathway. *Experimental Neurology*, 261:698–709, 2014.
- C. Mueller-Dieckmann, S. Kernstock, M. Lisurek, J. P. von Kries, F. Haag, M. S. Weiss, and F. Koch-Nolte. The structure of human ADP-ribosylhydrolase 3 (ARH3) provides insights into the reversibility of protein ADP-ribosylation. *Proceedings of the National Academy of Sciences*, 103(41):15026–15031, 2006.
- M. S. Nawaz, E. Giarda, F. Bedogni, P. La Montanara, S. Ricciardi, D. Ciceri, T. Alberio, N. Landsberger, L. Rusconi, and C. Kilstrup-Nielsen. CDKL5 and shootin1 interact and concur in regulating neuronal polarization. *PLOS ONE*, 11(2):e0148634, 2016.

-
- M. Niere, M. Mashimo, L. Agledal, C. Dölle, A. Kasamatsu, J. Kato, J. Moss, and M. Ziegler. ADP-ribosylhydrolase 3 (ARH3), not poly(ADP-ribose) glycohydrolase (PARG) isoforms, is responsible for degradation of mitochondrial matrix-associated poly(ADP-ribose). *Journal of Biological Chemistry*, 287(20):16088–16102, 2012.
- S. Nowsheen, T. Cooper, J. A. Stanley, and E. S. Yang. Synthetic lethal interactions between EGFR and parp inhibition in human triple negative breast cancer cells. *PLOS ONE*, 7(10):e46614, 2012.
- K. Oda, Y. Matsuoka, A. Funahashi, and H. Kitano. A comprehensive pathway map of epidermal growth factor receptor signaling. *Molecular Systems Biology*, 1(1):2005.0010, 2005.
- E. Ohashi, K. Tanabe, Y. Henmi, K. Mesaki, Y. Kobayashi, and K. Takei. Receptor sorting within endosomal trafficking pathway is facilitated by dynamic actin filaments. *PLOS ONE*, 6(5):e19942, 2011.
- S. Oka, J. Kato, and J. Moss. Identification and characterization of a mammalian 39-kDa poly(ADP-ribose) glycohydrolase. *Journal of Biological Chemistry*, 281(2):705–713, 2006.
- Oliveros, Juan Carlos. Venny. An interactive tool for comparing lists with Venn’s diagrams, 2007–2015. URL <http://bioinfogp.cnb.csic.es/tools/venny/index.html>.
- C. J. O’Neal, M. G. Jobling, R. K. Holmes, and W. G. Hol. Structural basis for the activation of cholera toxin by human ARF6-GTP. *Science*, 309(5737):1093–1096, 2005.
- S. Packham, Y. Lin, Z. Zhao, D. Warsito, D. Rutishauser, and O. Larsson. The nucleus-localized epidermal growth factor receptor is SUMOylated. *Biochemistry*, 54(33):5157–5166, 2015.
- E. A. Papakonstanti and C. Stournaras. Cell responses regulated by early reorganization of actin cytoskeleton. *FEBS Letters*, 582(14):2120–2127, 2008.
- H. N. Pfäffle, M. Wang, L. Gheorghiu, N. Ferraiolo, P. Greninger, K. Borgmann, J. Settlementan, C. H. Benes, L. V. Sequist, L. Zou, and H. Willers. EGFR-activating mutations correlate with a Fanconi Anemia-like cellular phenotype that includes PARP Inhibitor sensitivity. *Cancer Research*, 73(20):6254–6263, 2013.
- X. Pham, G. Song, S. Lao, L. Goff, H. Zhu, D. Valle, and D. Avramopoulos. The *DPYSL2* gene connects mTOR and schizophrenia. *Translational Psychiatry*, 6:e933, 2016.
- J. M. Pleschke, H. E. Kleczkowska, M. Strohm, and F. R. Althaus. Poly(ADP-ribose) binds to specific domains in DNA damage checkpoint proteins. *Journal of Biological Chemistry*, 275(52):40974–40980, 2000.

- E. A. Ponomarenko, E. V. Poverennaya, E. V. Ilgisonis, M. A. Pyatnitskiy, A. T. Kopylov, V. G. Zgoda, A. V. Lisitsa, and A. I. Archakov. The size of the human proteome: the width and depth. *International Journal of Analytical Chemistry*, 2016:7436849, 2016.
- K. Pritchard and C. J. Moody. Caldesmon: a calmodulin-binding actin-regulatory protein. *Cell Calcium*, 7(5–6):309–327, 1986.
- M. Rajaram, J. Zhang, T. Wang, J. Li, C. Kuscu, H. Qi, M. Kato, V. Grubor, R. J. Weil, A. Helland, A.-L. Borrenson-Dale, K. R. Cho, D. A. Levine, A. N. Houghton, J. D. Wolchok, L. Myeroff, S. D. Markowitz, S. W. Lowe, M. Zhang, A. Krasnitz, R. Lucito, D. Mu, and R. S. Powers. Two Distinct categories of focal deletions in cancer genomes. *PLOS ONE*, 8(6):e66264, 2013.
- J. Rakotomamonjy, M. Brunner, C. Jüschke, K. Zang, E. J. Huang, L. F. Reichardt, and A. Chenn. Afadin controls cell polarization and mitotic spindle orientation in developing cortical radial glia. *Neural Development*, 12(1):7, 2017.
- F. A. Ran, P. D. Hsu, J. Wright, V. Agarwala, D. A. Scott, and F. Zhang. Genome engineering using the CRISPR-Cas9 system. *Nature Protocols*, 8(11):2281–2308, 2013.
- S. Raychaudhuri, C. Loew, R. Körner, S. Pinkert, M. Theis, M. Hayer-Hartl, F. Buchholz, and F. U. Hartl. Interplay of acetyltransferase EP300 and the proteasome system in regulating heat shock transcription factor 1. *Cell*, 156(5):975–985, 2014.
- C. Revenu, R. Athman, S. Robine, and D. Louvard. The co-workers of actin filaments: from cell structures to signals. *Nature Reviews Molecular Cell Biology*, 5(8):635–646, 2004.
- A. A. Riccio, G. Cingolani, and J. M. Pascal. PARP-2 domain requirements for DNA damage-dependent activation and localization to sites of DNA damage. *Nucleic Acids Research*, 44(4):1691–1702, 2016.
- P. J. Rijken, W. J. Hage, P. M. van Bergen en Henegouwen, A. J. Verkleij, and J. Boonstra. Epidermal growth factor induces rapid reorganization of the actin microfilament system in human A431 cells. *Journal of Cell Science*, 100(3):491–499, 1991.
- M. I. Rodríguez, A. Peralta-Leal, F. O’Valle, J. M. Rodriguez-Vargas, A. Gonzalez-Flores, J. Majuelos-Melguizo, L. López, S. Serrano, A. G. de Herreros, J. C. Rodríguez-Manzanegue, R. Fernández, R. G. del Moral, J. M. de Almodóvar, and F. J. Oliver. PARP-1 regulates metastatic melanoma through modulation of vimentin-induced Malignant transformation. *PLOS Genetics*, 9(6):e1003531, 2013.
- S. Rom, N. L. Reichenbach, H. Dykstra, and Y. Persidsky. The dual action of poly(ADP-ribose) polymerase-1 (PARP-1) inhibition in HIV-1 infection: HIV-1 LTR inhibition and diminution in Rho GTPase activity. *Frontiers in Microbiology*, 6:878, 2015.

-
- F. Rosenthal, K. L. H. Feijs, E. Frugier, M. Bonalli, A. H. Forst, R. Imhof, H. C. Winkler, D. Fischer, A. Caffisch, P. O. Hassa, B. Lüscher, and M. O. Hottiger. Macrod domain-containing proteins are new mono-ADP-ribosylhydrolases. *Nature Structural & Molecular Biology*, 20(4):502–507, 2013.
- M. Rouleau, V. Saxena, A. Rodrigue, E. R. Paquet, A. Gagnon, M. J. Hendzel, J.-Y. Masson, M. Ekker, and G. G. Poirier. A key role for poly(ADP-ribose) polymerase 3 in ectodermal specification and neural crest development. *PLOS ONE*, 6(1):e15834, 2011.
- E. T. Roussos, J. S. Condeelis, and A. Patsialou. Chemotaxis in cancer. *Nature Reviews Cancer*, 11(8):573–587, 2011.
- K. J. Roux, D. I. Kim, M. Raida, and B. Burke. A promiscuous biotin ligase fusion protein identifies proximal and interacting proteins in mammalian cells. *The Journal of Cell Biology*, 196(6):801–810, 2012.
- K. W. Ryu, D.-S. Kim, and W. L. Kraus. New facets in the regulation of gene expression by ADP-ribosylation and poly(ADP-ribose) polymerases. *Chemical Reviews*, 115(6):2453–2481, 2015.
- R. Sannerud, I. Declerck, A. Peric, T. Raemaekers, G. Menendez, L. Zhou, B. Veerle, K. Coen, S. Munck, B. De Strooper, G. Schiavo, and W. Annaert. ADP ribosylation factor 6 (ARF6) controls amyloid precursor protein (APP) processing by mediating the endosomal sorting of BACE1. *Proceedings of the National Academy of Sciences*, 108(34):E559–E568, 2011.
- T. Sapir, T. Levy, A. Sakakibara, A. Rabinkov, T. Miyata, and O. Reiner. Shootin1 Acts in concert with KIF20B to Promote polarization of migrating neurons. *Journal of Neuroscience*, 33(29):11932–11948, 2013.
- M. Scaltriti and J. Baselga. The Epidermal growth factor receptor pathway: a model for targeted therapy. *Clinical Cancer Research*, 12(18):5268–5272, 2006.
- M. Schnoor, T. E. Stradal, and K. Rottner. Cortactin: Cell functions of a multifaceted actin-binding protein. *Trends in Cell Biology*, 28(2):79–98, 2018.
- B. T. Seet, I. Dikic, M.-M. Zhou, and T. Pawson. Reading protein modifications with interaction domains. *Nature Reviews Molecular Cell Biology*, 7(7):473–483, 2006.
- R. Sharifi, R. Morra, C. D. Appel, M. Tallis, B. Chioza, G. Jankevicius, M. A. Simpson, I. Matic, E. Ozkan, B. Golia, M. J. Schellenberg, R. Weston, J. G. Williams, M. N. Rossi, H. Galehdari, J. Krahn, A. Wan, R. C. Trembath, A. H. Crosby, D. Ahel, R. Hay, A. G. Ladurner, G. Timinszky, R. S. Williams, and I. Ahel. Deficiency of terminal ADP-ribose protein glycohydrolase TARG1/C6orf130 in neurodegenerative disease. *The EMBO Journal*, 32(9):1225–1237, 2013.

- J. H. Shin, Y. N. Kim, I. Y. Kim, D.-H. Choi, S. S. Yi, and J. K. Seong. Increased cell proliferations and neurogenesis in the hippocampal dentate gyrus of Ahnak Deficient mice. *Neurochemical Research*, 40(7):1457–1462, 2015.
- T. Shirao, K. Hanamura, N. Koganezawa, Y. Ishizuka, H. Yamazaki, and Y. Sekino. The role of drebrin in neurons. *Journal of Neurochemistry*, 141(6):819–834, 2017.
- D. Slade, M. S. Dunstan, E. Barkauskaite, R. Weston, P. Lafite, N. Dixon, M. Ahel, D. Leys, and I. Ahel. The structure and catalytic mechanism of a poly(ADP-ribose) glycohydrolase. *Nature*, 477(7366):616–620, 2011.
- M. A. Smith, E. Blankman, M. L. Gardel, L. Luettjohann, C. M. Waterman, and M. C. Beckerle. A zyxin-mediated mechanism for actin stress fiber maintenance and repair. *Developmental Cell*, 19(3):365–376, 2010.
- D. P. Srivastava, B. A. Copits, Z. Xie, R. Huda, K. A. Jones, S. Mukherji, M. E. Cahill, J.-E. VanLeeuwen, K. M. Woolfrey, I. Rafalovich, G. T. Swanson, and P. Penzes. Afadin is required for maintenance of dendritic structure and excitatory tone. *Journal of Biological Chemistry*, 287(43):35964–35974, 2012.
- J. B. Strosznajder, G. A. Czapski, A. Adamczyk, and R. P. Strosznajder. Poly(ADP-ribose) polymerase-1 in amyloid beta toxicity and Alzheimer’s disease. *Molecular Neurobiology*, 46(1):78–84, 2012.
- M. Szántó, A. Brunyánszki, B. Kiss, L. Nagy, P. Gergely, L. Virág, and P. Bai. Poly(ADP-ribose) polymerase-2: emerging transcriptional roles of a DNA-repair protein. *Cellular and Molecular Life Sciences*, 69(24):4079–4092, 2012.
- X. Tan, P. F. Lambert, A. C. Rapraeger, and R. A. Anderson. Stress-Induced EGFR trafficking: mechanisms, functions, and therapeutic implications. *Trends in Cell Biology*, 26(5):352–366, 2016.
- H. Tanaka, R. Morimura, and T. Ohshima. Dpysl2 (CRMP2) and Dpysl3 (CRMP4) phosphorylation by Cdk5 and DYRK2 is required for proper positioning of Rohon-Beard neurons and neural crest cells during neurulation in zebrafish. *Developmental Biology*, 370(2):223–236, 2012.
- J. Tang and D. J. Gross. Regulated EGF receptor binding to F-actin modulates receptor phosphorylation. *Biochemical and Biophysical Research Communications*, 312(4):930–936, 2003.
- F. Teloni and M. Altmeyer. Readers of poly(ADP-ribose): designed to be fit for purpose. *Nucleic Acids Research*, 44(3):993–1006, 2016.
- M. Terashima, C. Yamamori, and M. Shimoyama. ADP-ribosylation of Arg28 and Arg206 on the actin molecule by chicken arginine-specific ADP-ribosyltransferase. *European Journal of Biochemistry*, 231(1):242–249, 1995.

-
- S. Thalappilly, P. Soubeyran, J. L. Iovanna, and N. J. Dusetti. VAV2 regulates epidermal growth factor receptor endocytosis and degradation. *Oncogene*, 29(17):2528–2539, 2010.
- T. Tiganis. Protein tyrosine phosphatases: dephosphorylating the epidermal growth factor receptor. *IUBMB Life*, 53(1):3–14, 2002.
- G. Timinszky, S. Till, P. O. Hassa, M. Hothorn, G. Kustatscher, B. Nijmeijer, J. Colombelli, M. Altmeyer, E. H. K. Stelzer, K. Scheffzek, M. O. Hottiger, and A. G. Ladurner. A macrodomain-containing histone rearranges chromatin upon sensing PARP1 activation. *Nature Structural & Molecular Biology*, 16(9):923–929, 2009.
- J. Tong, P. Taylor, and M. F. Moran. Proteomic Analysis of the epidermal growth factor receptor (EGFR) interactome and post-translational modifications associated with receptor endocytosis in response to EGF and stress. *Molecular & Cellular Proteomics*, 13(7):1644–1658, 2014.
- M. Toriyama, T. Shimada, K. B. Kim, M. Mitsuba, E. Nomura, K. Katsuta, Y. Sakumura, P. Roepstorff, and N. Inagaki. Shootin 1: a protein involved in the organization of an asymmetric signal for neuronal polarization. *The Journal of Cell Biology*, 175(1):147–157, 2006.
- D. Toyoshima, K. Mandai, T. Maruo, I. Supriyanto, H. Togashi, T. Inoue, M. Mori, and Y. Takai. Afadin regulates puncta adherentia junction formation and presynaptic differentiation in hippocampal neurons. *PLOS ONE*, 9(2):e89763, 2014.
- L. Tweedy, D. A. Knecht, G. M. Mackay, and R. H. Insall. Self-generated chemoattractant gradients: attractant depletion extends the range and robustness of chemotaxis. *PLOS Biology*, 14(3):e1002404, 2016.
- S. Tyanova, T. Temu, P. Sinitcyn, A. Carlson, M. Y. Hein, T. Geiger, M. Mann, and J. Cox. The Perseus computational platform for comprehensive analysis of (prote)omics data. *Nature Methods*, 13(9):731–740, 2016.
- F. Ubelmann, T. Burrinha, L. Salavessa, R. Gomes, C. Ferreira, N. Moreno, and C. Guimas Almeida. Bin1 and CD2AP polarise the endocytic generation of betaamyloid. *EMBO reports*, 18(1):102–122, 2017.
- O. Ullrich, T. Reinheckel, N. Sitte, R. Hass, T. Grune, and K. J. A. Davies. Poly-ADP ribose polymerase activates nuclear proteasome to degrade oxidatively damaged histones. *Proceedings of the National Academy of Sciences*, 96(11):6223–6228, 1999.
- O. Ullrich, A. Diestel, I. Y. Eyüpoglu, and R. Nitsch. Regulation of microglial expression of integrins by poly(ADP-ribose) polymerase-1. *Nature Cell Biology*, 3(12):1035–1042, 2001.

- S. van Delft, C. Schumacher, W. Hage, A. J. Verkleij, and P. M. P. van Bergen en Henegouwen. Association and colocalization of Eps15 with adaptor protein-2 and clathrin. *The Journal of Cell Biology*, 136(4):811–821, 1997.
- E. van den Broek, M. J. J. Dijkstra, O. Krijgsman, D. Sie, J. C. Haan, J. J. H. Traets, M. A. van de Wiel, I. D. Nagtegaal, C. J. A. Punt, B. Carvalho, B. Ylstra, S. Abeln, G. A. Meijer, and R. J. A. Fijneman. High prevalence and clinical relevance of genes affected by chromosomal breaks in colorectal cancer. *PLOS ONE*, 10(9):e0138141, 2015.
- P. J. M. Van Haastert and P. N. Devreotes. Chemotaxis: signalling the way forward. *Nature Reviews Molecular Cell Biology*, 5(8):626–634, 2004.
- P. Verheugd, A. H. Forst, L. Milke, N. Herzog, K. L. H. Feijs, E. Kremmer, H. Kleine, and B. Lüscher. Regulation of NF- κ B signalling by the mono-ADP-ribosyltransferase ARTD10. *Nature Communications*, 4:1683, 2013.
- C. Vidal, B. Geny, J. Melle, M. Jandrot-Perrus, and M. Fontenay-Roupie. Cdc42/Rac1-dependent activation of the p21-activated kinase (PAK) regulates human platelet lamellipodia spreading: implication of the cortical-actin binding protein cortactin. *Blood*, 100(13):4462–4469, 2002.
- R. Villaseñor, H. Nonaka, P. Del Conte-Zerial, Y. Kalaidzidis, and M. Zerial. Regulation of EGFR signal transduction by analogue-to-digital conversion in endosomes. *eLife*, 4:e06156, 2015.
- C. A. Viveiro, R. Wat, C. Agrawal, H. Y. Tee, and A. K. L. Leung. ADPriboDB: The database of ADP-ribosylated proteins. *Nucleic Acids Research*, 45(D1):D204–D209, 2017.
- S. Vyas and P. Chang. New PARP targets for cancer therapy. *Nature Reviews Cancer*, 14(7):502–509, 2014.
- S. Vyas, M. Chesarone-Cataldo, T. Todorova, Y.-H. Huang, and P. Chang. A systematic analysis of the PARP protein family identifies new functions critical for cell physiology. *Nature Communications*, 4:2240, 2013.
- F. Wang. The signaling mechanisms underlying cell polarity and chemotaxis. *Cold Spring Harbor Perspectives in Biology*, 1(4):a002980, 2009.
- Z. Wang, G. A. Michaud, Z. Cheng, Y. Zhang, T. R. Hinds, E. Fan, F. Cong, and W. Xu. Recognition of the *iso*-ADP-ribose moiety in poly(ADP-ribose) by WWE domains suggests a general mechanism for poly(ADP-ribosyl)ation-dependent ubiquitination. *Genes & Development*, 26(3):235–240, 2012.
- P. Wee and Z. Wang. Epidermal growth factor receptor cell proliferation signaling pathways. *Cancers*, 9(5):52, 2017.

-
- H. Wei and X. Yu. Functions of PARylation in DNA damage repair pathways. *Genomics, Proteomics & Bioinformatics*, 14(3):131–139, 2016.
- D. Wu and W. Pan. GSK3: a multifaceted kinase in Wnt signaling. *Trends in Biochemical Sciences*, 35(3):161–168, 2010.
- B. Xu, A. Woodroffe, L. Rodriguez-Murillo, J. L. Roos, E. J. van Rensburg, G. R. Abecasis, J. A. Gogos, and M. Karayiorgou. Elucidating the genetic architecture of familial schizophrenia using rare copy number variant and linkage scans. *Proceedings of the National Academy of Sciences*, 106(39):16746–16751, 2009.
- T. Yamaoka, M. R. Frey, R. S. Dise, J. K. Bernard, and D. B. Polk. Specific epidermal growth factor receptor autophosphorylation sites promote mouse colon epithelial cell chemotaxis and restitution. *American Journal of Physiology–Gastrointestinal and Liver Physiology*, 301(2):G368–G376, 2011.
- D. Z. Ye and J. Field. PAK signaling in cancer. *Cellular Logistics*, 2(2):105–116, 2012.
- K. G. Young and R. Kothary. Dystonin/Bpag1 - A link to what? *Cell Motility and the Cytoskeleton*, 64(12):897–905, 2007.
- J. Yue, Q. Wang, H. Lu, M. Brenneman, F. Fan, and Z. Shen. The cytoskeleton protein filamin-A is required for an efficient recombinational DNA double strand break repair. *Cancer Research*, 69(20):7978–7985, 2009.
- J. Yue, S. Huhn, and Z. Shen. Complex roles of filamin-A mediated cytoskeleton network in cancer progression. *Cell & Bioscience*, 3(1):7, 2013.
- F. Zhang, Y. Chen, M. Li, and X. Yu. The oligonucleotide/oligosaccharide-binding fold motif is a poly(ADP-ribose)-binding domain that mediates DNA damage response. *Proceedings of the National Academy of Sciences*, 111(20):7278–7283, 2014.
- F. Zhang, J. Shi, S.-H. Chen, C. Bian, and X. Yu. The PIN domain of EXO1 recognizes poly(ADP-ribose) in DNA damage response. *Nucleic Acids Research*, 43(22):10782–10794, 2015.
- Y. Zhang, S. Liu, C. Mickanin, Y. Feng, O. Charlat, G. A. Michaud, M. Schirle, X. Shi, M. Hild, A. Bauer, V. E. Myer, P. M. Finan, J. A. Porter, S.-M. A. Huang, and F. Cong. RNF146 is a poly(ADP-ribose)-directed E3 ligase that regulates axin degradation and Wnt signalling. *Nature Cell Biology*, 13(5):623–629, 2011.
- Q. Zheng, X. Cai, M. H. Tan, S. Schaffert, C. P. Arnold, X. Gong, C.-Z. Chen, and S. Huang. Precise gene deletion and replacement using the CRISPR/Cas9 system in human cells. *BioTechniques*, 57(3):115–124, 2014.

Acknowledgements

I would like to thank the chair of the department Andreas Ladurner for giving me the chance to join his stimulating, international department.

I would also like to thank my supervisor Gyula Timinszky for giving me a great research project, for his door being literally always open, and for his trust in me which allowed me to shape my project according to my own interest, instincts, and passion.

I would like to thank the whole Timinszky laboratory for their help and support throughout the years. I would like to thank Rebecca Smith for always having an open ear, many scientific discussions, fixing the microscope a thousand times, for helpful comments on my thesis, and all the fun we had over the years.

I would like to thank Barbara Golia for two great, fun years together and for many discussions about MacroD2. Thanks for your support and friendship.

I would like to thank Julia Preisser and Anna Hegele for their help and especially for showing me how the lab worked in the beginning.

I would like to thank the whole Ladurner department for all the fun, coffee breaks, lunches, and scientific and non-scientific talks. I will miss seeing all of you every day.

I would like to thank my TAC members Andreas Ladurner, Gyula Timinszky, Axel Imhof, and Michael Boshart for providing excellent help and feedback to guide me and my project in the right direction.

I would like to thank Andreas Schmidt and Axel Imhof for their help with the proteomics, Stefan Zahler and Simone Braig for their help with cellular migration and attachment assays, and Sebastian Bultmann and the FACS Core Facility for the use of their FACS machines.

I would like to thank all my students: Mai Ly Tran, Irene Chen, Regina Bichler, and Maria Richter. You did a great job on your projects and I had a fantastic time with each and every one of you. I wish you guys all the best for the future.

Last but not least, I want to thank my parents and my brother for their support and encouragement. I could not have done this without you. I would like to thank Tobi's family for their support and their believe in me. I would like to thank Tobi for being there for me, being my best friend, and encouraging me in everything I want to do.